COMBUSTION AND EMISSIONS OF A DIRECT INJECTION GASOLINE ENGINE USING BIOFUELS

by

Chongming Wang

A thesis submitted to
The University of Birmingham
for the degree of

DOCTOR OF PHILOSOPHY

UNIVERSITY OF BIRMINGHAM

University of Birmingham Research Archive

e-theses repository

ABSTRACT

This thesis exams the combustion characteristics and emissions of bioethanol and two other novel biofuel candidates, 2-methlyfuran (MF) and 2,5-dimethylfuran (DMF) in a spray-guided GDI engine. The impact of fuels, injector pressure and fouled injectors on PM emissions, and oxidation of soot produced from GDI engines are also investigated.

Biofuels are one part of the solutions for the renewable energy supply and emission reduction. Research interests cover detailed combustion characteristics and emissions, especially particulate matter (PM) emissions. Gasoline is used as the benchmark fuel. A spray-guided single-cylinder direct-injection (DISI) engine is used in this thesis. A Horiba MEXA-7100DEGR Gas Analyser is used to measure gaseous emissions such as hydrocarbon (HC), nitrogen oxide (NO_x) and carbon monoxide (CO). Aldehyde emissions and key HCs have been investigated using the High Performance Liquid Chromatography (HPLC) and Gas Chromatography Mass Spectrum (GC-MS) techniques. A Scanning Mobility Particle Sizer (SPMS) is used to measure the particle size distributions. A Thermo-gravimetric analyser (TGA) is applied in the study of the PM composition and soot oxidation process.

The combustion of DMF and MF in DISI engines demonstrates better knock resistance properties and faster burning rates compared to those of gasoline. DMF and MF have much lower fuel consumptions than ethanol due to their higher energy density. The combustion of DMF and MF produces much lower hydrocarbon (HC) and PM emissions than those of gasoline. However because of much higher combustion temperatures, their NO_x emissions are significantly higher than those of gasoline, when fuel-optimized spark timings are used. This issue can be solved by either retarding ignition timing at the price of fuel consumption penalties,

or by using exhaust gas recirculation (EGR) which is more efficient and has a less negative impact on fuel economy, if it is optimized. DMF and MF produce much lower aldehyde emissions compared with gasoline and ethanol. The majority of HCs in the exhaust are unburned fuel. Toluene and benzene are detected in the exhaust; however their concentrations are relatively low.

Since biofuels such as bioethanol have oxygen in their molecule, PM emissions from ethanol are lower than those from gasoline, giving it good potential in PM emission reduction. Therefore, the impact of fuels (ethanol and gasoline) on PM emissions from a GDI engine under various injection pressure and injector fouling has been studied. Particles are classified into nucleated and accumulated particles, a distinction not made by most other researchers. Results show that PM emissions vary to fuels, injection pressure, and injector fouling. Ethanol produces less PM mass emission compared to gasoline. Unlike gasoline, PM emissions from the DISI engine fuelled with ethanol are not sensitive to injection pressure. This thesis highlights the significant negative impact of fouled injectors on PM emissions when using gasoline as the fuel, and it also highlights how ethanol is able to keep PM emissions low from fouled injectors. A trade-off between particle number (PN) and PM mass emissions is observed when using ethanol.

Further work has been done to investigate PM composition and soot oxidation of PM produced in a GDI engine fuelled with DMF, ethanol and gasoline. This is one of the few investigations focusing on the PM oxidation characteristics from a GDI engine. It is found that even under rich combustion and later injection timing operating conditions, soot only accounts for a small fraction (<30%) of PM mass whilst volatility components are the main contributors. Soot produced from the combustion of oxygenated fuels such as DMF and ethanol is more easily oxidized than gasoline soot due to their unique capsule type oxidation mode, smaller primary, and agglomerated particles.

ACKNOWLEDGEMENTS

I wish to dedicate this thesis

To my father, Jiansheng Wang

To my mother, Yuezhen Shen

To my fiancé,

To my sister,

And friends

CONTENTS

LIST OF FIGURES

LIST OF TABLES

LIST OF NOTATIONS

AECC	Association for Emissions Control by Catalyst
AFR	Air-Fuel Ratio
aTDC	After Top Dead Centre
BSFC	Brake Specific Fuel Consumptions
bTDC	Before Top Dead Centre
BUT	Butanol
CAD	Crank Angle Degrees
CCD	Combustion Chamber Deposits
CD	Combustion Duration n Duration
CEC	Coordinating Research Council
CID	Initial Combustion
CO	Carbon Dioxide
CO2	Coefficient of Variation
COV	Direct Injection
CRC	Carbon Monoxide
DC	Direct Injection Spark Ignition
DI	Direct Injection
DISI	Diesel Particulate Filters
DMF	2,5-Dimethylfuran
DNPH	2,4-Dinitrophenylhydrazine
DPFs	Diesel Particulate Filters
E25	Gas Chromatography–Mass Spectrometry
EDX/EDS	Energy Dispersive X-Ray
EGR	Engine Management System
EMS	Exhaust Valve Closing
EOI	Volumetric 25% Ethanol in Ethanol/Gasoline Blend

EPSRC	Engineering and Physical Sciences and Research Council
ETH	End of Injection
EVC	Fourier Transform Infrared Spectroscopy
FID	Flame Ionization Detector
FTIR	Fourier Transform Infrared Spectroscopy
GCMS	Gas Chromatography Mass Spectrometry
GDI	Homogeneous Charge Compression Ignition
GHG	Greenhouse Gas
GisFC	Gravimetric Indicated Specific Fuel Consumption
GPFs	Gasoline Particulate Filters
HCCI	Homogeneous Charge Compression Ignition
HC	Hydrocarbons
HMF	5-hydroxymethylfurfural
HPLC	High Performance Liquid Chromatography
HRR	Heat Release Rate
HV	Heat of Vaporization
IBP	Initial Boiling Point
IMEP	Indicated Mean Effective Pressure
IR	Infrared Spectroscopy
IVC	Intake Valve Closing
IVO	Intake Valve Opening
isCO	Indicated specific Carbon Monoxide
isHC	indicated specific Hydrocarbon
LHV	Lower Heating Value
λ	Minimum Spark Advance for Best Torque
KLSA	Knock-limited Spark Advance
LCV	Lower Calorific Value
LTC	Low Temperature Combustion

MBT/KLSA	Maximum Brake Torque/ Knock-Limited Spark Advance
MMLRT	Maximum Mass Loss Rate Temperature
MBT	Minimum Spark Advance for Best Torque
MF	2-Methylfuran
MFB	Mass Fraction Burned
MTH	Methanol
MON	Motor Octane Number
NO	Nitric Oxide
NO_X	Oxides of Nitrogen
NVO	Negative Valve Overlap
OEMs	original equipment manufacturers
PAH	Polycyclic Aromatic Hydrocarbons
PDPA	Phase Doppler Particle Analyser
PEAs	Polyether Amines
PFI	Port Fuel Injection
PM	Particulate Matter
Φ	Equivalence Ratio (Fuel to Air)
PM	Particulate Matter
PN	Particle Number
PID	Proportional Integral Differential
PPM	Parts per Million
PRF	Primary Reference Fuel
TDC	Top Dead Centre
TEM	Transmission electron microscopy
TGA	Thermo-gravimetric Analyser
TWCs	Three Way Catalysts
rpm	Revolutions per Minute
RON	Research Octane Number

SI	Spark Ignition
SEM	Scanning Electron Microscope
SMPS	Scanning Mobility Particle Sizer
SOC	Start of Combustion
SOI	Start of Injection
T90	90% distillation temperature
TDC	Top Dead Center
TGA	Thermo-gravimetric Analyser
TWCs	Three-Way Catalysts
ULG	Unleaded Gasoline
VCT	Variable Cam Timing
VD	Valve Deposits
VisFC	Volumetric Indicated Specific Fuel Consumption
VOC	Volatile Organic Compounds
VVT	Variable Valve Timing
WOT	Wide Open Throttle
WWFC	Worldwide Fuel Charter
XRF	X-Ray Fluorescence Analysis

LIST OF PUBLICATION

1.   **Fuel Injector Deposits in Direct-Injection Spark-Ignition,** Hongming Xu, <u>Chongming Wang</u>, Xiao Ma, Asish K Sarangi, Adam Weall, Jens Krueger-Venus, Progress in Energy and Combustion Science, Review report received (minor correction), 2014.

2.   **Impact of Fuel and Injection System on Particle Emissions from a GDI Engine,** <u>Chongming Wang</u>, Hongming Xu, Jose Martin Herreros, Jianxin Wang, Roger Cracknell, Applied Energy, 132 (1), 178-191, 2014.

3.   **Fuel Effect on Particulate Matter Composition and Soot Oxidation in a Direct-Injection Spark Ignition (DISI) Engine,** <u>Chongming Wang</u>, Hongming Xu, Jose Martin Herreros, Thomas Lattimore, Shijin Shuai, Energy & Fuels, 28, 2003-12, 2014.

4.   **Combustion characteristics and emissions of 2-methylfuran compared to 2,5-dimethylfuran, gasoline and ethanol in a DISI engine,** <u>Chongming Wang</u>, Hongming Xu, Ritchie Daniel, Jose Martin Herreros, Shijin Shuai, Xiao Ma, Fuel, 103, 200-11, 2013.

5.   **Impacts of Low-level MF content in gasoline on DISI engine combustion behaviour and emissions,** <u>Chongming Wang</u>, Hongming Xu, and Thomas Lattimore, SAE technical paper 2013-01-131, 2013.

6.   **Comparison of Gasoline, Bio-ethanol and 2,5-Dimethylfuran in a DISI Engine using the Miller cycle with Late Inlet Valve Closure Timing,** <u>Chongming Wang</u>, Ritchie Daniel, Hongming Xu, SAE technical paper 2012-01-1147, 2012.

7.   **Research of the Atkinson Cycle in the Spark Ignition engine,** <u>Chongming Wang</u>, Ritchie Daniel, Hongming Xu, SAE technical paper 2012-01-0390, 2012.

8.   **Effects of Combustion Phasing, Injection Timing, Relative Air-Fuel Ratio and Variable Valve Timing on SI Engine Performance and Emissions using 2,5-Dimethylfura**n, Ritchie Daniel, <u>Chongming Wang</u>, Hongming Xu, International Journal of Fuels and Lubricants 2012-01285, 2012.

9.   **Split-Injection Strategies at Wide Open Throttle using Gasoline, Ethanol and 2,5-Dimethylfuran in a Direct-Injection SI Engine,** Ritchie Daniel, <u>Chongming Wang</u>, Hongming Xu, SAE technical paper 2012-01-0403, 2012.

10.   **Dual-Injection as a Knock Mitigation Strategy using pure Ethanol and Methanol,** Ritchie Daniel, <u>Chongming Wang</u>, Hongming Xu, SAE technical paper 2012-01-1152, 2012.

11.   **Combustion Performance of 2,5-Dimethylfuran Blends using Dual-Injection compared to Direct-Injection in a SI Engine,** Ritchie Daniel, Hongming Xu, <u>Chongming Wang</u>, Guohong Tian and Dave Richardson, Applied Energy, 98, (0), 59-68, 2012.

12.   **Gaseous and Particulate Matter Emissions of Oxygenated Fuel Blends using Dual-Injection compared to Direct-Injection in a SI Engine,** Ritchie Daniel, Hongming Xu, <u>Chongming Wang</u>, Guohong Tian and Dave Richardson, Applied Energy, 105, (0), 252-261, 2013.

13.   **Speciation of Hydrocarbon and Carbonyl Emissions of 2,5-Dimethylfuran in a DISI Engine,** Ritchie Daniel, Lixia Wei, <u>Chongming Wang</u>, Hongming Xu and Miroslaw L. Wyszynski, Energy & Fuels, 26 (11), pp 6661–6668. DOI: 10.1021/ef301236f, 2012.

CONFERENCE PRESENTATION

1.   **Comparison of Gasoline, Bio-ethanol and 2,5-Dimethylfuran in a DISI Engine using the Miller cycle with Late Inlet Valve Closure Timing**, Chongming Wang, Ritchie Daniel, Hongming Xu, SAE World Congress, Detroit, USA, 2012.

2.   **Dual-Injection as a Knock Mitigation Strategy using pure Ethanol and Methanol**, Ritchie Daniel, Chongming Wang, Hongming Xu, SAE World Congress, Detroit, USA, 2012.

3.   **Split-Injection Strategies at Wide Open Throttle using Gasoline, Ethanol and 2,5-Dimethylfuran in a Direct-Injection SI Engine**, Ritchie Daniel, Chongming Wang, Hongming Xu, SAE World Congress, Detroit, USA, 2012.

4.   **Combustion Characteristics and Emissions of Low2-Methylfuran/Gasoline Blend in a DISI Engine**, Chongming Wang, Hongming Xu, and Thomas Lattimore, SAE World Congress, Detroit, USA, 2013.

5.   **Impact of DMF and MF on Engine Performance and Emissions as a New Generation of Sustainable Biofuel**, Chongming Wang, Hongming Xu, Ritchie Daniel, Dublin, Ireland, 2013.

6.   **The New Generation of Sustainable Biofuel in GDI engines**, Chongming Wang, Future Powertrain Conference Birmingham, UK, 2014.

7.   **Fuel Effect on Particulate Matter Composition and Soot Oxidation in a Direct-Injection Spark Ignition (DISI) Engine,** Chongming Wang, Hongming Xu, Jose Martin Herreros, Thomas Lattimore, Shijin Shuai, UnICEG, University of Birmingham, 2014.

CHAPTER 1

1   INTRODUCTION

This introductory chapter is intended to give an overview of the author's PhD research, which is mainly about combustion and emissions of biofuels in a GDI engine. The study of biofuels is driven by the call for renewable energy supply and stringent emission regulations. Two biofuel candidates, DMF and MF, are introduced. The overall research outline, objectives and corresponding investigation approach are briefly presented, followed by a thesis outline.

1.1   Overview

The transportation sector is facing two challenges, which are renewable energy supply and clean transportation. The fossil fuel was, is, and will be the main energy source for the transportation for many decades; however this trend cannot last forever. On the other hand, because of increased environmental awareness, regulatory authorities across the world are putting more and more pressure on the automobile and petroleum industry to invent and develop technologies for reducing emissions and improving fuel economy. The author believes that electric vehicles will be the ultimate solution; however the advanced battery technologies and the battery disposal issues will potentially take decades to be fully resolved. The related infrastructure requirements such as charging outlets are barriers stopping electric vehicle from being applied quickly in the short term. There are some medium term solutions such as the hydrogen fuel cell and hybrid vehicles. For the

hydrogen fuel cell, there are still technical issues such as hydrogen production, transportation, and storage.

In spark ignition engines there are many technologies available for improving fuel economy and reducing emissions. Those technologies include in-cylinder approaches such as direct injection, 2/4 stroke engine mode switch, turbo-charging, variable valve lift and valve timing, learn burn stratified-charge combustion, and engine-out approaches such as high efficiency catalytic converters and particle captures. By using those technologies, GDI engines reduced fuel consumption at part load by 20~25% compared to PFI engines (S. Kono, 1995, Jackson et al., 1997, Park et al., 2012, Tomoda et al., 1997).

It is also believed that biofuels such as bio-ethanol are part of the solutions. Bioethanol is widely blended into gasoline because of high anti-knock abilities, and the benefits of low HC and PM emissions. However, bio-ethanol has some drawbacks: low fuel economy, solubility in water, and high production costs. The search for a superior alternative to bioethanol is critical to energy development.

In 2007, improved MF and DMF production methods were published using fructose as the feedstock (Roman-Leshkov, 2007, Zhao, 2007). MF and DMF produced by this method are considered to be renewable biofuels. Before DMF and MF can be widely used as gasoline alternatives, their impact on engine performance and emissions need to be assessed.

1.2 Objectives and Approaches

The research aim was to assess the feasibility of using biofuels (MF, DMF and bioethanol) in a DISI engine. The following are the specific objectives of the author's PhD study:

- Effect of MF, DMF and ethanol on combustion and regulated emissions in a GDI engine.

- Identification of key HCs and aldehyde emissions from a GDI engine fuelled with MF.

- Impact of fuels (ethanol and gasoline) on PM emissions from a GDI engine under various injection pressure and injector fouling conditions.

- Study of PM composition and soot oxidization characteristics in a GDI engine fuelled with DMF, ethanol and gasoline.

A spray-guided single-cylinder DISI engine is used for engine experiments. A Horiba MEXA-7100DEGR Gas Analyser is used to measure gaseous emissions. Aldehyde emissions and key HCs are investigated using the High Performance Liquid Chromatography (HPLC) and Gas Chromatography Mass Spectrum (GC-MS) techniques. A Scanning Mobility Particle Sizer (SPMS) is used to measure the particle size distributions. A Thermo-gravimetric analyser (TGA) is applied in the study of PM composition and the soot oxidation process.

The novelty of this thesis includes:

- Detailed combustion analysis of a GDI engine fuelled with two novel biofuel candidates; MF and DMF.

- Assessment of the toxic HC and aldehyde emissions from MF combustion.

- This thesis highlights the significant negative impact of fouled injectors on PM emissions, and how ethanol is able to reduce PM emissions from fouled injectors.

- Unlike most other investigations, PM analysis in the thesis is detailed into the nature of the particles. Particles are classified into the nucleation and accumulation modes.

  - This is one of the few investigations focusing on oxidation characteristics of soot produced in a GDI engine. This is one of the few investigations focusing on the PM oxidation characteristics from a GDI engine.

1.3   Research Outline

In this thesis, the main focus is on the investigation of the impact of biofuels (MF, DMF and bioethanol) on combustion characteristics and emissions in a DISI engine.

The study of engine combustion characteristics includes a comprehensive analysis of engine in-cylinder pressure, heat release rate, and combustion phase. A Ricardo Wave model is used for the calculation of in-cylinder temperatures. Regulated emissions such as CO, NO_x, and HC have been measured and compared with those of gasoline. EGR and retarded spark timing strategies are used to control NO_x emissions. Unregulated emissions such as individual HCs and aldehyde emissions have been also measured. Since oxygenated fuels such as ethanol have the advantage of reduced PM emissions, the impact of fuels (ethanol and gasoline) on PM emissions from a GDI engine under various injection pressure and injector fouling is studied. Further investigation is carried out for a comprehensive study of PM composition and soot oxidization characteristics.

1.4   Thesis Outline

This thesis is comprised of eight chapters. A brief outline of each followed chapters is presented below.

Chapter 2 – Literature Review

This chapter covers a brief literature review of topics related to this thesis. Firstly, GDI technologies are introduced. Secondly, physiochemical properties of gasoline, DMF and MF, and the review of previous publications investigating those fuels, are presented. Thirdly, emissions, especially PM emissions, are reviewed. Lastly, the GDI injector fouling issue, one of major challenges in GDI combustion system development, is reviewed.

Chapter 3 – Experimental Setup

This chapter provides detailed information of engine and instrument setup, data acquisition, and recording systems. Emission analysers are also briefly presented. Finally, key calculations used in this thesis are presented.

Chapter 4 – Combustion Characteristics and fuel consumptions of MF, DMF and Ethanol in a GDI Engine

This chapter assesses combustion of MF, DMF, and ethanol in a DISI engine. The experiments were conducted at stoichiometric combustion, 1500 rpm engine speed, and 3.5 to 8.5 bar IMEP. The analysed combustion characteristics include in-cylinder pressure, heat release rate and combustion phase. A Ricardo Wave model has also been used for the calculation of in-cylinder temperatures. The importance of this chapter is that it compares

the combustion of biofuels with that of gasoline, and assesses the feasibility of using those biofuels as gasoline alternatives.

Chapter 5 – Emission Characteristics of MF in a GDI Engine compared with DMF, Ethanol, and Gasoline

Engine-out gaseous emissions of MF, DMF and ethanol have been investigated under the engine condition of 1500 rpm engine speed, 3.5-8.5 bar IMEP load and stoichiometric air-fuel ratio. EGR and retarded spark timing have been applied to reduce NO_x emissions. Key HCs and aldehyde emissions in DISI engines fuelled with MF at 6.5 bar IMEP are detected using the GCMS and HPLC techniques. The importance of this chapter is that it compares gaseous emissions of biofuels with those of gasoline, and it also assesses the toxic HC and aldehyde emissions from MF combustion.

Chapter 6 – Impact of Fuels on PM Emissions from a GDI Engine under various Injection Pressure and Injector Fouling conditions

Impact of fuels on PM Emissions from a GDI engine under various injection pressure and fouled injectors was studied. The experiments were conducted in a DISI research engine (λ=1, engine speed=1500 rpm, load=3.5-8.5 bar IMEP). Two fuels (gasoline and ethanol), four injection pressures (50, 100, 150, 172 bar) and three injectors (one clean and two fouled injectors with 5.3% and 8.5% fuel flow rate loss) were tested. Results show that PM emissions vary significantly between different fuels and different injection systems. Ethanol combustion produced less PM emissions compared to gasoline. Unlike gasoline, PM emissions from the ethanol powered the DISI engine are not sensitive to injection system; a low injector pressure and fouled injectors have very limited impacts on PM emissions. This chapter highlights the importance of keeping injectors clean in order to

keep PM emissions low, and also the benefit of using ethanol to reduce PM emissions, even when injectors are fouled.

<u>Chapter 7 – PM Composition and Soot Oxidation for PM Emissions from a GDI Engine Fuelled with DMF, Ethanol, and Gasoline</u>

PM composition and soot oxidization characteristics from a DISI engine were investigated using the TGA technique. A kinetic model was used to quantitatively describe soot oxidization reactivity. The engine was operated at 1500 rpm with rich combustion and late fuel injection strategy. A TGA method was developed and then applied to the study of PM produced from the combustion of ethanol, low ethanol/gasoline blend (E25), and DMF. The importance of this chapter is that it provides key information about the soot oxidation characteristics, which are key information for GPF regeneration and GPF thermal modelling.

<u>Chapter 8 – Summary, Conclusion and Future Work</u>

This chapter gives the key conclusions of this thesis, followed by recommendations for future work.

CHAPTER 2

2   LITERATURE REVIEW

This chapter is intended to provide literature review and background knowledge needed for the author to carry out his PhD research, which is mainly about combustion and emissions of biofuels in a GDI engine. Since the experiments were carried out in a modern GDI engine, therefore a general review of GDI technology is presented. Then DMF and MF are introduced, along with the related investigations done by previous researchers. Because gasoline is used as the benchmark fuel, it is also introduced. Reducing emissions by using biofuel is another important theme of this thesis, thus review of emissions especially PM emissions is presented. Injector fouling is one of the major challenges during GDI combustion system development, due to its highly negative impact on engine performance. The author is one of the few that studied the impact of injector fouling on PM emissions, and the results show that injector fouling affect PM emissions more than the engine combustion and other emissions such as HC emissions. For the importance of injector fouling, a review of injector fouling is provided at the end of this chapter.

2.1   GDI Engines

Vehicles powered by GDI engines aiming to improve fuel economy and reduce CO_2 emissions started to enter the car market in the late 1990s (Zhao et al., 1999). GDI is a technology where high pressure fuel (50~150 bar) is injected directly into the cylinder with the quantity and timing precisely controlled by an electronic control unit (ECU). Direct injection offers precise fuel metering and improved spray atomization compared with the

PFI injection system. The first GDI vehicle by Mitsubishi was released in 1996, and Volkswagen launched fuel stratified injection (FSI) GDI engines in 2000. When coupled with other advanced technologies such as VVT, turbo-charging, and lean stratified combustion technologies, GDI engines further reduced fuel consumption at part load by 20~25% due to the use of wasted energy in the exhaust, the use of high compression ratio engines, optimised combustion and less throttling (S. Kono, 1995, Jackson et al., 1997, Park et al., 2012, Tomoda et al., 1997). Table 2-1 provides a summary of carburettor, PFI, and GDI injection systems.

Table 2-1:   Summary of Carburettor, PFI and GDI Injection System

	Advantages	**Disadvantages**
Carburettor	Basic fuel metering	1) No precise fuel metering 2) Bad emissions 3) Bad engine response and driveability
PFI	1) Improved fuel metering compared with carburettor 2) Three Way Catalyst (TWC) works well under steady state operation 3) Better engine response and improved driveability compared to the carburettor engine 4) Low PM emissions	1) Bad fuel metering in cold start and transient operating conditions, which affects emissions 2) potential intake valve deposit issue
GDI	1) Precise fuel metering, better fuel spray atomization, superior transient response 2) high compression ratio, high engine power output, and low fuel economy 3) Lower emissions due to faster catalyst light-off in cold start 4) More flexible choice of combustion mode	1) Issues regarding fuel economy and emission in cold start compared with hot steady state operations are still persist 2) Bad HC and PM emission compared with PFI engines 3) High requirement for high fuel quality, potential injector plugging problem 4) Piston and cylinder liner wetting thus more severe combustion chamber deposits 5) High system complexity, high manufacturing cost, and durability problem

Based on the mixture preparation process, GDI engines are classified into three categories. In the air-guided (wide-space concept) combustion system, fuel is transported to the region near the spark plug by a strong air motion generated by inlet ports with a specially designed shape. Injector tip wetting is much reduced since the air dries the injector tip. However, the air-guided combustion system is highly sensitive to air flow motion therefore it suffers from severe cylinder-by-cylinder and cycle-by-cycle variations. In the wall-guided combustion system, the injector and spark plug are away from each other (wide-spacing concept), and fuel spray is directed to the spark plug by a piston with a cavity on the crown. The wall-guided GDI engines are also referred to as first generation GDI engines. However, due to the severe piston wetting issue, emissions such HC, CO, and particulate matter (PM) in the wall-guided combustion system are concerns. In the spray guided GDI system which is referred to as second generation GDI technology, the injector is located near the spark plug (close-spacing concept), and one or multiple fuel jets are delivered to the spark by the injector. The injector of the spray guided GDI system is often centrally mounted, differing from the side-mounted injectors near the intake port in both air and wall guided combustion systems.

2.2   Gasoline in SI Engines

Fuel is an important factor in meeting stringent emission requirements for fuel economy and emissions; it is also a key in guaranteeing the reliability and durability of GDI engines and after treatment systems. In the past decade in developing countries such as China and India, and in Africa, significant progress has been made towards low sulphur, lead-free, and metal-free gasoline, in order to protect human health and the environment, and to improve catalyst durability.

Fuel standards vary significantly across the world. Table 2-2 lists fuel specifications of the US (ASTM D4814-2011), the EU (EN228 -2012), and China (GB 17930 – 2013). Additionally the automotive industry from their perspective describes the requirements on fuels in their "Worldwide Fuel Charter" (WWFC), currently available as a draft in its 5th version. The main focus of these fuel standards is on the sulphur, aromatics, olefins, gum, volatility, and octane rating.

The biggest development in the regulations is the sulphur limit. In the past 20 years, the EU has applied ever stricter standards regarding sulphur content, starting from a 2000 ppm limit in the year of 1994, to a 150 ppm limit in the year of 2000. Currently, the EU markets have already regulated the sulphur content below 10 ppm. In China, the sulphur content is also regulated, starting from 500 ppm limit in the year of 2006, to 50 ppm limit in the year of 2013. In the year of 2017, China plans to enforce a 10 ppm sulphur limit nationwide. In the USA, the sulphur cap is also tightened from 300 ppm in the year of 2004 to 80 ppm in the year of 2006.

The investigation of sulphur in GDI engines is still of interest from a global perspective. Sulphur not only contributes to SO_2 emissions and therefore acid rain, it is also partially responsible for PM emissions. Fuel with high sulphur content can rapidly and irreversibly damage the oxygen sensor and exhaust after treatment devices (TWC and NO_x absorbers), therefore it leads to high emissions (Schifter et al., 2003, Yao et al., 2008, Hochhauser, 2009). The poisoned catalysts demonstrated a longer light-off time, increased light-off temperature, and reduced conversion efficiency (WWFC, 2012).

Table 2-2: Fuel Specifications in US, EU and China

Parameter	EU EN 228-2012	US ASTM D4814 Rev B - 2011	China GB 17930 – (Dec. 2013
Density (kg/m ³)	720-775 (at 15 ℃)		720-775(at 20 ℃)
T10 (℃)		≤70	≤70
T50 (℃)		≤77-121	≤120
T90 (℃)		≤190	≤190
End of distillation point (℃)			≤205
E70 summer (volume %)[a]	20-48		
E70 Winter (volume %)[a]	22-50		
E100 (volume %)	46-71		
E150 (volume %)	≥75		
Sulphur (ppm)	≤10	≤80	≤(50
Aromatics (m/m)	≤35%	≤20.9%	≤40%
Olefins (%m/m)	≤18%	≤11.9%	≤28%
Max. washed/unwashed Gum(mg/100mL)	5 (washed)	5 (washed)	5 (washed)/30 (unwashed)

[a] Depends on volatility class of region, country and season

Aromatics are chemicals containing at least one benzene ring in their molecule. Research evidence shows that aromatics are responsible for carcinogenic emissions such benzene and toluene (Barnes et al., 2005). Similar to aromatics, olefins are responsible for deposit formation in the fuel and combustion systems (Aradi et al., 1999, Uehara et al., 1997, Ashida et al., 2001). Gum also causes deposit problems in the fuel and combustion system. Research evidence shows that the T90 parameter of fuel is directly related to injector deposit formation (Aradi et al., 2000a, Kinoshita et al., 1999, Bacho et al., 2009, Sandquist et al., 2001).

The fuel volatility property indicated by vapour pressure and driveability index is directly linked to the performance and emissions of GDI engines. Highly volatile fuel is preferred in the winter to ensure a better cold start performance. If fuel formulated for the winter is used in the summer mistakenly, there is a risk of vapour lock in the fuel system,

resulting in engine driveability problems. Therefore there is a maximum and minimum limit for vapour pressure, depending on the season.

Octane rating, a function of the motor octane number (MON) and the research octane number (RON), is an indicator of the antiknock property of the fuel. GDI engines lead to less knock tendency due to the fuel cooling effect. Fuel with a high octane rating is used in high compression ratio GDI engines to avoid engine knock, for the purpose of increasing engine efficiency.

2.3   Bio-ethanol, DMF and MF

The use of ethanol as an engine fuel dates back to the 1890s. In 1896 Henry Ford built an automobile running on pure ethanol (Goettemoeller and Goettemoeller, 2007). The ethanol consumption in the transportation sector has been expanded three times in the past ten years (Berg and Licht, 2011).

Bio-ethanol is the most widely used biofuel in the world, especially in the EU, Brazil, and the United States. The United States is the largest bio-ethanol producer (made mainly from corn crops) and Brazil is the largest exporter (made mainly from sugar cane) (Berg and Licht, 2011). The first generation bio-ethanol is made from high end stocks such as sugar cane, wheat, corn, etc., and is highly controversial, because of its consumption of food supplies. The second generation bio-ethanol is produced from low end stocks such as grass, wood chips, and agricultural wastes, therefore proving to be less controversial.

Ethanol is a favourable gasoline alternative. Sustained research has been carried out using ethanol in SI engines (Kintisch, 2007, Atsumi et al., 2008, Agarwal, 2007, Demirbas, 2007). It can be used in its pure form in specially designed SI engines or in blended forms

with minor engine modifications. Ethanol has a high octane rating and a high heat of vaporization, making it a favourable choice in the application of high compression ratio engines. Due to ethanol's partially oxygenated nature and its fast flame speed, its combustion and post-oxidation is more complete than gasoline. The HC, NO_x, and PM emissions from ethanol combustion are lower than those from gasoline (Masum et al., 2013, Wang et al., 2013a). The difference in vehicle-out HC, NO_x and CO emissions between engines fuelled with ethanol and gasoline will be diminished due to the high efficiency of TWCs. Publications about the use of diesel-ethanol blends in CI engines are also available (Rakopoulos et al., 2011, Scania, 2007, Song et al., 2010, Sayin, 2010). Generally, the ignition delay of the diesel engine powered by an ethanol and diesel blend is increased, compared to when it's powered purely by diesel. As a result, HC, CO emissions and smoke opacity are reduced.

However, bio-ethanol has some drawbacks as an engine fuel, the most significant being low energy content and high production costs. Due to its solubility in water, its production, transportation, and storage cost are all increased. Engine performance and emissions in cold start are issues due to its high heat of vaporization, and low saturated vapour pressure at low temperature (Iodice and Senatore, 2013). Therefore, the search for new biofuel candidates is a focus of future fuel research. The new biofuel candidates for SI engines should meet the following requirements:

- Safe, easy, and low-cost storage and transportation

- Use of biomass as raw feedstock

- High production efficiency with competitive cost

- High energy density

- Easily adapted to current-existing SI engines

- Competitive combustion characteristic and emissions

DMF and MF has become attractive biofuel candidates, after a new production method was published in 2007, using fructose as the feedstock (Roman-Leshkov, 2007, Zhao, 2007). Figure 2-1 shows the rationale for converting carbohydrates to DMF and MF. Selective oxygen removal can be achieved in two steps: firstly, by removing three oxygen atoms from fructose through dehydration to produce 5-hydroxymethylfurfural (HMF); and secondly, by removing two oxygen atoms through hydrogenolysis to produce DMF and MF (Yuriy Román-Leshkov, 2009, Tian et al., 2011). Fructose is abundant and renewable, and biomass can be used as the feedstock. Since the feedstock for DMF and MF production is renewable, DMF and MF produced by this method are also considered to be renewable.
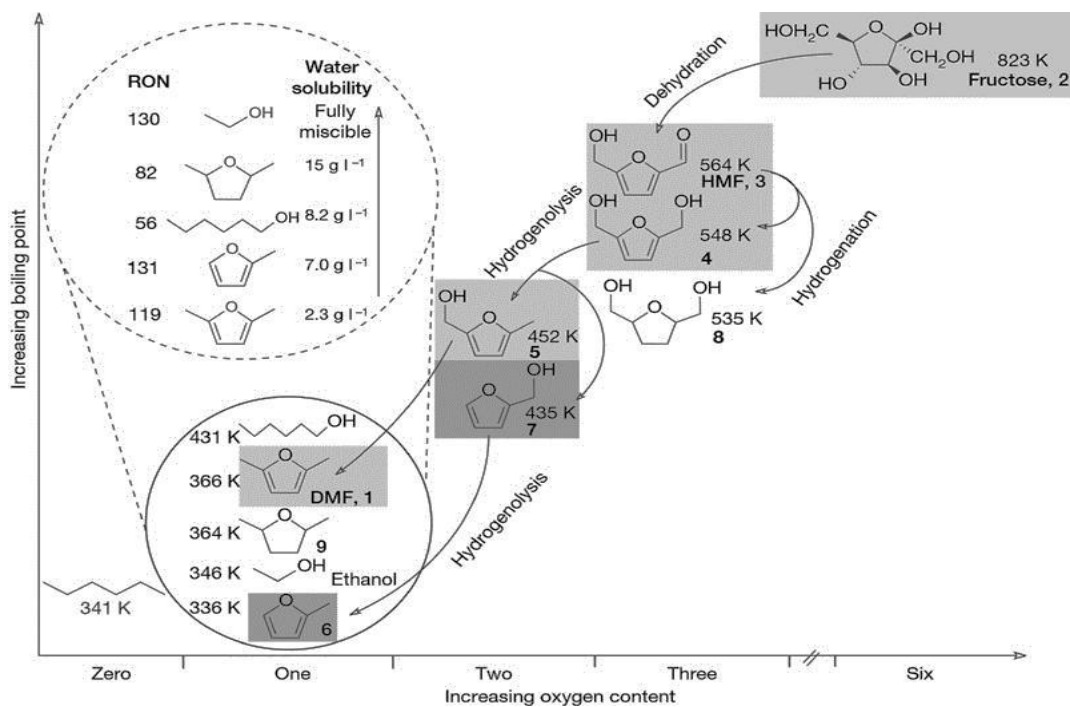
Figure 2-1: Rationale for Converting Carbohydrates to DMF and MF (Roman-Leshkov, 2007, Zhao, 2007)

Before commercial mass production of any new biofuels, the costs, energy efficiency, and carbon footprint, which largely depend on the availability of raw feedstock and production methods, need to be assessed.

For the analysis of energy and GHG emissions, there are two methodologies available, well to wheels (WTW) and life cycle analysis (LCA). WTW can be separated into well to tank (WTT) and tank to wheels (TTW). WTT assessment considers energy required and GHG emitted in the procedures of crop growing and harvesting, crop transportation, biofuel refinery, and delivering fuels into the tank of vehicles. The TTW assessment accounts for the energy required and GHG emitted by vehicles during the driving process. Apart from all the factors considered in the WTW analysis, LCA assesses other energy required and GHG emitted such as the plant construction, water, and emission of all kind of pollutants. As a result, LCA is a more accurate methodology; however it requires more data input. In this work, the WTW of bioethanol, instead of LCA, is reviewed.

The WTW analysis of future automotive fuels and powertrains in the European context is currently in the fourth edition (Edwards et al., 2014). Figure 2-2 shows the WTW fossil energy expended and GHG emissions for ethanol pathways when using 2020 model year DISI vehicles. Table 2-3 shows the code for the pathways presented in Figure 2-2, where NG stands for nature gas; CHP stands for combined heat and power; DDGS stands for distiller's dried grain with solubles (the residue left after ethanol production from wheat grain).
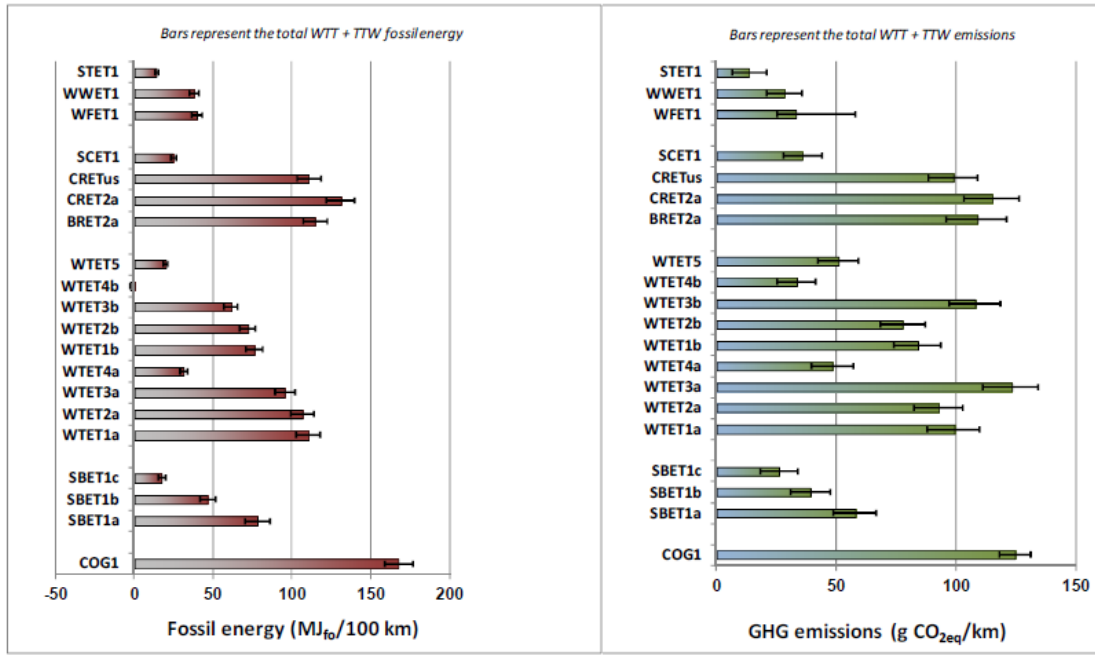
Figure 2-2: WTW fossil energy expended and GHG emissions for ethanol pathways (2020+ DISI vehicles) (Edwards et al., 2014)

Table 2-3: Key to pathway codes (Edwards et al., 2014)

STET1	Wood (wheat)
WFET1	Wood (farmed)
WWFET1	Wood (waste)
SCET1	Sugar Cane (Brazil), surplus biogas to electricity
CRET2a	Maize (EU), NG to CHP, DDGS to animal feed
CRETus	Corn (US)
BRET2a	Barley/Rye, NG to CHP, DDGS to animal feed
WTET5	Wheat, convention boiler, DDGS to electricity via biogas
WTET4b	Wheat, straw to CHP, DDGS to electricity
WTET3b	Wheat, lignite to CHP, DDGS to electricity
WTET2b	Wheat, NG to CHP, DDGS to electricity
WTET1b	Wheat, convention boiler, DDGS to electricity
WTET4a	Wheat, straw to CHP, DDGS to animal feed
WTET3a	Wheat, lignite to CHP, DDGS to animal feed
WTET2a	Wheat, NG to CHP, DDGS to animal feed
WTET1a	Wheat, convention boiler, DDGS to animal feed
SBET1c	Sugar beet, pulp to fuel, slops to biogas
SBET1b	Sugar beet, pulp to animal feed, slops to biogas
SBET1a	Sugar beet, pulp to animal feed, slops not used
COG1	Conventional gasoline

In Brazil, the feedstock for bioethanol production is mainly sugar cane. If the surplus biogas is used to produce electricity, the WTW average energy and GHG saving compared to gasoline is around 80% and 70% respectively. In the USA, corn is the primary feedstock for bioethanol production, and the WTW average energy and GHG saving compared to convention gasoline is around 30% and 20% respectively. The variation of GHG saving is so big that in some cases it is negative. The WTW energy and GHG saving in the EU using maize as feedstock is less than those in the USA using corn as the feedstock.

Sugar beet leads to over 50% energy and GHG saving, especially when co-products such as pulp and slops are used as the energy source. By using wood or straw as part of the fuel, advanced processes lead to even higher savings in energy and GHG.

The WTW analysis of DMF and MF is challenging, since both of them are new biofuel candidates, and the production method is still in the improvement process. Limited data are available. If wasted biomass is used in the DMF and MF production, the production of feedstock involves almost no extra energy input, which is an advantage over bioethanol production. Unlike the feedstock for bioethanol, production of DMF and MF does not need to involve the conversion of forests into agricultural land, which leads to increased GHG emissions. The collection of feedstock requires some energy; therefore it involves GHG emissions. The energy required and GHG emitted during feedstock conversion into DMF and MF is hard to quantitatively assess at this stage, and no literature is available. However, one advantage of DMF and MF is that they consume only one-third of the energy in the purification process (evaporation) compared to bioethanol because they are not soluble in water. The TTW CO_2 emission of bio-ethanol, DMF and MF is related to the engine-out CO_2 emissions, and will be discussed in the Chapter 4.

Worldwide, around 170 billion tons of biomass are produced annually through photosynthesis, among which 75%, or 128 billion tons, are classified as carbohydrates (Röper, 2002). Only 3-4% of those carbohydrates are consumed by humans for food and other purposes. The first generation bioethanol mainly uses corn and sugar cane as feedstock, which accounts only a very small fraction of carbohydrates that can be used as human food. Therefore, compared to the feedstock for the production (mainly corn and sugar cane) of first generation bioethanol, there are widely abundant biomass carbohydrates, which are viewed as feedstock for the Green Chemistry of the future (Lichtenthaler and Peters, 2004). The production of DMF and MF does not compete with food since it uses non-food biomass carbohydrates as feedstock. McCormick et al. estimated that by the year of 2050, there is potentially 80+ billion annual gallons of biofuel capacity in the US, compared to 400 million tons available today (McCormick et al., 2014).

The properties of DMF, MF, ethanol and gasoline (supplied by Shell, UK) are listed in Table 2-4. The chemical structure of MF is very similar to that of DMF, except that MF has one methyl group only on its furan ring whilst DMF has two methyl groups. Both MF and DMF have higher octane ratings than gasoline, making them more knock resistant in SI engines. MF and DMF have around 19% higher energy densities than ethanol, thus they have a better fuel consumption. The oxygen atom in their molecule makes DMF and MF competitive in engine-out emissions. The initial boiling point of MF (63 °C) is much closer to gasoline (25.4 °C) than DMF (92 °C).

The properties of MF are slightly different from those of DMF. Compared to DMF, MF has a higher density (913.2 kg/m^3 at 20 °C) than DMF (889.72 kg/m^3 at 20 °C) and its flash point (-22 °C) is lower than DMF (16 °C), which would also overcome the cold

engine start problems usually associated with bio-ethanol. Finally, its latent heat of vaporization (358.4 kJ/kg) is higher than DMF (330.5 kJ/kg), thus the cooling effect from MF is better than DMF. Consequently, MF has a higher maximum power output in a DISI engine than DMF.

Table 2-4: Fuel Properties

	Gasoline*	DMF	MF	Ethanol
Formula	C_2-C_{14}	C_6H_8O	C_5H_6O	C_2H_6O
Gravimetric Oxygen Content (%)	2	16.67	19.51	34.78
Density @ 20 °C (kg/m^3)	726.7	889.7	913.2	790.9
RON	96.8	101.3	102.5	107
MON	85.3	88.1	86.1	89
Stoichiometric AFR	14.27	10.72	10.04	8.95
LHV (MJ/kg)	42.9	32.89	31.2	26.9
Flash Point (°C)	-40	1	-22	13
Heat of Vaporization (kJ/kg)	373	332	358	840
Stoichiometric Heat of Vaporization (kJ/kg air)	25.8	31	35.5	93.9
Initial Boiling Point (°C)	25.4	92	63	78.4
Reid Vapour Pressure (kPa)	86	3.45	18.5	5.83
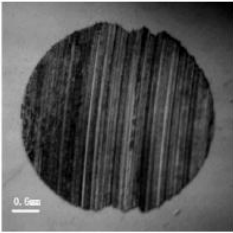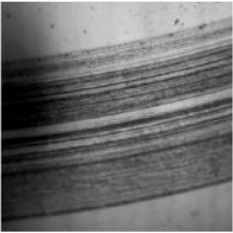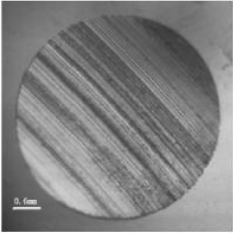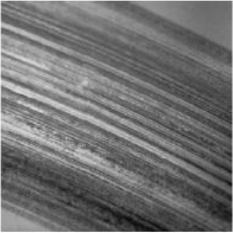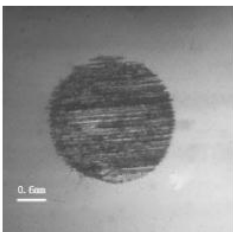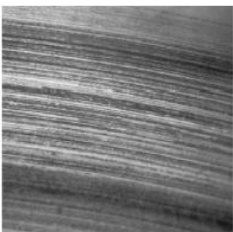
*gasoline, labelled as ULG95, is supplied by Shell, with 5 vol% ethanol

The engine research group at the University of Birmingham was the first to study DMF as an engine fuel (Zhong et al., 2010, Daniel et al., 2011, Tian et al., 2011). The research subjects covered lubricity properties, spray characteristics, optical combustion imaging, laminar flame speed study, thermal engine testing, and numerical modelling.

Hu et al. (Hu et al., 2012) assessed the lubricity properties of DMF using an MQ-800 four-ball tribometer, under the load of 100 N and at 500 rpm. They tested DMF and various DMF blends for 30 min at humidity of 55%. Gasoline was used as the benchmark.

Table 2-5 shows some selected results. It is clear that DMF has a better wear resistance than gasoline, indicated by 49% smaller average wear scar diameter (AWSD) and 91% lower roughness of rotational ball. The SMD is defined as six times droplet volume divided by droplet surface. However, it seems that adding 20% DMF into gasoline had limited impact on the lubricity properties.

Table 2-5: Images of steel ball surface, AWSD and ball roughness after 30 min test under different DMF concentration (Hu et al., 2012)

DMF (Vol%)	Image of stationary ball	Image of rotating ball	AWSD	Roughness of rotational ball, R_a (μm)
0			0.443 ± 0.015	0.086 ± 0.01
20			0.477 ± 0.015	0.081 ± 0.012
100			0.297 ± 0.015	0.045 ± 0.013

Spray characteristics, including spray angle, penetration length, and droplet diameter are essential for fuel/air mixture preparation in GDI engines. High-speed imaging and PDPA tests were carried out at room temperature and pressure (Tian et al., 2010a). Even though the temperature and pressure in the GDI engine during the injection event is much higher than the test condition in (Tian et al., 2010a), the data is still valuable as a reference. It was found that the spray structure of DMF, including spray angle, and penetration length, shows a limited difference to that of ethanol and gasoline, however a significant

difference is observed with their droplet size. Figure 2-3 shows the Sauter Mean Diameter (SMD) for DMF, ethanol, and gasoline at 50-150 bar injection pressure, with the measurement position at 32 mm from the nozzle. The SMD is defined as six times droplet volume divided by droplet surface. DMF has similar droplet size to gasoline and their difference in SMD is within 1 μm. Ethanol has a larger SMD compared to gasoline and DMF when the injection pressure is higher than 100 bar. The maximum difference in SMD between DMF and ethanol is 3 μm at 150 bar injection pressure.
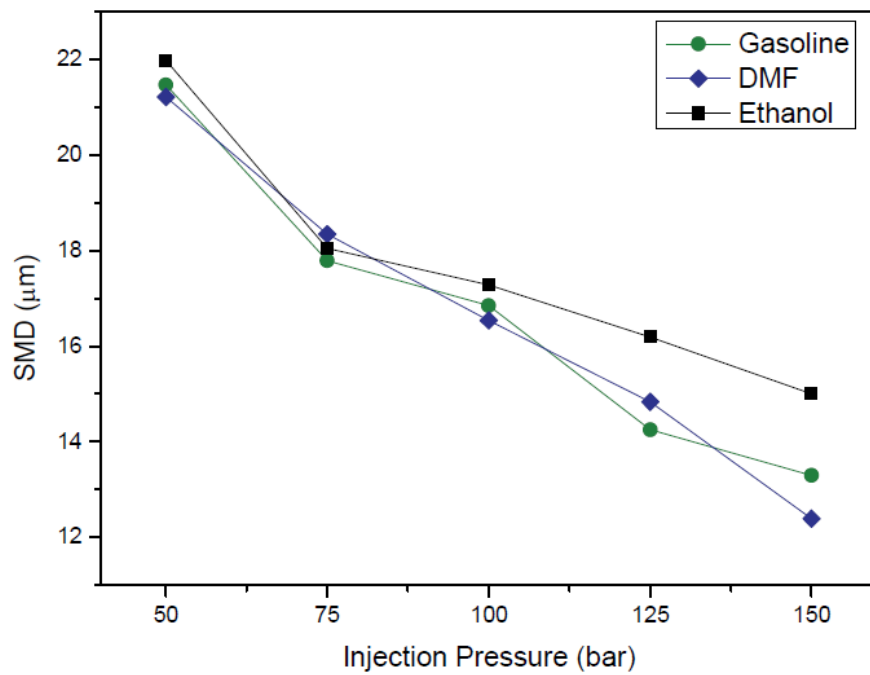
Figure 2-3: SMD for DMF, ethanol and gasoline at 50-150 bar injection pressure, with the measurement position at 32 mm from the nozzle (Tian et al., 2010a)
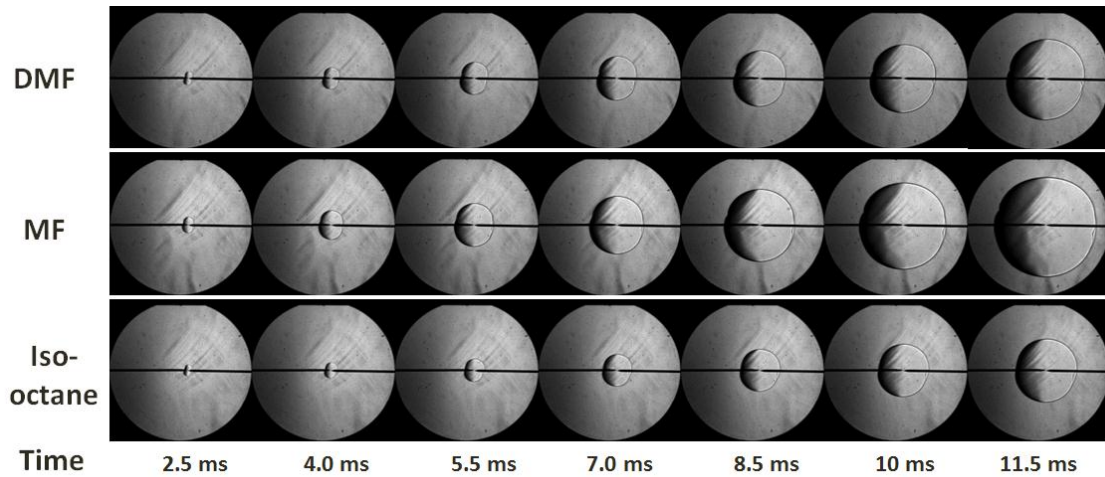
Figure 2-4:   Chronological Schlieren images of stoichiometric fuel/air mixture of DMF, MF, and iso-octane at an initial temperature of 90 ℃ and 0.1 Mpa initial pressure (Ma et al., 2013)

Laminar flame characteristics are fundamental fuel properties, and are important information for the combustion modelling. Schlieren imaging is a commonly used technique for the study of laminar frame characteristics. Many studies have been conducted regarding the laminar flame speeds of DMF, MF, and iso-octane (Ma et al., 2014, Ma et al., 2013, Tian et al., 2010b, Li et al., 2012, Wu et al., 2009b). Iso-octane is used to represent gasoline due to their similar properties. Figure 2-4 shows the Chronological Schlieren images of the stoichiometric fuel/air mixture of DMF, MF, and iso-octane at an initial temperature of 90 ℃ and 0.1 MPa initial pressure (Ma et al., 2013). It is clear that MF has the fastest laminar flame speed and iso-octane has the slowest. Tests were also conducted under various initial temperatures and air/fuel ratios, as shown in Figure 2-5. Again, the ranking of laminar burning velocity for those three fuels is: MF>DMF>iso-octane.
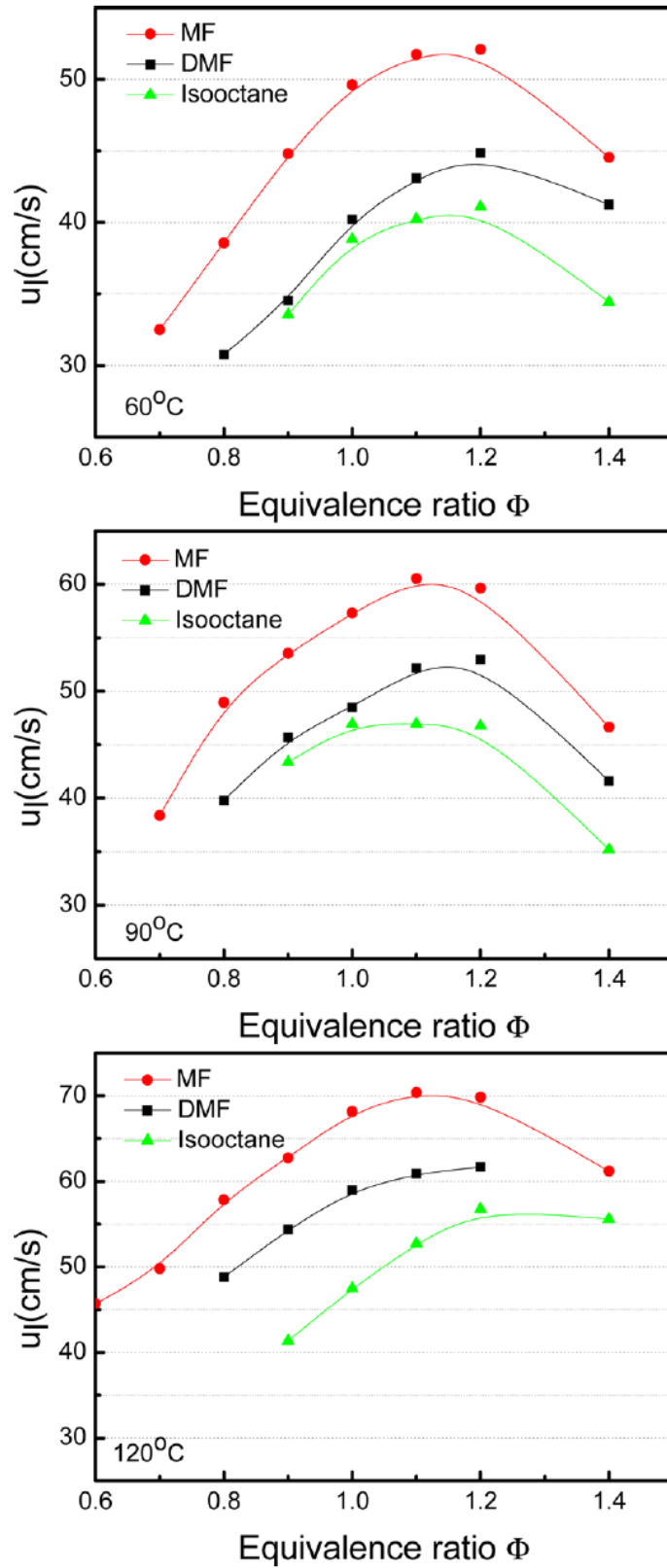
Figure 2-5: Upstretched flame speed of the test fuels at different temperatures and equivalence ratios (Ma et al., 2013)

Ma et al. (Ma et al., 2012) studied the combustion of DMF in a single cylinder optical GDI engine, using the high-speed imaging technique. Figure 2-6 shows flame images of DMF, gasoline, and ethanol at various crank angles at the engine speed of 1500 rpm and engine loads of 3 and 4 bar IMEP. The same spark timing, 1 degree delayed from MBT/KLCA timing of gasoline, was used for all the fuels, for the purpose of avoiding engine knock. DMF, in both engine loads, has a much brighter flame due to high combustion temperature and has bigger flame areas than gasoline at every crank angle.
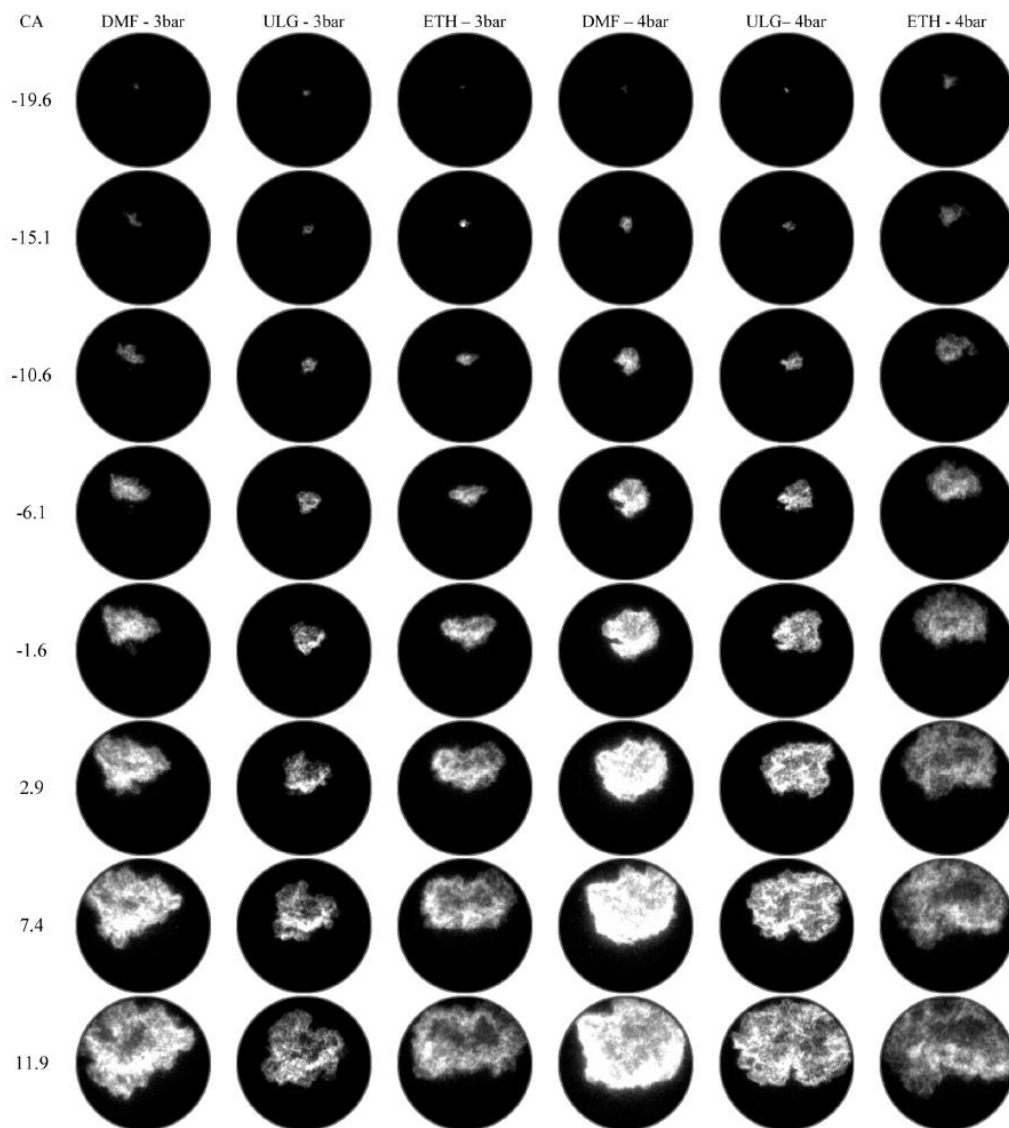
Figure 2-6:   Flame images of DMF, gasoline and ethanol in an optical engine at the engine speed of 1500 rpm and engine load of 3 and 4 bar IMEP (Ma et al., 2012)

Engine tests were also carried out to compare the engine performance and emissions when using DMF, ethanol, and gasoline fuel in a GDI engine with a compression ratio of 11.5 (Daniel et al., 2011, Zhong et al., 2010). MBT/KLSA was used for fuels at 3.5-8.5 bar IMEP. It was found that at 1500 rpm engine speed, DMF allowed a more advance spark timing to be used than gasoline; however knock was observed at high engine loads. Ethanol did not knock, even at high engine loads. DMF combustion was faster than ethanol and gasoline. The full throttle power output ranking when using DI was: ethanol > DMF > gasoline. The volumetric fuel consumption of DMF was much closer to gasoline than ethanol, due to its higher energy density. DMF produced less HC emissions than gasoline, however not as low as ethanol. Due to DMF's significantly high combustion temperature, its NO_x emissions were the higher than gasoline and ethanol. The difference in vehicle-out HC, NOx and CO emissions between engines fuelled with ethanol and gasoline will be diminished due to the use of highly efficient TWCs.

Various combustion strategies were tested when using DMF as an engine fuel, such as split and dual injection. Split injection strategy, with one injection in the induction stroke and another in compression stroke, was used at full throttle, for the purpose of supressing engine knock and thus increasing engine power output (Daniel et al., 2012b). The cooling effect of first fuel DI injection is used to increase volumetric efficiency and the second fuel DI injection generates a stratified air/fuel mixture charge. It is found that the increase in power output over single injection is less consistent with and more sensitive to the second injection timing when using bio-fuels, compared to gasoline. A 2.3% increase of IMEP was observed when using DMF and ethanol using a split injection strategy. The dual-injection concept, with gasoline being injected in using PFI and bio-fuel being injected in using DI, was proposed, for the purpose of taking advantage of both PFI

and DI injection (Daniel et al., 2012d, Wu et al., 2011). Dual-injection allows the flexibility of in-cylinder blending of one or two fuels at any blending ratio, which offers the flexibility and potential to optimize the combustion process at any engine operating condition. Dual-injection was also used for PM emission reduction (Daniel et al., 2013). It is well proven that PM emissions are lower when using the PFI injection system; therefore, compared with DI injection alone, dual injection is reduces PM emissions.

An in-house KIVA 3V spray model was developed and validated using the data from experiments (Li et al., 2013). It is found that more significant spray-wall interaction exists with DMF compared to gasoline, resulting from DMF's slower evaporation rate and larger amount of injected fuel due to its lower energy density. Therefore, a richer mixture is found in the case of DMF compared to the case of gasoline.

The first engine report about MF concluded that MF is more competitive in cold engine starts than the widely used biofuel, ethanol, because of its better vaporization and higher combustion stabilities (Thewes et al., 2011). The knock suppression ability of MF is better than gasoline, which makes it more suitable in suppressing engine knock in the application of higher compression ratio downsized SI engines. HC emissions from MF are less than half of those from gasoline. However, because of high combustion flame temperatures of MF, its high NO_x emission is a concern.

2.4 Emissions in SI Engines

Table 2-6 shows the European emission standards for light duty commercial petrol vehicles (<1305 kg).

Table 2-6:   EU Emission Limits For Light duty SI Vehicles (Delphi, 2012)

Tier	Unit	CO	THC	NO$_x$	PM	PN
Euro 1		2720	-	-	-	-
Euro 2		2200	-	-	-	-
Euro 3	mg/km	2300	200	150	-	-
Euro 4		1000	100	80	-	-
Euro 5		1000	100	60	5 (4.5*)	-
Euro 6		1000	100	60	4.5	6×10^{11}/km**

*Euro 5b
**PN is proposed however the limit has not been confirmed

2.4.1   Regulated Emissions

GDI engines significantly improve the fuel metering by delivering fuel directly into each cylinder with a high fuel injection pressure commonly ranging from 50 to150 bar, leading to low HC emissions in cold start and transient conditions (Zhao et al., 1999).

However, there are still some issues related to the HC emissions in GDI engines: (1) inhomogeneous fuel/air mixture in the cylinder, (2) Incomplete fuel vaporization due to limited time window for fuel spray evaporation, (3) Fuel impingement on the cylinder liner and piston crown (Zhao et al., 1999, Stevens and Steeper, 2001), (4) Fuel trapped in the piston ring crevice, (5) fuel absorbed and disrupt by piston deposits, and (6) Flame quench near the piston and cylinder wall.

Drake et al. studied the correlation between piston fuel film and the engine-out HC emissions from a wall-guided GDI engine using a high-speed refractive-index-matching imaging technique for quantitative time and space resolved fuel-film mass measurements (Drake et al., 2003). They found that for off-optimum injection timings, the wall firm can account for up to 35% of Unburned Hydrocarbons (UBHC). The fuel trapped in the fuel film, formed by droplets impinging on the piston surface has been shown to be an

important source of UBHC. The piston temperature is lower than the surrounding air temperature so the evaporation rate is lower for fuel trapped in the wall film. The film creates an under-mixed area outside the ignition limits, where the combustion rate is limited and the unburned fuel leaves the engine as UBHC emissions.

NO_x formations are highly sensitive to combustion temperature (Heywood, 1989). NO_x emissions are related to fuel H/C ratio (Harrington and Shishu, 1973, Daniel et al., 2011). Fuel with higher H/C ratio tends to have a higher adiabatic flame temperature, thus it produces a higher NOx emission. There are several strategies for in-cylinder NO_x reductions, such as EGR, retarded spark timing, water injection, and the use of fuels with high heat of vaporization such as ethanol and methanol. TWCs and NO_x trappers are also used for engine-out NO_x reductions.

CO is a colourless and odourless chemical, with a lower density than air. It is indirectly toxic to humans at high concentrations. An immediately dangerous to life concentration is proposed as 1200 ppm (NIOSH, 1994). CO can disable haemoglobin in blood which delivers oxygen to all parts of the body. When insufficient oxygen is delivered to the body, especially the brain, the consequence can be fatal. CO emissions are formed when there are insufficient oxidizers, or when temperature is too low, or when time is not sufficient for a complete combustion (NIOSH, 1994). Even though GDI engines are operated in global stoichiometric conditions, there are still local rich regions. CO emissions increase significantly with an increase in the fuel/air ratio. The solution to reduce CO emissions is to improve the homogeneity of air/fuel mixture inside the cylinder, and regular vehicle maintenance.

2.4.2   PM Emissions

As listed in Table 2-6, Euro 5+ enforced a limit on PM mass emissions (<4.5 mg/km) for light duty commercial petrol vehicles. The PN limit is proposed in the coming Euro 6 regulations.

(1) <u>What are the PM emissions?</u>

PM size distributions (Figure 2-7) are composed of particles of different nature: (a) HC nuclei which mainly compose the nucleation mode and (b) soot agglomerates with HCs condensed or adsorbed on their surface, which mainly compose the accumulation mode (Kittelson, 1998).
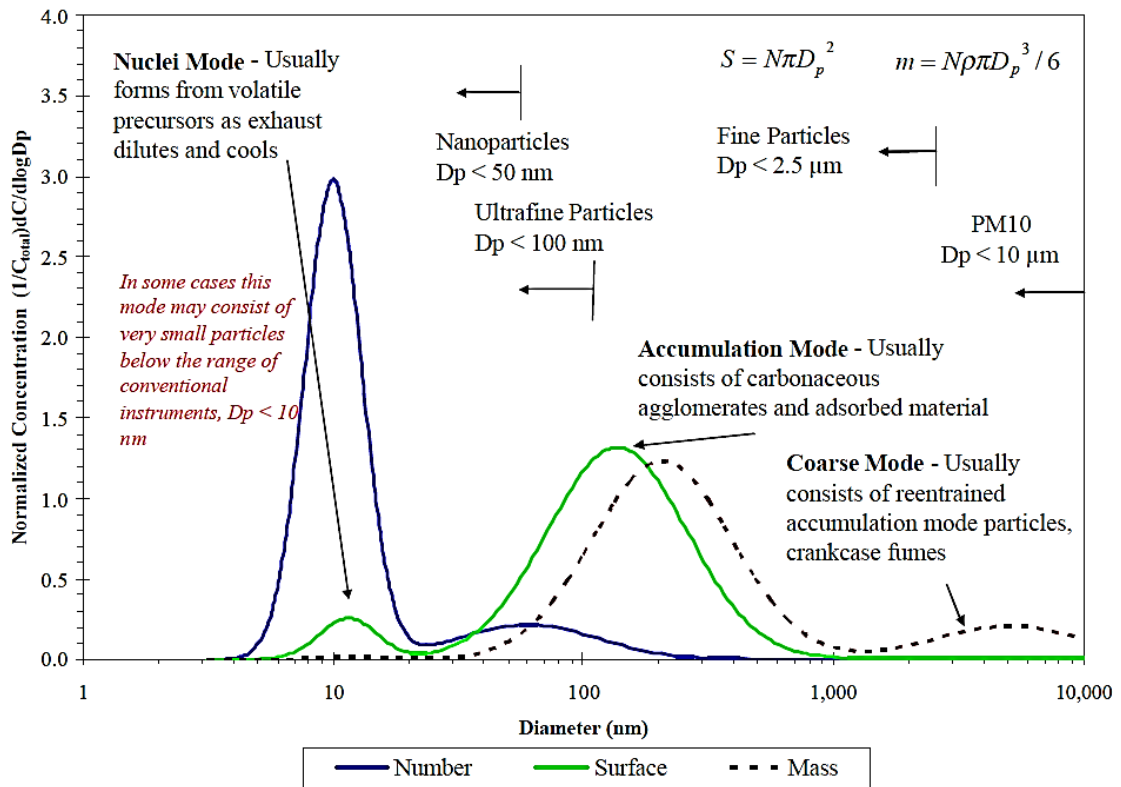
Figure 2-7:   Ideal Engine Exhaust Size Distribution (Kittelson, 1998)

(2)   Dangers of PM emissions

Nano-particulates are difficult to be trapped by filters and their residence time in the atmosphere is very long. Ultrafine particulates (UFPs) with diameters less than 100 nm have significantly high surface to volume ratios, making them highly active. Some particles containing benzpyrene have carcinogenic properties and potentially cause DNA damage and mutation, resulting in risks of lung and lymphatic term bladder cancers (Charlton et al., 2011, Agency, 2009, Mansurov, 2005). Apart from the damage to human health, particles can affect the climate by scattering and absorbing solar and infrared radiation in the atmosphere. PM is responsible for global warming according to some research evidence (Ramanathan and Carmichael, 2008). There is also research evidence showing that TWCs plugged by ash or soot have reduced conversion efficiency and require a high light-off temperature (Kittelson et al., 2013).

(3)   Soot formation mechanism

Soot is formed under rich fuel/air ratio conditions ($\lambda<0.5$) (Dec, 2009). Hydrocarbon fuels break down to short chain unsaturated hydrocarbon such as acetylene and then form polycyclic aromatic hydrocarbons (PHAs); the so called soot particle precursors. Precursors grow and develop into soot by aggregation agglomeration and coagulation processes (Mansurov, 2005).

(4)   PM emissions in various engine types (PFI, GDI, diesel)

Mathis et al. concluded that GDI engines produce more PM emissions than their equivalent PFI engines, with PM mass exceeding those of diesel engines equipped with diesel particulate filters (DPFs) (Mathis et al., 2005). Conventional diesel engines have higher engine-out PM emissions (11-40 mg/km) than those of GDI engines (2-13 mg/km)

(Parkin, 2008). A DPF is capable of reducing the PM emissions from conventional diesel engines below the latest PM limit (5 mg/km). Theoretically, increasing the DPF load can reduce PM emissions; however DPFs lead to increased back pressure, thus increase fuel consumption. Therefore, there is a fuel economy penalty and a PM emission benefit when DPFs are used. Particle number (PN) emissions also vary significantly depending on the engine type (conventional diesel (5×10^{13} #/km) > GDI (5×10^{12} #/km), DPFs are able to reduce the PN emissions from conventional diesel engines below the latest PN limit (6×10^{11}/km). The data presented by the Association for Emissions Control by Catalyst (AECC) showed similar results, with GDI PM mass emissions in the range of 0.8 to 22.11 mg/km, and PN in the range of 6×10^{11} #/km to 1.5×10^{13} #/km, depending on the engine configurations and operating conditions (ACSS, 2013).

PM emissions from various GDI engines are notably different (Andersson et al., 1999, Price et al., 2007a). PM emissions from a wall-guided GDI engine were close to those from diesel engines, and elemental soot dominated the PM composition (72%) (Andersson et al., 1999). This is because the significant fuel impingement on the piston and cylinder liner. The fuel impingement leads to a favourable rich region for soot formation. PM emissions from a spray-guided GDI engine was largely composed of volatile components whilst the elemental soot formed 2-29% of PM mass, depending on the engine operating conditions (Price et al., 2007a). Compared to the wall-guided GDI engines, spray-guided GDI engines lead to less fuel impingement.

(5) <u>Effect of fuel and fuel composition on PM emissions in gasoline engines</u>

PM emissions vary widely depending on fuel properties such as aromatic content, vapour pressure, boiling range, and oxygen content are the mostly studied (Aikawa et al., 2010, Chen et al., 2012, Di Iorio et al., 2011, Liang et al., 2013, Leach, 2012). Fuel boiling

range is directly associated to fuel evaporation and thus PM emissions (Khalek et al., 2010). Liquid fuel like iso-octane generates higher PM emissions than gas fuel like propane (Xu, 2012). A 'PM Index', taking into account vapour pressure and fuel structure (double bond and aromatic ring), is used to predict PM emissions in gasoline vehicles, was concluded (Aikawa et al., 2010). They calculated the PM Index distribution of 1445 worldwide commercially available gasoline fuels and found that the PM Indices of gasoline fuels sold globally fall in a very wide band, ranging from 0.67 to 3.86. Leach et al. has studied the influence of fuel properties on PN emissions from a DISI engine by designing fuels with different volatility and aromatic content, and has validated a 'PN index' for evaluating the PM emissions from commercial gasoline fuel (Leach et al., 2013). It is well reported that compared to gasoline, pure ethanol produces much less PM emissions in GDI engines (Daniel et al., 2011, Di Iorio et al., 2011, Catapano et al., 2013). The effect of ethanol blend on PM emissions in GDI engine is not well understood. Mohammad et al. reported significant reduction of soot formation by using alcohol blends (Fatouraie et al., 2013), which is supported by other publications (Zhang et al., 2010, Storey et al., 2012, Storey et al., 2010). However Chen et al.'s data showed that increases in both PM mass and number based emissions were observed with ethanol addition, particularly in a cold engine (Chen et al., 2012). Other publication also concluded that low percentage ethanol-gasoline blends had higher or similar PM emissions compared with pure gasoline (Khalek et al., 2010, He et al., 2010, Di Iorio et al., 2011, Catapano et al., 2013).

(6) Research equipment and study methodologies

There are several facilities which are used for PM characterization. The DMS500 from Cambustion and SMPS/EEPS from TSI are widely used for PM size distribution

measurements (Khalek et al., 2010, Rubino et al., 2005, Price et al., 2006). Transmission electron microscopy (TEM) is used for structural characteristics of nano-particles. For the soot reactivity and the oxidation behaviour study, some techniques such as, TGA, differential scanning calorimetry (DSC), and X-ray diffraction (XRD) are widely used. There are other techniques for the study of PM composition, like energy dispersive X-ray (EDX) (D'ambrosio and Ferrari, 2012), infrared spectroscopy (IR) (VonBacho et al., 2005, Aradi et al., 1999, Schwahn et al., 2010), X-Ray fluorescence analysis (XRF) (Schwahn et al., 2010), and GC-MS.

TGA is an essential instrument for PM characterization in which the mass of a test sample is constantly monitored as it is heated by a furnace. The sample atmosphere can be an inert or reactive gas and its flow rate can be controlled to achieve the specific research objectives. Overall the operation of the TGA is relatively simple and its performance is reliable. The soot oxidization reaction rate can be affected by the TGA program settings. The oxidation reaction inside the TGA furnace is partially diffusion-controlled (Lapuerta et al., 2010, Gilot et al., 1993). There are some key factors (instrument and sample) affecting the TGA measurement reliability and repeatability: balance, furnace, temperature calibration, sample mass as mentioned earlier, sample atmosphere gas flow rate, and heating ramps are all such factors. The balance, furnace, and temperature calibration are independent of PM factors and can be calibrated according to standard operation procedures. However sample masses and heating ramps are both PM dependent necessitating further studies.

Much research has been conducted on diesel PM using TGA (Bhardwaj et al., 2013, Song et al., 2006, Lapuerta et al., 2012, Al-Qurashi and Boehman, 2008). A robust TGA method for the diesel soot has been developed by the University of Castilla-La Mancha

(Rodríguez-Fernández et al., 2011) however the application of TGA on PM generated from DISI engines is limited (Price et al., 2007a). PM emissions from spark ignition engines are far lower than those of diesel engines, making it substantially more difficult to collect. Moreover, PM oxidization characteristics are highly fuel-dependent (Rodríguez-Fernández et al., 2011).

Unlike diesel engines, PM size distribution measurement in the GDI engines can be extremely challenging. The measurement system developed by the Particle Measurement Programme (PMP) is not suitable for the measurement PM from GDI engines, because a high percentage of volatile components in the exhaust make the measurement unrepeatable. On the other hand, the separation of PM size distributions into the nucleation and accumulation modes is difficult. A thermo-denuder, or volatile particle remover, is needed to reduce the negative impacts of volatility on PM measurements.

(7) Reduction of PM solutions in DISI engines

PM emissions in GDI engines are complicated, especially when various fuel and fuel blends are used. The stringent PM regulations may not be satisfied by pushing the boundary of engine optimization, and/or by using green fuels alone. There is a potential that, in the future, GPFs will be required for GDI engines, just like DPFs on diesel engines. There are many studies focusing on GPFs (Richter et al., 2012, Chan et al., 2013, Ito et al., 2013, Chan et al., 2012, Kim et al., 2013, Mason et al., 2013). To ensure the durability and reliability of the GPF and thermal management in its regeneration, profound understanding about the oxidation characteristics of the PM is needed.

There are also some other solutions available for PM reduction, such as the use of ethanol and natural gas. Dual injection (DI+PFI) is also a good solution which has been proved by the University of Birmingham (Daniel et al., 2013).

2.5   GDI Injector Deposits

The effect of injector fouling on PM emissions in a GDI engine is investigated in this thesis; therefore, injector fouling is reviewed in this chapter.

Fuel injector deposits have been observed since the introduction of PFI system, and these issues may be worsened in GDI engines due to injectors' harsher operating conditions compared to those of PFI system (Zhao et al., 1999, Arters et al., 1999, Arters and Macduff, 2000, Bardasz et al., 1999, Brogan et al., 2000, Aradi et al., 2003, Aradi et al., 2000b).

The effects of injector deposits on engine performance and emissions have been widely reported (DuMont et al., 2009, Lindgren et al., 2003, Whitehead et al., 1998, Carlisle et al., 2001, Zhao et al., 1999, Arters et al., 1999, Sandquist et al., 2001). For example, Arters et al. reported that the correlation between injector fouling and vehicle performance (drivability, fuel consumption, HC, CO and PM emissions) is over 90% in GDI vehicles (Arters and Macduff, 2000). Similarly, deposit formation on fuel injectors can cause increased HC, CO and smoke emissions in GDI engines (Ohyama, 1998, Noma et al., 1998, Nogi et al., 1998, Joedicke et al., 2012, Sandquist et al., 2001). Research evidence showed that as the spray angle decreases, there is increased tendency of smoke formation (Nogi et al., 1998). Fouled injectors with 22% fuel flow rate losses led to 30% and 190% increased HC and CO emissions respectively (Joedicke et al., 2012). Similar

results were observed in the tests conducted in a four-cylinder GDI engine (Sandquist et al., 2001). It was found that HC emissions were increased by 80% after 60 hours of test and fell back to the initial levels when fouled injectors were replaced with new injectors. Lindgren et al. found that increased mass of fuel captured in the wall film resulting from higher spray jet velocity and larger droplet diameter was the primary reason for the increased HC emissions in the fouled injectors (Lindgren et al., 2003).

There are extensive studies on GDI injector deposit reduction methods, mainly including using of fuel detergents, improved injection system (injector and injection pressure) and engine design. The use of ethanol is also proven to be useful in suppressing injection fouling.

Detergent

Many studies have been carried out on PFI injector deposit control additives (Tupa and Koehler, 1986, Tupa, 1987, Richardson et al., 1989, Herbstman and Virk, 1991, Reading et al., 1992) with investigations of additives used in GDI being reported in recent years (Aradi et al., 2000a, Ashida et al., 2001, China and Rivere, 2003, Aradi et al., 2003, DuMont et al., 2009). A study of two types of detergents (Manniches and polyether amines (PEAs)) in a research GDI engine controlled to maintain five fixed injector nozzle temperatures ranging from 120 ℃ to 184 ℃ was reported in (Aradi et al., 2000a). The results show that Mannich detergents were more effective in injector deposit control especially at 173 ℃ injector tip temperature than PEAs. In another study of three GDI injector deposit detergents (Manniches, PEAs and polyisobutylene amines) (China and Rivere, 2003), it was found that some chemistries were more effective that the other at same treat rates, however the authors did not disclose the which chemistry performs best. Polyisobutylene amines performed the best amongst the three tested additives. In the study

of (DuMont et al., 2009), four additives were tested and it was found that three of them effectively removed injector deposits. Nevertheless, in almost all the literature, the performances of different types of additives were difficult to assess because of the lack of detailed information and contradictory results of similar detergent chemistries.

The concentrations of deposit control additives need to be optimized, since there are research evidence from Kalghatgi and Uehara et al. showing that they could accelerate combustion chamber deposit (CCD) formation (Uehara et al., 1997, Kalghatgi, 1995).

GDI Injector Design

Based on the proposed T90 theory as one important factor for deposit formation, studies have been done to reduce the injector temperature by modifying injector design. Saito et al. (Kinoshita et al., 1999) reduced nozzle temperature by changing cooling passages in the cylinder head, placing material with a high heat conductivity rate into the space between the nozzle and the engine head, and installing a heat insulator on the part of the nozzle surface exposed to combustion gases. Matsushita et al. (Matsushita et al., 1998) patented a GDI injector featuring an insulating material on the injector surface to reduce heat transfer from hot combustion gases to injectors. Katashiba et al. (Katashiba et al., 2006) examined a method of reducing the heat transfer by the combination of reducing the injector surface area exposed to the heat source and using a front seal.

Investigations have also been done on using various coatings on the injector key surface. A patent for injectors coated with an anti-deposit fluorine-coating amorphous hydrogenated carbon film is found in (Fleming et al., 2000). Another application for patent for an injection nozzle with coating which either had a higher or lower thermal conductivity than that of nozzle body is reported in (Green et al., 2001). Zhao et al. [1]

discussed the interfacial tension between the fuel deposit and the solid surface. It was also pointed out that the surface coating was found to be able to delay the onset of deposition. Once a deposit layer is formed, the coated and uncoated injectors exhibited very little difference in the deposition formation. Berndorfer et al. (Berndorfer et al., 2013) applied coating on the injector tip which could prevent deposit formation and also help deposit removal. They found that those coatings did not reveal a breakthrough in preventing coking layer formation on the GDI injector. Imoehl et al. (Imoehl et al., 2012) concluded that the use of an inert amorphous silicon coating is statistically insignificant.

Reducing injector SAC volume, better nozzle surface finishing and nozzle shape are also beneficial for supressing injector deposits. Imoehl et al. (Imoehl et al., 2012) pointed out that the surface finish was one of the most significant factors. Laser drilling holes with smooth inner-surface and sharp inlets could reduce injector fouling and the interactions between the jets (Rivera, 2014). Sharp hole entrances also contributed to injector deposit suppression probably due to increased cavitation and turbulence (Rivera, 2014, Imoehl et al., 2012). According to (Imoehl et al., 2012), protruded injector tip reduces the likelihood of the spray impacting the protruded seat by providing a roughly uniform step hole depth around the circumference of the step. The protrusion also reduces the likelihood of the spray contracting the face of the seat or combustion chamber surface by positioning the hole exit further away from these surfaces. The temperature profile of the seat is also affected by the protrusion. Since deposits in the injector nozzle are mainly fuel-derived; therefore any attempt to reduce the residual fuel inside the nozzles contributes to reduce the deposit formation tendency. Reducing the SAC volume, or even use valve covered orifices (VCO) benefit the control of residual fuels (Lindström and Ångström, 2008, Gilles-Birth et al., 2005, Sczomak, 1990, Imoehl et al., 2012). In the VCO layout, the

injector orifices are completely covered by injector needle when valve is closed. No fuel escapes from the injector after the injector event ends and therefore VCO layout can also reduce the diffusive combustion caused by fuel leakage. Besides, the step hole or counter bore in the outlet side can decrease the impact of the deposits formation (Imoehl et al., 2012). Optimized injector configurations found to inhibit deposit formation are listed in Table 2-7.

Table 2-7:   Summary for anti-deposit injector design

Factors	Optimised design
SAC volume[a]	Orifice holes outside the Sac volume (Imoehl et al., 2012);or valve covered orifice (VOC) (Lindström and Ångström, 2008, Gilles-Birth et al., 2005, Sczomak, 1990)
Tip design	Protruded injector tip is better than flat tip (Imoehl et al., 2012)
Combustion seal design	Not statistically significant (Imoehl et al., 2012)[b]
Orifice hole divergence	No taper (Imoehl et al., 2012)
Orifice hole surface finish	Smooth finish, mechanical micro-machining is recommended (Imoehl et al., 2012); Laser drilling is better than EDM (Rivera, 2014)
Hydro erosive grinding of orifice holes	No hydro erosive grinding (Imoehl et al., 2012)
Inlet shape	Sharp inlet (Rivera, 2014)
Outlet shape	Step holes or counter bore (Imoehl et al., 2012)
Injector type	outward opening injector> inward opening swirl injector> multi-hole injector (Preussner et al., 1998)

[a] Defined as the volume between the valve seat and the entrance to the metering orifice of the injector
[b] Contradicts with (Katashiba et al., 2006)

The injector formation and its impact on the injector performance are different for various types of GDI injectors which mainly include swirl-type, multi hole and outward opening injectors. Swirl injectors generate thin liquid sheets by opening the needle inwards (inward opening), with which the spray flexibility is less than with multi-hole injectors (Preussner et al., 1998). For a given deposit layer inside the swirl chamber, circumferential

and axial flow resistances inside the nozzle, which have opposite effects on the flow rate, are both increased where the overall result is a relatively increase in the robustness of swirl injectors against fouling (Preussner et al., 1998). Multi-hole injectors, which also open inwards, allow the best flexibility of the spray pattern by changing the position and orientation of the holes, making asymmetrical spray patterns possible. However, multi-hole injectors are highly vulnerable to deposits inside the nozzle because injector flow is highly sensitive to the change in the dimensions of the internal geometry (Aradi et al., 2000a, Arters et al., 1999). Unlike swirl and multi-hole injectors, outward opening injectors open the needle outwards and generate a hollow cone spray resembling to those of swirl injectors. Outward opening injectors have less cycle-to-cycle spray angle variation compared to swirl injectors, and do not have the poorly atomized pre-spray structure which exists in most swirl injectors (Xu and Markle, 1998, Arcoumanis et al., 2008). Outward opening injectors have the potential to address typical problems related to spray-guided configurations (close-spacing concept) due to better air utilization than multi-hole sprays, good penetration during early injection and spray angle almost independent of backpressure (March et al., 2010). The conical shape and zero SAC volume of the nozzle passage of outward opening injectors prevents carbon formation, and the robustness against fouling of the inward opening injectors can be improved by the appropriate design of needle tip and seat (Mathieu et al., 2010). The deposit built up may only influence spray pattern, not the flow rate (March et al., 2010). The new generation of outward opening piezo-driven injectors have better performances than, or comparable to those of the solenoid injectors (Skiba and Melbert, 2012, Smith et al., 2011, Mathieu et al., 2010). Preussner et al. (Preussner et al., 1998) compared those three types of injectors. They concluded that the multi-hole injectors have the least robustness against fouling, whilst outward opening injectors have the best robustness against fouling. Thus outward opening

piezo-driven injector design is a promising technology for future GDI injector deposit reduction.

Engine Design

The injector tip temperature is affected by the protrusion of its tip into the cylinder, the conductive path from the injector mounting boss to the coolant passage and the in-cylinder charge velocity near the tip location. The position of the injector relative to the spark plug is a critical feature; the longer the distance, the lower the injector nozzle temperature tends to be. Bacho et al. (Bacho et al., 2009) studied the GDI injector mounting location and observed that centre mounted injector tended to experience more deposit formation compared to side mounted injector (7.2% versus 2% in flow rate loss). Katashiba et al. (Katashiba et al., 2006) also pointed out that the primary issue for the centre injection structure was to reduce the spray structure changes resulting from the deposits built up near the injector nozzle holes. The spray-guided GDI engines, injectors could experience more deposit problem compared to the wall-guided GDI engines (Aradi et al., 1999). However, currently there is not enough data to support this viewpoint and therefore more investigation is required.

Increasing fuel injection pressure is also an effective way of limiting deposit formation. Bacho et al. (Bacho et al., 2009) studied the effect of injection pressure (5 MPa and 10 MPa) on injector flow rate loss. The results showed that a higher injector pressure (10 MPa) helped to reduce the injector deposit formation and the fuel flow rate losses was lower (3.8% vs 7.4%) than the case of a lower injector pressure (5 MPa). A higher injection pressure suppressed the injector deposition formation by increasing the deposit removal rate, which is supported by the mathematical model in (Aradi et al., 2000a). High

injection pressure also contributes to reduce PM emissions in GDI engines (He et al., 2012, Matousek et al., 2013). However, with all things being kept constant, the extra work required by fuel pump to offset some benefits derived from reduced injector deposit formation.

Ethanol

Many researchers reported the effect of blended ethanol on GDI injector deposit formation. Ashida et al. (Ashida et al., 2001) added 10% ethanol into the base fuel alkylate. They observed that injector deposit formation was reduced (4% versus 1.5% flow rate loss) after 8 hours' test. Dumont et al. reported that by adding 10% (volume) ethanol into gasoline (E10), the injector flow rate loss was reduced from 18.9% to 5.5% (DuMont et al., 2009).

Taniguhi et al. (Taniguchi et al., 2007) reported that an ethanol blend in the form of E20 (20% vol. ethanol in gasoline) is able to suppress injector deposit formation. In their study various ethanol blend fuels were examined in a V6 GDI engine. The test condition consisted of an injection pressure of 40 bar (reduced from nominal 120 bar) with an increased injector tip protrusion to increase the injector tip temperature. The test duration was 10 hours for each blend. They found that injectors had less flow rate loss and less deposit formation when using E20 compared with gasoline. They believed that the reduction of injector deposit formation was caused by the synergistic effects of both the injector nozzle temperature reduction and fuel composition in blended fuels.

2.6 Summary

The author's PhD is mainly about the study of performance and emissions in a modern GDI engine fuelled with biofuels, such as MF, DMF and ethanol. The author believe that biofuels can play an important part of role in securing renewable energy supply, and reducing greenhouse gas emission and other emission such as NO_x and PM.

Since the experiments were carried out in a modern GDI engine, therefore a general review of GDI technology is presented, along with its comparison with carburettor and PFI technologies. Special attention was paid on the various GDI concept, such as air-guided, wall-guided (wide-space concept) and spray-guided (close-space concept) GDI system. Of course, this review is not able to cover topics about GDI technology due to the page limit, such as engine downsizing which is currently. So the author does acknowledge that there are many other important topics about GDI engines that are not included in this review.

Some key properties of gasoline such as volatility and octane rating properties are briefly introduced, which are also top important properties for SI engine fuels. However the review of gasoline is not priority of this review, therefore it only accounts for a small fraction.

Followed by the review of gasoline, ethanol is introduced. Some key publications about the application of ethanol in SI engine are reviewed, and drawbacks of bio-ethanol as a renewable fuel are discussed, which inspired and motived the author to take on the research of the next generation biofuels. Review of promising biofuel candidates, DMF and MF, are given, including review of their production method, fuel properties. Review of research work done by other researchers on DMF and MF are also given. Those literature covered lubricity properties, spray characteristics using high-speed imaging and Phase

Doppler Particle Analyser, optical combustion imaging, laminar frame speed study, thermal engine testing and numerical modelling.

Since one of the points of using biofuels is for the reduction of emissions, emissions in SI engines are reviewed. The thesis has two chapters focusing on PM emissions, so special attention is put on the review of PM emissions.

In the end, one of the challenges in the development of GDI engines, injector fouling is reviewed, including effect of injector fouling on engine performance and emissions, and solutions for GDI injector fouling. The reason for review injector fouling is because, PM emissions and injector fouling can interact with each, and they have similar nature of carbon of particles and deposits. Injector fouling can increase PM emissions, and particles can be deposited on injector tip and form deposits. This inspired the author to study PM emissions from a GDI engine fuelled with biofuel when using fouled injectors. Actually, the author is not only involved in a biofuel project, also a GDI injector deposit project.

In summary, this literature reveals the main subject of this thesis, which is to study the biofuels' performance and emissions in a modern GDI engine, so as to pave the way for promoting the use of renewable biofuels as a part of solutions for renewable energy supply and emission reduction.

CHAPTER 3

3   EXPERIMENTAL SETUP

This chapter is intended to provide detailed information about the single-cylinder spray-guided DISI research engine along with its control systems. The data (temperature, pressure and emission) acquisition and recording system as well as data processing are briefly introduced, followed by the properties of fuels used in this thesis.

During the PhD research, the author updated the Labview control system, and built an in-house Labview combustion analysis program. The hardware of control system was updated due to circuit board failure. The DI fuel system and air flow rate measuring system was also updated.

3.1   Engine and Instrument

The engine and instrumentation setup (Figure 3-1) consists of a direct current (DC) dynamometer, single cylinder spray guided DISI research engine, control, data acquisition and recording system.
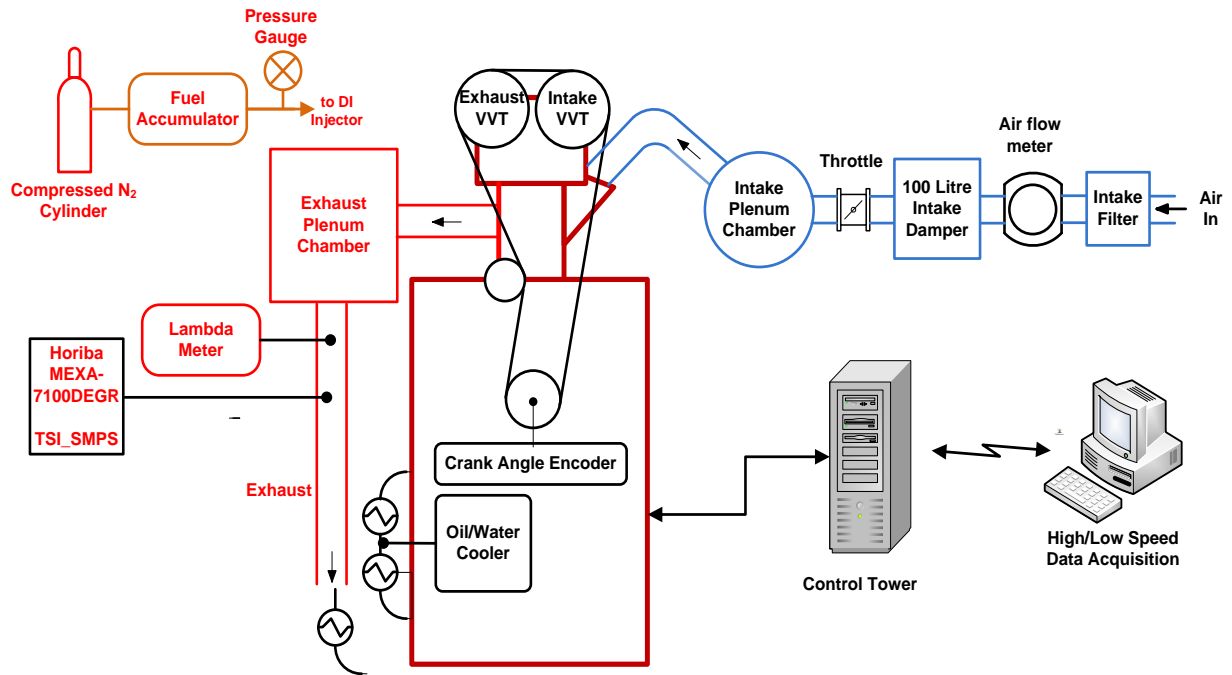
Figure 3-1: Schematic of engine and instrumentation setup

The engine is coupled to a DC dynamometer which is capable of maintaining engine at a fixed speed (resolution: ±1 rpm) regardless of the engine power output. The dynamometer is used as an engine starter when the engine starts and as a load absorber when the engine is fired. A 100 L intake buffer box made of steel is used to reduce intake flow oscillation introduced by the single cylinder engine, which improves the volumetric efficiency and the accuracy of air flow rate measurement. The engine is operated via a LabVIEW program. The controllable parameters including injection timing and pulse width, injection mode (DI or PFI, or dual-injection mode), ignition timing and ignition energy, intake and exhaust valve timing. The throttle is manually controlled via a cable. Gaseous emissions such as THC, CO_2, CO and NO_x were measured using a Horiba MEXA-7100DEGR gas Analyser. PM emissions were characterized by using the TGA and SMPS3936. Exhaust samples are taken 300 mm downstream of the exhaust valve and are pumped via a heated line (464 K) to the analysers. The engine running conditions such as intake manifold pressure, IMEP, COV of IMEP, in-cylinder pressure trace and combustion phase are real-time displayed by a Labview program.

The key parts such as engine, combustion system, control system, and data recording, acquisition and processing are discussed in the following sub-sections.

3.2   Single Cylinder Research Engine

The 4-valve, 4-stroke single-cylinder close-space concept (spray-guided) DISI research engine is presented in Figure 3-2.
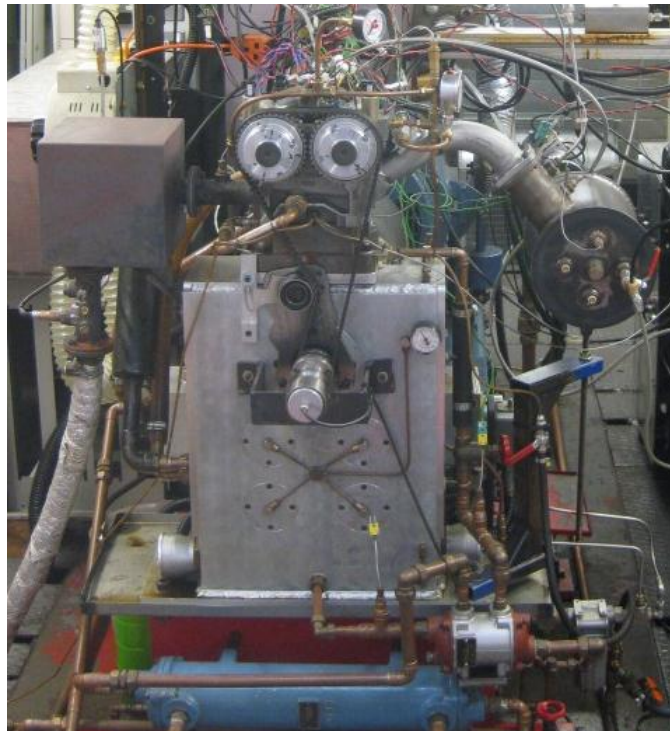
Figure 3-2:   Single cylinder GDI engine

The technical data and engine specification are listed in Table 3-1. The engine has a geometric compression ratio (CR) of 11.5, which can be changed by adjusting the number and the size of metal blocks between the crankcase and cylinder block. However the increase of CR is limited due to the risk of intake valves hitting the piston crown. The engine features a modern spray-guided direct-injection (SGDI) cylinder head as a single cylinder version of Jaguar AJ133 (V8) engines. The engine has compact double overhead camshafts (DOHC) and equipped with variable valve timing (VVT) systems in both intake and exhaust sides enabling

a 50 CAD valve timing adjusting window. The engine is equipped with both DI (150 bar) and

PFI (3 bar) injection systems. By adjusting the hardware settings, users are able to use those

two injection system either independently or simultaneously.

Table 3-1: Engine specification

Engine Type	4-Stroke, 4-Valve
Combustion System	Spray Guided DISI/PFI
Swept Volume	565.6 cc
Bore x Stroke	90 x 88.9 mm
Connecting Rod Length	160 mm
Geometric compression Ratio	11.5:1
Injection system	DI (150 bar) and PFI (3 bar)
Intake Valve Opening	-25~ 25 °aTDC*
Exhaust Valve Closing	0~ 50 °aTDC*

* 0 °aTDC refers to TDC in the combustion stroke

3.3 Combustion System

The engine features a SGDI combustion system (Sandford et al., 2009). A 3D cylinder

head diagram and a picture of piston are presented in Figure 3-3.

Figure 3-3: Combustion system of single cylinder GDI engine (a) 3D cylinder head

diagram, (b) piston

The combustion system features a flat top piston and a centrally-mounted, six-hole direct injector along with a side-mounted spark plug located closely beside the DI injector. The injector spray plume orientation is shown in Figure 3-4.
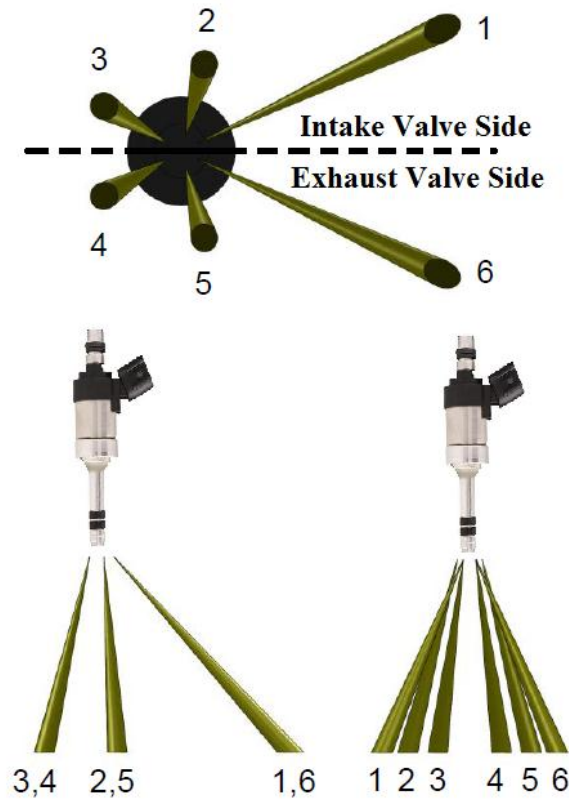
Figure 3-4:   Injector spray plume

The injector has two symmetric groups of holes with three in each side. The spark plug is at an angle of $18\,°$ to the cylinder axis and is located between fuel spray plumes 1 and 6. The injector delivers a desirable hollow-core spray, creating a locally fuel-rich zone near the spark plug with precise timing and quantity.

3.4   Intake and Exhaust System

The intake and exhaust runners are shown in Figure 3-5. 'A' and 'B' noted in the figure represents stable boxes for intake and exhaust system respectively.
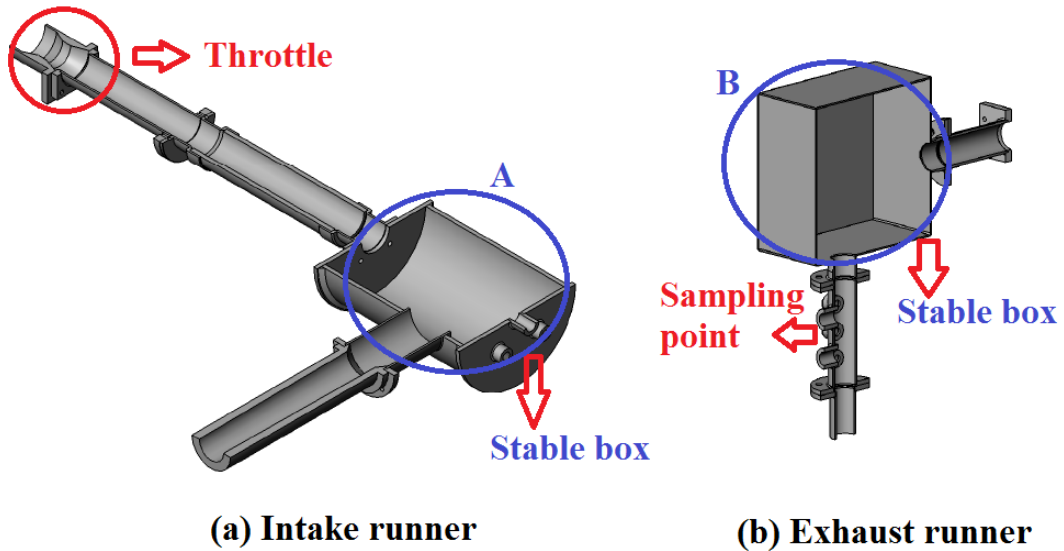
(a) Intake runner **(b) Exhaust runner**
Figure 3-5:   Runner for (a) intake, and (b) exhaust system

The intake and exhaust camshaft and valve geometry is listed in Table 3-2.

Table 3-2:   Camshaft and valve geometry

Intake Valve Lift	10.mm
Intake valve inner seat diameter	36 mm
Exhaust Valve Lift	9.3 mm
Exhaust valve inner seat diameter	33 mm
Intake Valve Duration	250 CAD
Exhaust Valve Duration	250 CAD

The designs of a larger lift and a larger inner seat diameter of intake valve than those of the exhaust valve are to ensure a maximum volumetric efficiency. In 2012 one intake valve failed. The intake valve was a prototype one and Jaguar did not have any in stock. The author modified one intake valve purchased from ebay and successfully solved the problem at a low cost.
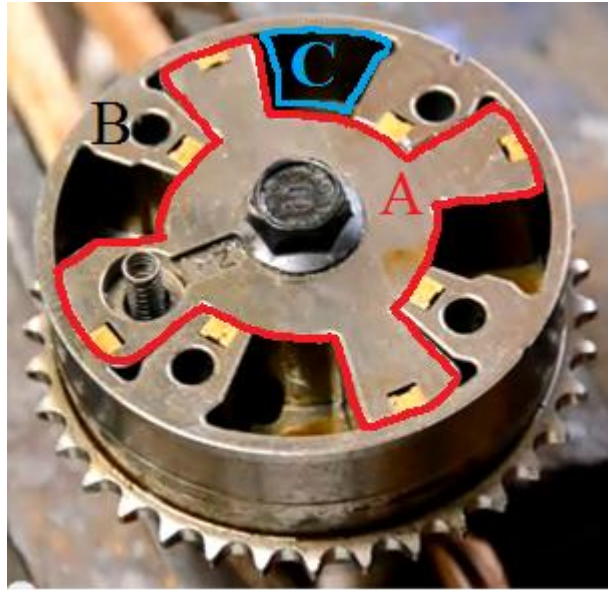
Figure 3-6:   VVT camshaft pulley

Both the exhaust and intake sides of this engine are equipped with VVT systems. The camshaft pulley (Figure 3-6) includes two parts: part 'A' (highlighted in red) and part 'B'. 'B' is driven by crankshaft through a belt, and 'A' is driven by 'B' and is connected to the camshaft. Part 'A' and 'B' can be relatively rotated up to 25 degrees enabling 50 CAD adjusting window for both intake and exhaust valve timing. The relative rotating is depending on the volume of oil (highlighted by C noted in Figure 3-6). A solenoid is used to control pressurized oil (3 bar) in and out of 'C'.

3.5   Fuel System

The engine is equipped with both high pressure DI (150 bar) and low pressure PFI (3 bar) injection system. The high pressure DI system design is shown in Figure 3-7.
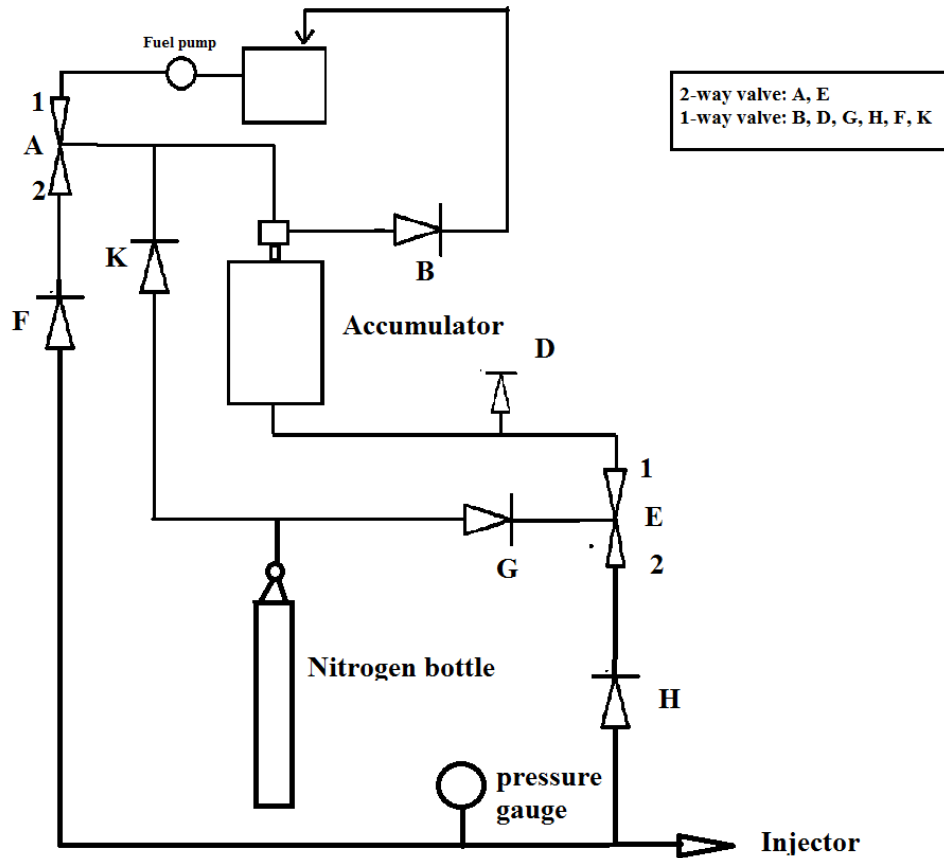
Figure 3-7: Direct injection system

The DI injection system has functions of fuelling, pressurizing, refuelling and purging, featuring a free piston accumulator and a high pressure nitrogen bottle. Pressure is delivered by high pressure nitrogen bottle pressurizing on the accumulator piston. When different fuels are used, the whole system is purged to avoid any contamination, ensuring the reliability and repeatability of the test data. Because the piston seal for the accumulator is specifically designed for gasoline usage, the system is washed by gasoline on a daily basis if fuels other than gasoline are used. Several seal replacements were required during the author's PhD, possibly related to the use of ethanol, DMF or MF.

The PFI system features a 5 bar PFI pump, a low pressure regulator, a fuel cooler and a PFI injector supplied by Siemens. The pressure gauge is used to monitor the fuel pressure throughout the test. Both PFI and DI systems can be operated under the split injection mode.

3.6 Engine Control System

This sub-section provides a brief description of the engine control system (Figure 3-8).
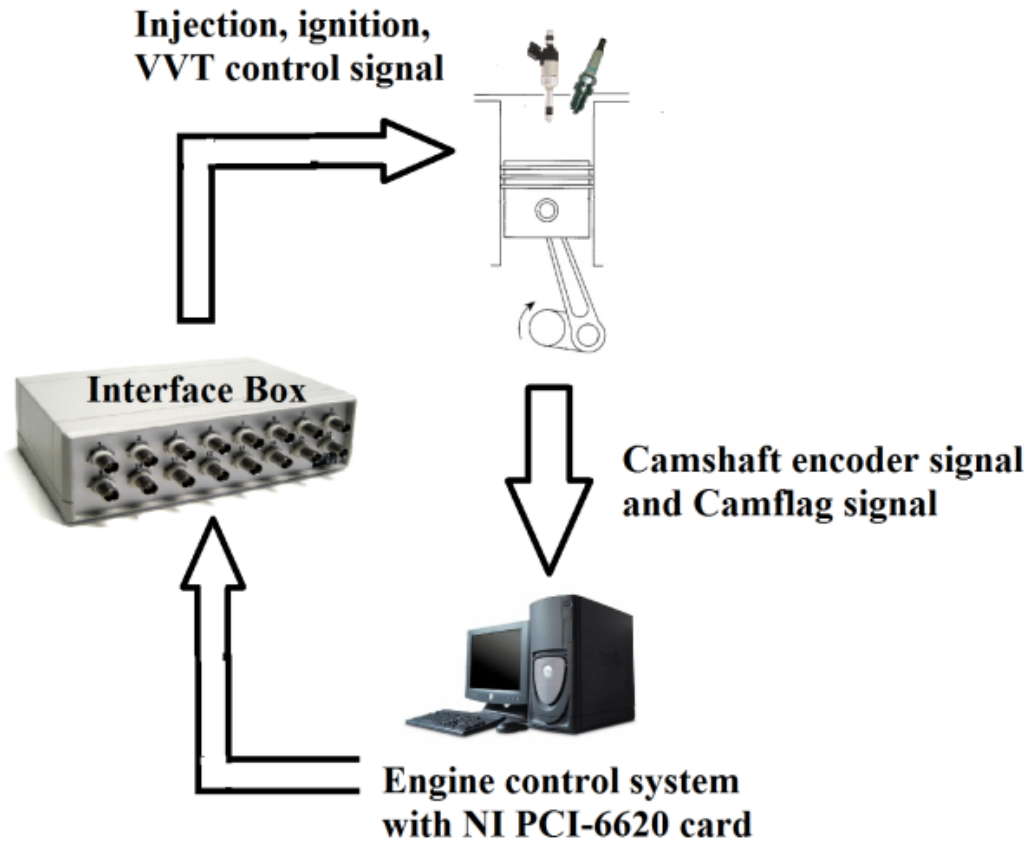
Figure 3-8:   Engine control system

A Labview program was used to control the engine via a National Instruments card (model 6202). This program receives the camshaft encoder and camflag signals as inputs and outputs injection, ignition and VVT control signals.
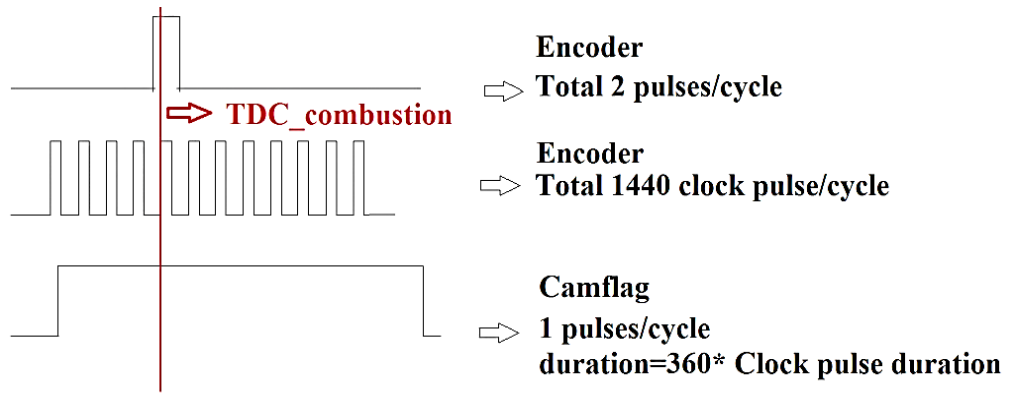
Figure 3-9:   TDC identification in engine control program

All the control signals are based on the 1440 TTL pulses per cycle clock signals (2 pulse/CAD) generated by the crankshaft encoder. The encoder is also capable of outputting two TTL pulses per cycle at a fixed encoder shaft position. By using those two type of signals, TDC position can be identified (Figure 3-9). The further identification of TDC_{Comb} and TDC_{Intake} is made by using a camflag signal from the intake camshaft flag (Figure 3-10).

Figure 3-10:   Camshaft flag

To ensure the control system outputting accurate engine control signals, the TDC_{Comb} position identified by the encoder must be exactly the same as TDC mark on the engine flywheel. The TDC defined in the control software is checked and adjusted by motoring the engine at very low speed and at the same timing using a timing light flashing at the mark of flywheel when spark timing is set at TDC. Because the camflag (Figure 3-10) is fixed on the

camshaft and their relative position is certain, the engine control system is able to identify the inlet and exhaust valve opening time (Figure 3-9). The VVT system (include intake and exhaust side) works by controlling the solenoid controls pressurized oil in and out of camshaft Pulley (C in Figure 3-6) using PID strategy.

During the experiments, coolant and oil temperatures are heated up by heating elements and precisely maintained at 358 K and 368 K (±3 K) respectively, using PID controllers and heat exchangers. The engine coolant and lubricant are pumped using separate electric pumps. The coolant is cooled by external water through a Bowman heat exchanger.

3.7   Temperature and Pressure Measurement

In-cylinder pressure is sampled by a Kistler water-cooled pressure transducer (Type: 6041A). Signals are amplified by a Kistler 5011B charge amplifier. EPT 3100 media isolated pressure transmitters supplied by EuroSensor were used for measuring the intake, exhaust manifold pressure. The sensors were calibrated by the author on an annual basis.

K type stainless thermocouples (steel sheath, 3 mm $\times$ 0.15 m) supplied by RS are used for the temperature measurement. The thermocouples and pressure transmitters (except for in-cylinder pressure sensor) outputs are sent to TCK-4 thermocouple amplifier units before being sampled by the data acquisition card. A Ricardo Wave Model was used for simulating in-cylinder temperature (see Figure 3-16). WAVE is a widely used 1D engine & gas dynamics simulation software developed by Ricardo, featuring engine performance simulations based on customized intake, combustion and exhaust system configuration.

3.8 Emission Measurement

The emissions being measured are gaseous emissions, PM emissions, and aldehyde emissions. Horiba MEXA-7100DEGER analyser is used for the analysis of gaseous emissions. SMPS are used for the analysis of PM emissions. TGA is used for further study of PM composition and soot oxidization characteristics. GC-MS and HPLC are used for HC speciation and aldehyde emissions measurement respectively.

3.8.1 Gaseous Emissions

The specification of MEXA-7100DEGER is listed in Table 3-3.

Table 3-3: Specifications for MEXA-7100DEGER

	HC	CO	CO_2	NO_x
Methods	FID (hot-wet)	NDIR (dry)	NDIR (dry)	CLD (dry)
Min. (ppm)	0-10	0-100	0-5000	0-10
Max. (ppm)	0-50000	0-12%	0-20%	0-10000
Zero gas	N_2/ air	N_2	N_2	N_2
Span gas	C_3H_8	CO/N_2	CO/N_2	NO/N_2

The flame ionization detector (FID) is widely used for the analysis of THC. The sample gas is introduced from a nozzle charged with a high voltage into a hydrogen flame. In the high-temperature hydrogen flame environment, a portion of hydrocarbon molecules in the sample gas is ionized resulting in a current flow between the nozzle and a collector. By detecting this ion current and converting it into a voltage output, it is possible to measure the concentration of the total HCs. To keep HCs from condensation and preventing it from dissolving in water, the sample gas is maintained at 191 $^\circ$C. The chemiluminescence detector

(CLD) is used for NO analysis. NO reacts with ozone; as a result, photon is emitted. The voltage output converted from photon current is a function of the sample NO concentration. For the NO_2 measurement, NO_2 is first converted to NO before reacting with ozone. O_2 balanced in N_2 is used to generate ozone. Non-dispersive infra-red (NDIR) is a detector for carbon oxides (CO and CO_2) analysis. Carbon oxides absorb infrared. By measuring the light intensity change before and after infra-red beam passing through a sample gas chamber, the NDIR detector is capable of the analysis of carbon oxides concentration.

3.8.2   PM Emission

PM emissions are characterized by a Scanning Mobility Particle Sizer (SMPS) Model 3936 which measures the size and number distribution. The settings used in this study are illustrated in Table 3-4. Before the sample is analysed by SMPS, the sample is diluted using a rotating disk diluter (Model 379020A) which is also supplied by TSI.

Table 3-4:   SMPS measurement settings

Sample Flow Rate (L/min)	1
Sheath Flow Rate (L/min)	10
Scan Time (s)	120
Min. Particle Diameter (nm)	7.23
Max. Particle Diameter (nm)	294.3

The particle classifier charges the particles into a known charge distribution. In DMA a narrow size band of particles is selected according to their mobility in the electrical field and then the selected particles are introduced into the CPC where their number is counted.

PM emissions from DISI engines are fundamentally different from those of diesel engines and most of which are composed of volatilities. The existence of large amounts of volatilities in the PM emissions makes the measurement of PM size distribution significantly difficult. Volatilities not only exist in nucleation mode, but also the accumulation mode.

Therefore it is necessary to use thermo-denuder to remove volatilities before the measurement of PM size distributions.

Table 3-5: TGA specification

Standard furnace	Temperature Range	Sub-ambient to 1000 ℃
	Scanning Rates	0.1 ℃/minute to 200 ℃/minute
	Temp. Precision	±2 ℃
Balance	Tare	Reproducible to ±2 μg
	Sensitivity	0.1 μg
	Accuracy	Better than 0.02%
	Capacity	1300 mg
Sample pan	Standard Furnace	Platinum or Ceramic with capacity of 60 μL

Apart from the PM size distribution, PM composition and soot oxidization characteristics are measured by using a TGA supplied by Perkin Elmer. The TGA specification is listed in Table 3-5. TGA is an essential instrument used for material characterization in which the mass of a sample is constantly monitored as it is heated by a furnace. The sample atmosphere can be an inert or reactive gas and its flow rate can be varied for specific research objectives.

The PM sample collection system is shown in Figure 3-11. Exhaust samples were taken 300 mm downstream of the exhaust valve and diluted by air. The diluted sample was then pumped via a heated line (maintained at 464 ± 2 K) and was collected by glass micro-fibre filters. The sampling flow (after the dilutor) was controlled at 10 L/min.
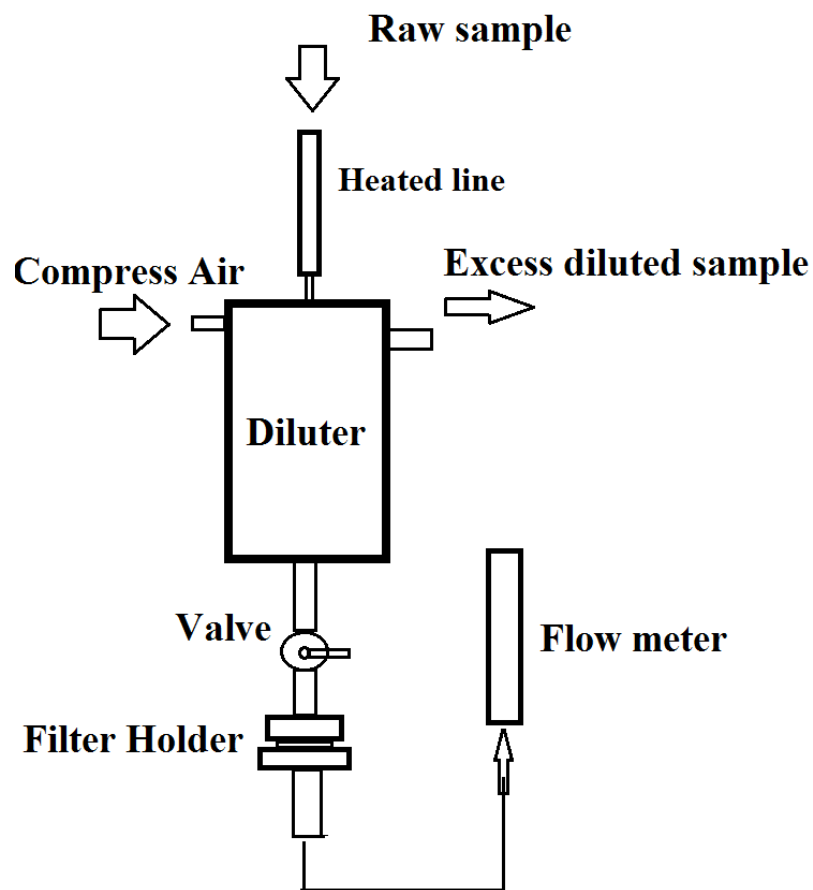
Figure 3-11: PM collection setup

3.8.3 HC and Aldehyde Emissions

GCMS and HPLC are used for HC emission speciation and aldehyde emissions analysis respectively. The specifications of GCMS and HPLC used in this study are shown in Table 3-6.

In this study, the temperature of raw exhaust gas was maintained at 191 $^{\circ}$C by a heating line and introduced into GCMS for analysis. GC is used to separate individual HC which has their unique detention time as it travels through the column. MS is used to identify each HC. The principle is as follows: each HC molecule separated in GC is broken into several ionized fragments. Each ionized fragment is identified based on their electrical mobility (m/z). The whole ionized fragment spectrum is searched in a NIST (National Institute of Standards and Technology) library and possible matches are outputted.

Table 3-6:   Specifications of GCMS and HPLC

	GC/MS	HPLC
Separation	Perkin-Elmer Clarus600	Shimadzu LC20
Detection	Perkin-Elmer Clarus600T	Shimadzu SPD-M20A
Column	Elite-1: 30m x 0.32mm x 3μm	Luna: 250 4.6mm x 5μm
Sample	Tedlar Bag (10-15:1)	DNPH (20ml)
Injection Size	1ml	25μl
Split Ratio	20:1	-
Flow Rate	2mL/min	1mL/min
Test Conditions	50 ℃, 1min; 12 ℃/min; 200 ℃, 1min	10:90 to 70:30 v/v MeCN/water, 120mins; UV λ = 360nm
Test Duration	14.5mins	130mins

In this study, carbonyls were analysed by using HPLC. The raw exhaust sample is bobbling into a glass (20 ml DNPH solution) immersed in an ice bath (Figure 3-12). The aldehyde components in the exhaust react with DNPH (Figure 3-13) and the DNPH-derivative products are retained in the solvent. The solvent then is then analysed by HPLC.
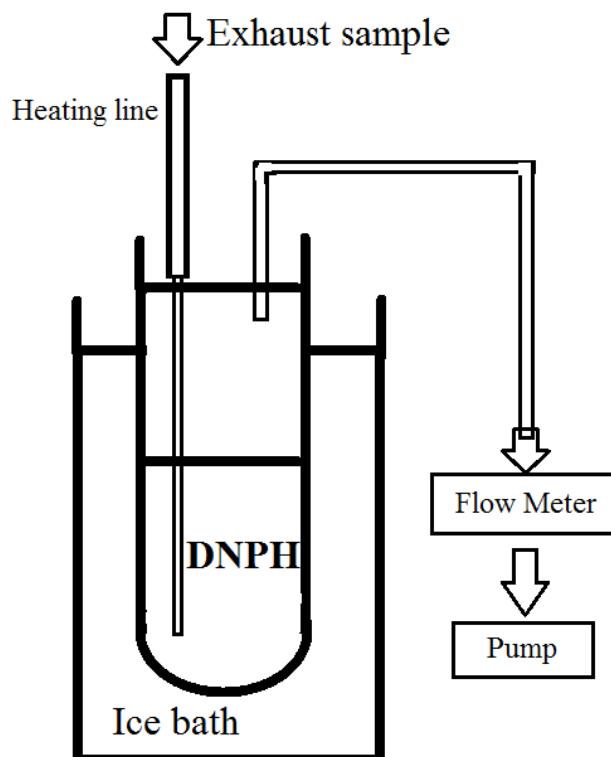
Figure 3-12:　Sample collection set up
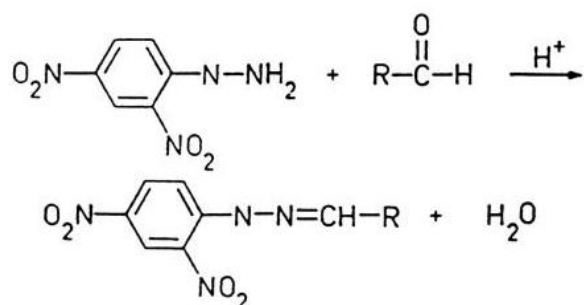
Figure 3-13:　Reaction scheme

3.9　Data Acquisition and Record System

A general overview of the data acquisition and recording system used in this study is introduced. The system consists of high and low speed acquisition channels (See Table 3-7).

The high speed channel recording system features an in-house LABVIEW program and a National Instruments card model 6251with a sample frequency of 1440/cycle. The low

speed channel recording system features an in-house LABVIEW program and a National Instruments card model 6220.

Table 3-7: Data Acquisition Channel

High speed channel	In-cylinder and intake manifold pressure
	Intake and camshaft flag
	HC emissions
Low speed channel	Exhaust gas, cylinder block, intake air, lubricant, coolant temperature
	Torque
	CO, O_2 and NO_X emissions
	Air flow rate
	Throttle position

3.10   Data Processing

3.10.1   In-Cylinder Pressure Processing

For each engine operation condition, 300 sequence cycles of in-cylinder pressure was recorded. The Kistler water-cooled pressure transducer (Type: 6041A) is a piezoelectric type pressure sensor with a high measurement frequency however it has the problem of drifting caused by temperature fluctuations. A widely used practice for solving this issue is to peg the in-cylinder pressure at the end of intake stroke with the intake manifold pressure at the same crank angle degree (in-cylinder P_BDC_{INTAKE} = intake manifold P_BDC_{INTAKE}). The 300 cycle pressure is then averaged. Mathematical smooth function is used to reduce the signal noise.

3.10.2   Heat Release Rate and Mass Fraction Burned Calculation

The heat release rate and mass fraction burned (MFB) are calculated and used to characterize the combustion process. In-cylinder pressure and the corresponding cylinder volume data are used to calculate the heat release rate based on (Equation 3-1.

$$dQ/d\theta = \gamma/(\gamma - 1) * P * dV/d\theta + 1/(\gamma - 1) * V * dP/d\theta \qquad \text{(Equation 3-1)}$$

where γ is the polytrophic exponent. In this study, γ are separately calculated in both the compression and expansion stroke and each value is used to calculate the heat release rate in their corresponding crank angle range. The definition of MFB is the accumulated released heat in successive crank angle ranging from the start of combustion to certain crank angle degree divided by the total heat released in the entire combustion process.

3.10.3   Combustion Efficiency

The combustion efficiency is calculated based on the exhaust gas composition (CO and HCs) as shown in Equation 3-2, which is a simplified version of that used by Christensen and Johansson (2000).

$$\eta_{combustion} = 1 - \frac{x_{CO} Q_{LHV_{CO}} + x_{HC} Q_{LHV_{fuel}}}{\left[\dot{m}_{air} \big/ (\dot{m}_{air} + \dot{m}_{fuel}) \right] Q_{LHV_{fuel}}}$$

Equation 3-2: Combustion Efficiency Calculation

where X_{CO} and X_{HC} are the mass fractions of CO and HC. Q_{LHVco} and $Q_{LHVfuel}$ are the low heating values of carbon monoxide and the fuel respectively. The calorific value of the unburned HCs is assumed to be equal to the calorific value of fuel times a correction factor. Because HCs are not individually measured, and thus the actual aggregated hydrocarbon calorific value is unknown. The correction factor for gasoline, MF and DMF is assumed to be

1, and the correction factor for ethanol is 0.68 (Wallner and Miers, 2008). However, in the exhaust of gasoline, DMF and MF, there are many oxygenated HCs. Therefore, it is expected that there are errors in the calculation of combustion efficiency for gasoline, DMF and MF. FTIR can be used to calculate the combustion efficiency more calculatedly, which measure all the combustion productions enabling the calculation of unreleased energy in the exhaust gas.

3.10.4 Air Flow Rate

An encoder is coupled to the shaft of air flow meter. TTL signals generated by the encoder are processed by a National Instruments counter-timer card (model 6202) where the rotation frequency is calculated. The actual air flow rate is a function of the rotation frequency. The calibration curve for the air flow rate and rotation frequency is generated by using an orifice plate. The air flow rate calibration setup is shown in Figure 3-14.
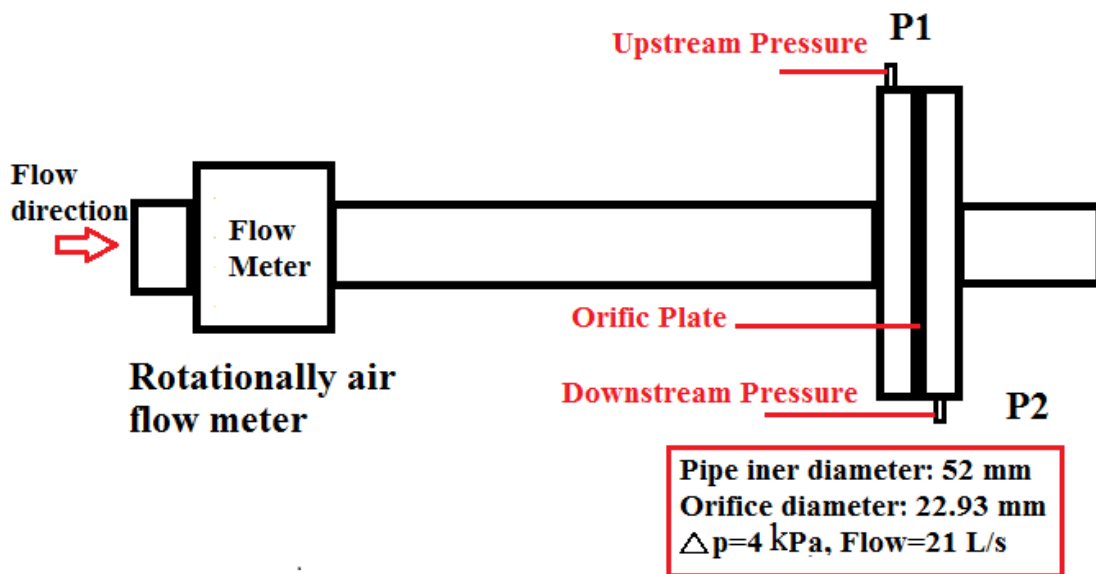
Figure 3-14: Air flow rate calibration

It is known from the orifice plate flow meter that at 4 kPa pressure drop, the actual flow rate is 21 L/s. The charge coefficient C_d can be indirectly obtained by dividing the actual flow

rate with the theoretical flow rate calculated in Equation 3-3. The gravimetric air flow rate is

the function of volumetric air flow rate and air density (Equation 3-3).

$$\rho_{air} = P * \frac{M_{air}}{R * T}$$

$$Q_{actual} = 21 \ (L/s)$$

$$Q_{theoretical} = A_1 * \sqrt{\frac{2*\rho_{air}*\Delta P}{1-(\frac{A_2}{A_1})^2}} = 35.361 \ (L/s)$$

$$C_d = \frac{Q_{actual}}{Q_{theory}} = 0.593881$$

$$Q_{actual} = C_d * A_1 * \sqrt{\frac{2 * \rho_{air} * \Delta P}{1 - (\frac{A_2}{A_1})^2}}$$

Equation 3-3: Airflow Rate Calculation

where P and T are the intake air pressure and temperature, M_{air} represents the molar

mass of air, R is the gas constant. The air pressure presented here has already excluded the

moisture pressure which is calculated based on the humidity value measured by humidity

sensor and temperature measured by thermocouple. Figure 3-15 shows the air flow meter

calibration curve.
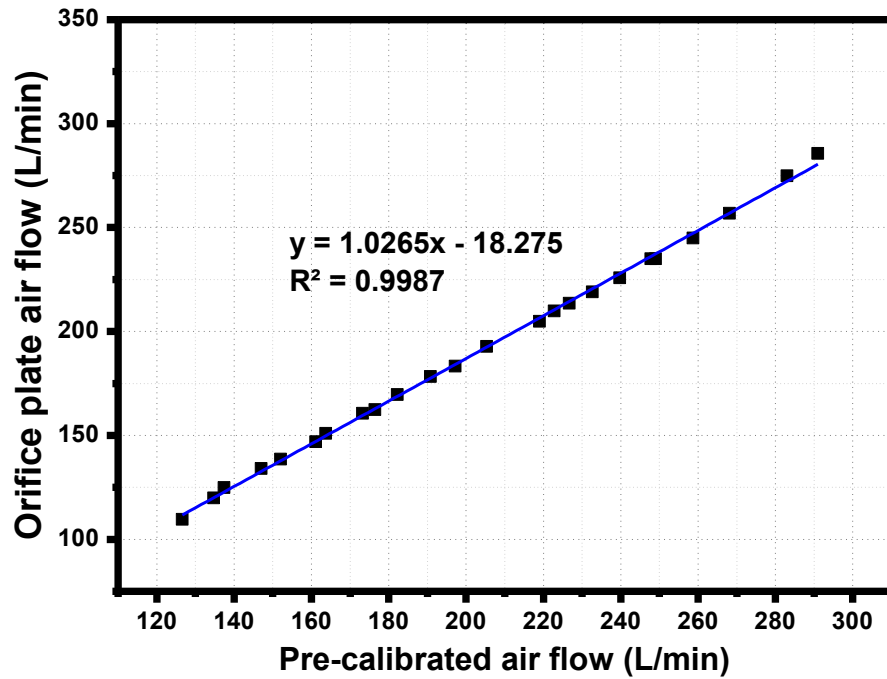
Figure 3-15:   Air flow meter calibration curve

3.10.5   Gravimetric Emissions Calculation

The indicated specific gravimetric emissions rather than volumetric fraction (ppm) are presented in this study. An example of ISCO calculation is given here. First of all the molar mass of exhaust stream is calculated based on the fraction of each component (NOx, CO, HC, N_2 and CO_2). Then the exhaust stream mass flow stream is calculated based on the fuel and air consumption data. The density of CO gas is calculated using (Equation 3-4. In the end the ISCO is calculated by (Equation 3-5.

$$\rho_{CO} = P * \frac{M_{CO}}{R*T} \qquad \text{(Equation 3-4)}$$

where P and T are the exhaust stream pressure and temperature, M_{co} represents the molar mass of CO, R is the gas constant.

$$ISCO = \rho_{CO} * CO_{ppm} * \frac{\dot{V}_{exh}}{Power} \qquad \text{(Equation 3-5)}$$

where CO_{ppm} represents the reading of CO emissions from Horiba, $\dot{V}_{exh}$ is the exhaust stream volumetric flow rate.

3.10.6   Fuel Consumption

The indicated specific fuel consumption is calculated by using the gravimetric air flow rate, λ value from an ETAS Lambda Meter (model LA3) and the engine power output ((Equation 3-6).

$$ISFC = \frac{m_{air} * F\_A * \lambda}{Power} \quad \text{(Equation 3-6)}$$

where F_A, λ and Power represent stoichiometric fuel air rate, lambda value and engine power output.

3.10.7   In-cylinder Temperature

The in-cylinder temperature is calculated using the Ricardo Wave software. When simulating a certain engine running condition, mass fraction burned data (MFB50 and MFB10-90) are used as key inputs of combustion characteristics. The volumetric efficiency and in-cylinder peak pressure of one case matches as well as possible with thermal engine data. When simulating the combustion of gasoline, the fluid properties of indolence were used. Some properties of DMF and MF, viscosity-temperature behaviour, were taken from indolence.

Model

The following steps were taken to build up the model.

1. Gathering data of intake and exhaust manifold configurations.

2. Measuring engine parameter data including bore, stroke, valve diameters and cam profiles.

3. Build up Ricardo Wave Model based on the above information (see Figure 3-16).

4. Check model using self-checking function embedded in the Wave software.
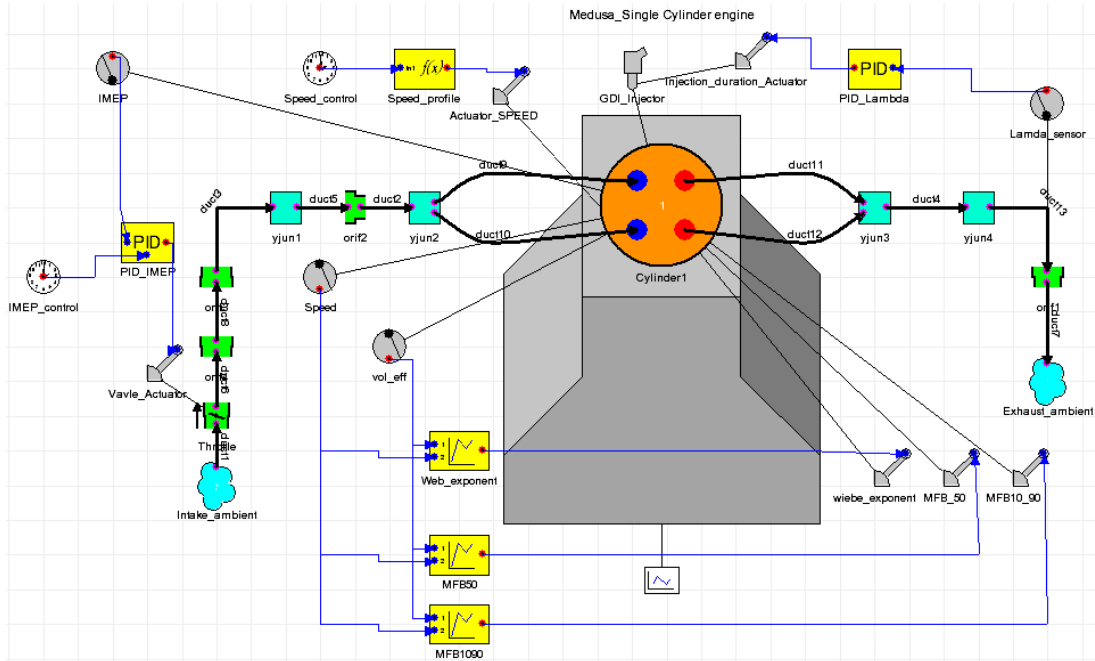
Figure 3-16: Ricardo Wave model for the single cylinder DISI engine

Calibration

Figure 3-17 shows the procedure for calibrating the single cylinder DISI Engine Wave model. Table 3-8 shows five operating points being used for the model calibration. The valve timing used is IVO=4.4 ° bTDC, EVC =36.5 ° aTDC. Figure 3-18 and Figure 3-19 shows simulated and experimental data of IMEP, in-cylinder peak pressure, volumetric efficiency and indicated efficiency.

Choose ten operation points, match each volumetric efficiency (±1%), and input heat release rates into combustion model

Set heat transfer, friction loss multiply factors in the model

Check the matchup of engine parameters such as power output, in-cylinder pressure, and efficiency with real engine data collected from thermal engine

NO

YES

DONE
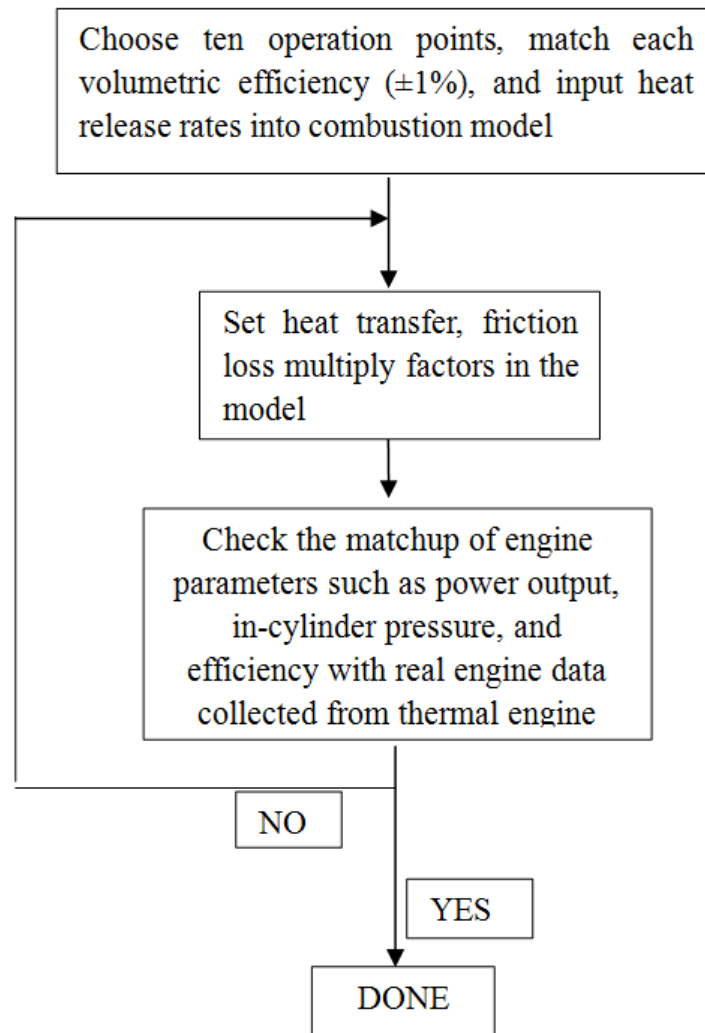
Figure 3-17:   Calibration procedure for the Ricardo Wave model

Table 3-8:   Calibration cases for the Ricardo Wave model

	IMEP (bar)
Case 1	3.40
Case 2	4.52
Case 3	6.38
Case 4	7.57
Case 5	8.32
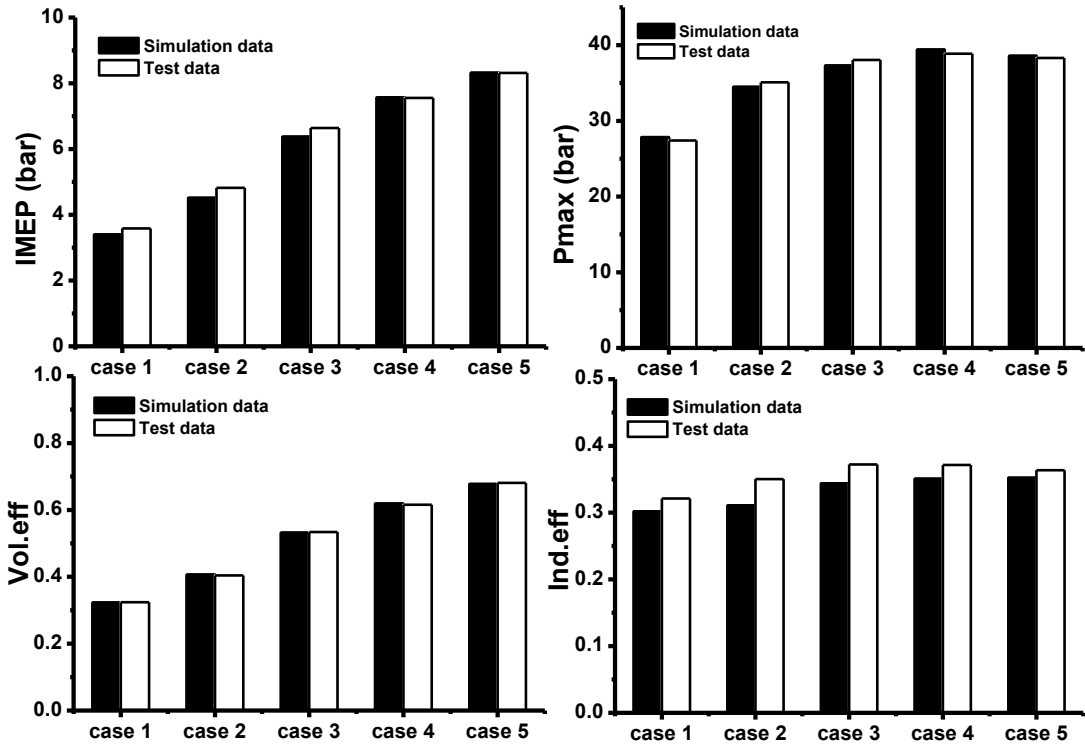
Figure 3-18: Comparison of IMEP, peak pressure, volumetric efficiency and indicated efficiency between simulation data and test data at various engine loads
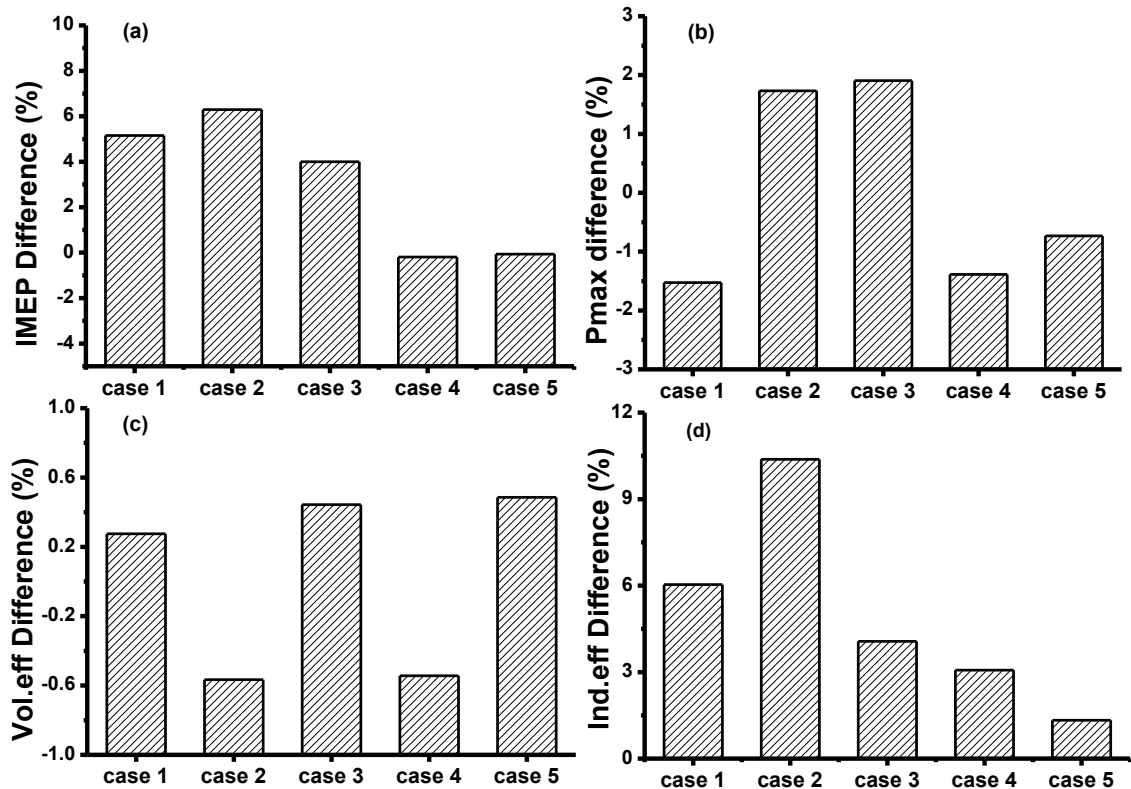
Figure 3-19: Deviation of IMEP, peak pressure, volumetric efficiency and indicated efficiency between simulation data and test data at various engine loads

Validation

Table 3-9 shows five operating points being used for model calibration. The valve timing used is IVO=20 ᵇTDC, EVC =36.5 ᵃTDC. Figure 3-20 and Figure 3-21 shows the tested data and simulated IMEP, in-cylinder peak pressure, volumetric efficiency and indicated efficiency.

Table 3-9:   Validation cases for the Ricardo Wave model

	IMEP (bar)
Case 1	3.53
Case 2	4.66
Case 3	6.42
Case 4	7.63
Case 5	8.43
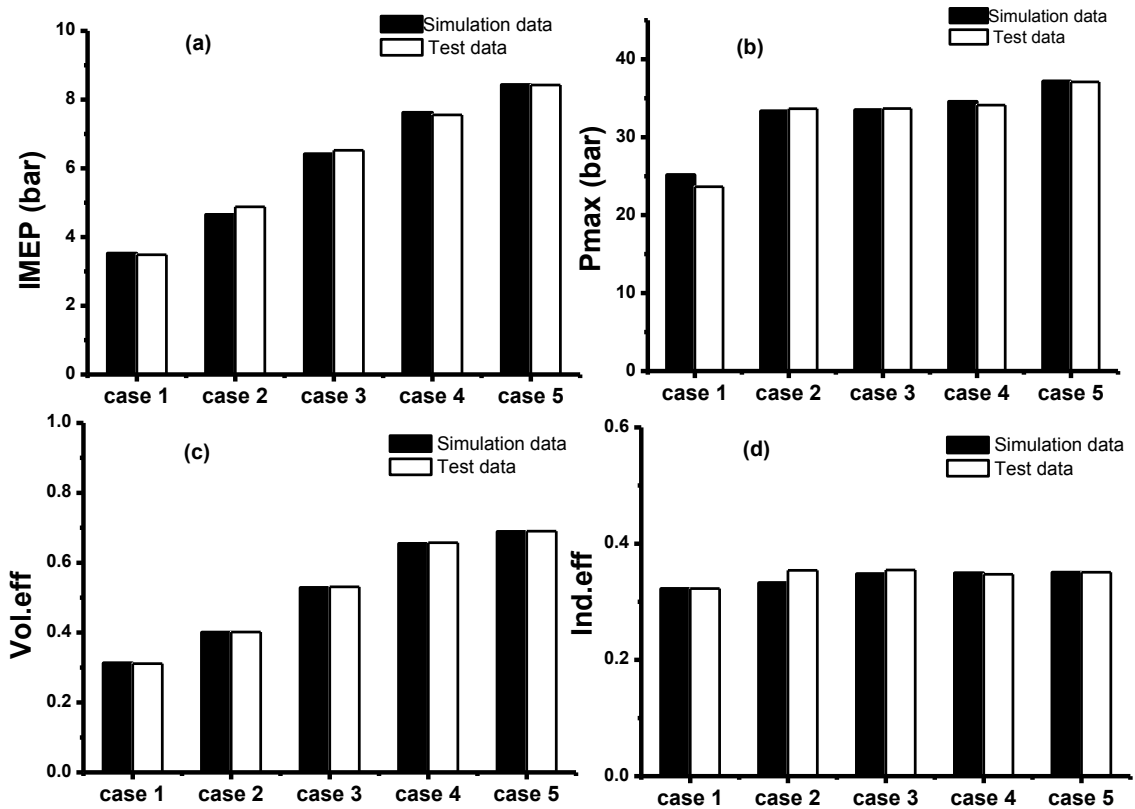
Figure 3-20:   Comparison of IMEP, peak pressure, volumetric efficiency and indicated efficiency between simulation data and test data at various engine loads
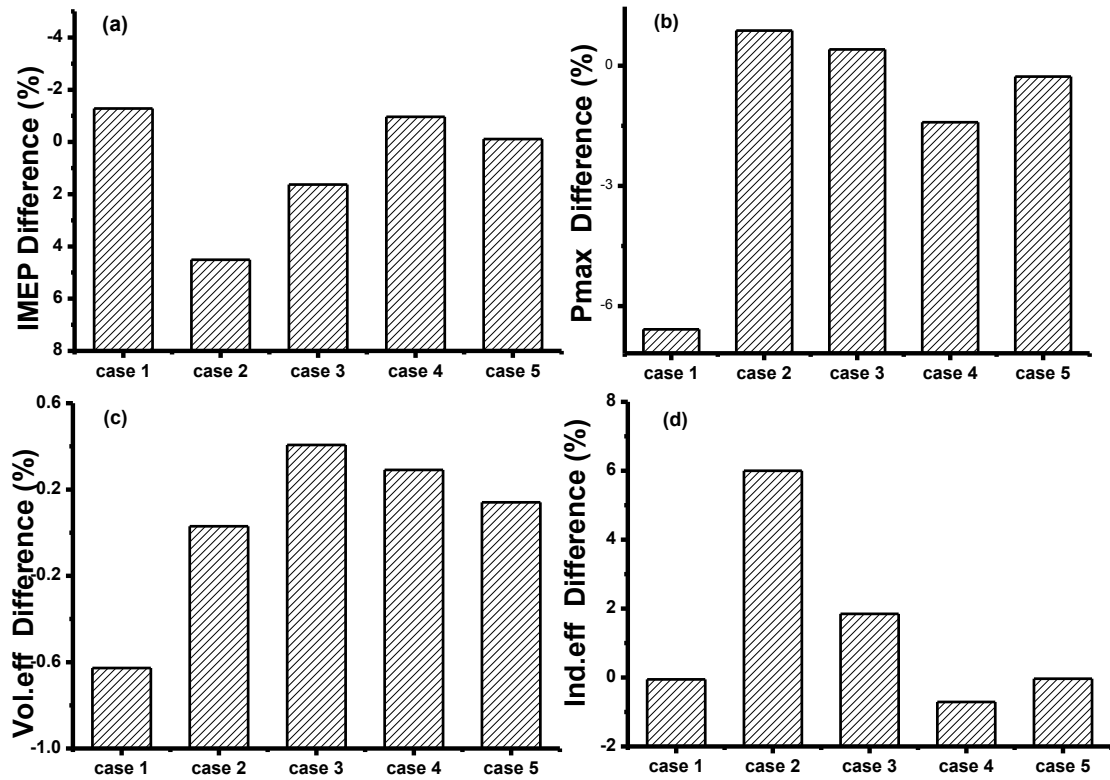
Figure 3-21: Deviation of IMEP, peak pressure, volumetric efficiency and indicated efficiency between simulation data and test data at various engine loads

This Ricardo Wave model is a simple 1D model, only for the purpose of acquiring the in-cylinder temperature. The parameters such as volumetric efficiency, peak in-cylinder pressure, IMEP and indicated efficiency are used to calibrate and validate the model. The author acknowledges that more work could be done to improve the accuracy of modelling, such as the use of a detailed 3D KIVA model; therefore the simulated in-cylinder temperatures are approximate of the real in-cylinder temperatures.

3.10.8   Injector Flow Rate

The injector flow rate is measured by weighing the fuel injected in a thousand pulses of injection. Each measurement is repeated for three times, and then an average is made, in order to minimize the uncertainties associated with the measurement process. Iso-octane is used as the testing fluid.

3.11   Statistical Data Analysis

The variability or error bars of parameters tested has been assessed based on the sample standard deviation, sample size and t distribution, which are presented in (Equation 3-7.

$$\text{Error bar} = \pm t_{(\frac{a}{2}, n-1)} \frac{s}{\sqrt{n}} \qquad \text{(Equation 3-7)}$$

where a represents   significance level; n represents sample size; s represents the sample standard deviation. The reason of using t distribution is that in most cases the sample size is less than 30. If the sample size is more than 30, then a normal or Gaussian distribution will be used instead of t distribution. However, those error bars only address the random errors occurred in the measurements. System errors such as zero errors, calibration errors are not excluded.

3.12   Fuels

Gasoline and ethanol were supplied by the Shell Global Solutions, UK. Although in every delivery the gasoline supplied by Shell is different especially the winter and summer gasoline, the properties of gasoline listed in Table 2-4 represents the most used gasoline throughout of the author's tests. MF was supplied by the Fisher Scientific, UK. DMF was supplied by the Shijiazhuang Lida Chemical Co. Ltd. and the Beijing LYS Chemicals Co. Ltd. with a purity of 99%. It has to be noted that the DMF was produced from crude-oil, rather than from bio-mass using the method mentioned by nature and science.

CHAPTER 4

4 Combustion Characteristics and Fuel Consumptions of MF, DMF and Ethanol in a GDI Engine

This chapter examines combustion characteristics of a GDI engine fuelled with MF, DMF and ethanol. Gasoline is used as the benchmark fuel. Tests are carried out at the condition of stoichiometric combustion, 1500 rpm engine speed and engine loads ranging from 3.5 to 8.5 bar IMEP. A fixed geographic compression ratio of 11.5 is used. Fuel-optimized maximum brake torque (MBT) or knock limited spark advance (KLSA) is used.

4.1　Introduction

This chapter focuses on the application of MF, DMF and ethanol in a DISI research engine. The combustion analysis includes antiknock ability, combustion phase, in-cylinder pressure and temperature, indicated thermal efficiency, combustion efficiency and indicated specific fuel consumption. A Ricardo Wave model was used for the simulation of in-cylinder peak temperature.

Limited publication is available for combustion characteristics of MF. One report (Thewes et al., 2011) found that MF is more robust in the application of cold start compared to ethanol due to its higher volatility and higher combustion stability. The octane rating of MF is better than gasoline, which would be an advantage in downsized SI engines.

The results presented in this chapter are representative due to the use of a modern single-cylinder spray-guided (close-space concept) GDI research engines and much detailed analysis.

4.2   Experimental Procedure

The engine was firstly run for at least 20 minutes, using the PFI injection system. When the coolant and oil temperatures were stabilized at 358 K, the engine was considered to be warm and then GDI injection system was switched on to replace the PFI injection system. Tests were done at 1500 rpm engine speed and stoichiometric combustion.

Fuel-optimized spark timings, also known as the MBT timings, were used in the tests. The definition of MBT timing was where the maximum power output at a fixed throttle position was achieved while keeping the air/fuel ratio the same. When engine knocking was detected, the spark timing was retarded by 2 CAD, which was referred as KLSA.

4.3   Results and Discussion

4.3.1   MBT/KLSA

Since a fixed geometric compression ratio of 11.5 is used, fuels with higher octane rating will experience less engine knocking at high engine load. Knocking is observed when MF, DMF and gasoline are used; therefore, spark timing has to be retarded to avoid potential engine damage. For MF and DMF, knock occurs from 6.5 bar IMEP whereas for gasoline it is 5.5 bar IMEP. No engine knock is detected with ethanol.

The fuel-optimized MBT/KLSA timings at engine load of 3.5-8.5 bar IEMP for MF and other tested fuels are presented in Figure 4-1. At 3.5 bar IMEP, fuel-optimized MBT/KLSA timings for MF and other three fuels are similar. Difference is observed from 4.5 bar IMEP and is increased with load. MF and DMF show a similar MBT/KLSA at all tested load. Ethanol has the most advanced MBT/KLSA timings while gasoline the least. If

fuel-optimised compression ratio is used, engine knocking may be avoided even at wide open throttle condition.

If the compression ratio is lowed to the extent that used for gasoline, DMF and MF,
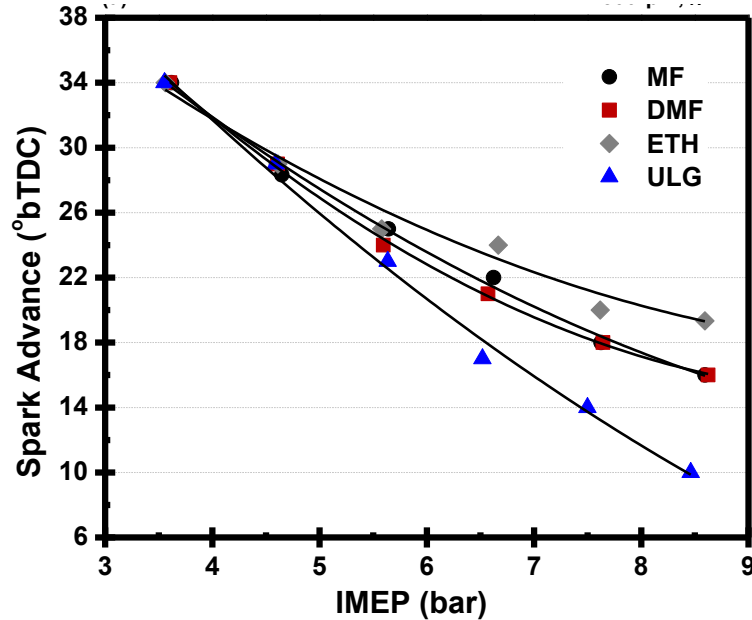
Figure 4-1: Spark timings for MF and other three fuels

The anti-knock ability of fuel is closely associated with its molecule structure. MF has similar molecule structure to DMF; the only difference is the number of methyl group on their cyclobenzene ring. The structure of MF is compact whilst gasoline is a complexes mixture with carbon number ranging from 2 to 14. The long chains of heavy HCs in gasoline make knock easily happen. Ethanol has only two carbons in its molecule. As molecule length increases, fuel has increased knock tendency in a SI engine. This partially explains that MF has a better anti-knock ability than gasoline.

The cooling effect of fuel direct injection also helps to supress knocking (Daniel et al., 2011). Vaporization of fuel spray lowers charge temperature in the cylinder. The ratio of heat of vaporization (HV) and lower heating value (LHV) is an indicator for the cooling

effect (Figure 4-2), which tells the amount of heat absorbed during the vaporization of one

energy unit of fuel. MF shows a higher cooling effect than DMF and gasoline.
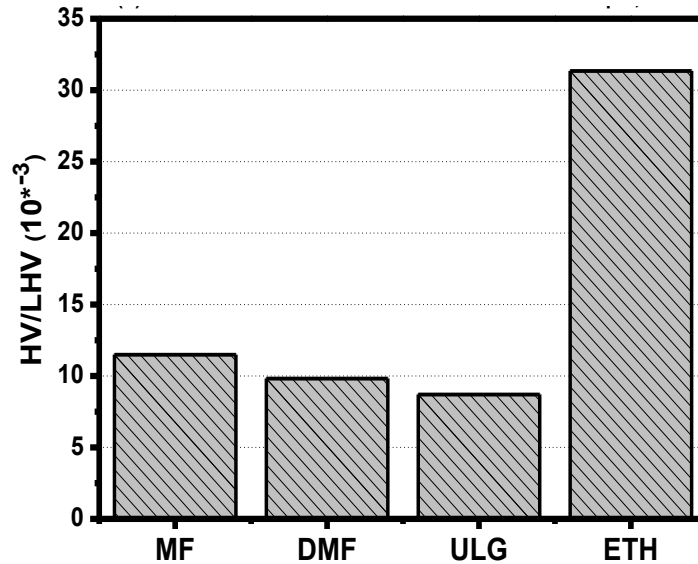
Figure 4-2:   HV/ LHV Ratio for MF and other three fuels

4.3.2   Combustion Phase

The MFB profiles for MF and other three fuels at 3.5, 5.5 and 8.5 bar IMEP are

shown in Figure 4-3. MF burns the fastest among the tested fuels. At 3.5 and 5.5 bar IMEP,

the spark timing of MF and ethanol are the same however MF burns faster. At 8.5 bar

IMEP, the combustion of gasoline is significantly slower than other fuels, which is because

of retarded spark timing, and a weak turbulence inside the cylinder at the timing of

ignition. Low combustion rate of gasoline at 8.5 bar IMEP is a negative factor for engine

efficiency. If compression ratio is optimised for each fuel, combustion phase will be

optimised and therefore it is expected that the combustion of gasoline will be quicker due

to higher in-cylinder charge turbulence at the time of ignition.
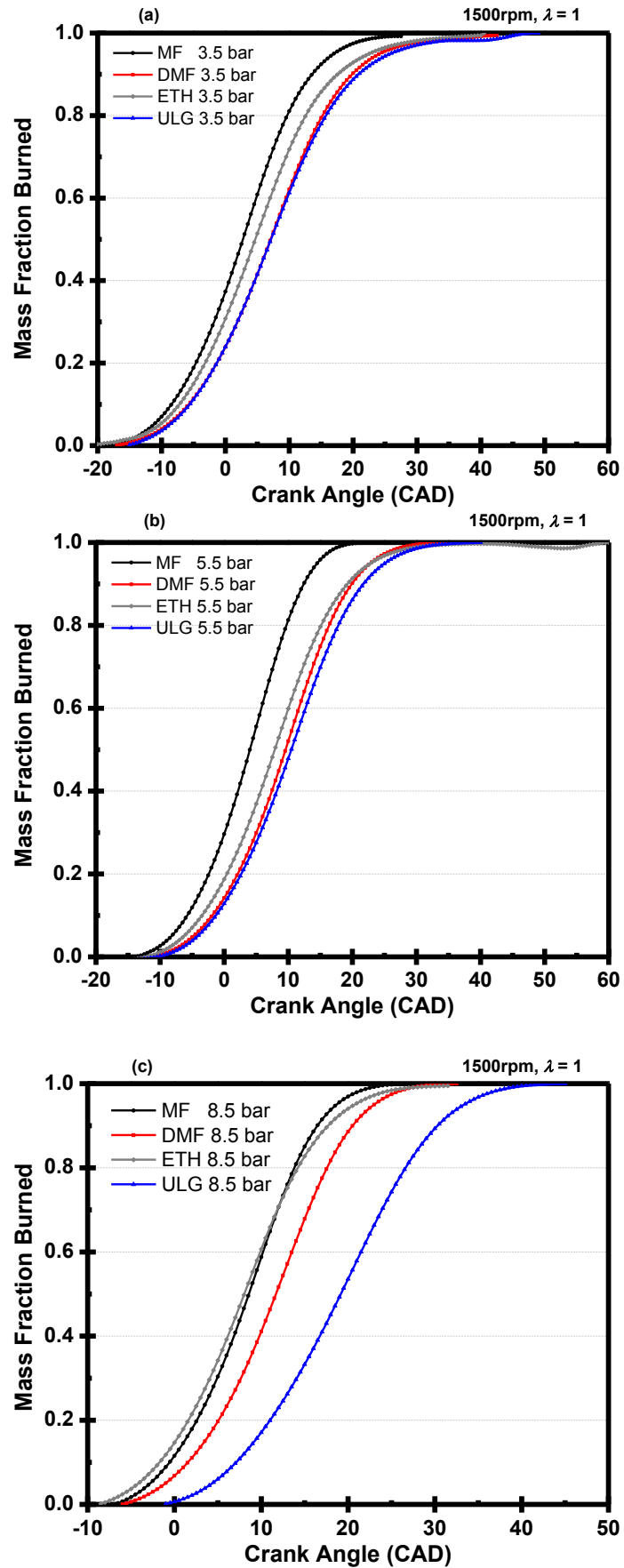
Figure 4-3: MFB profiles for MF and other three fuels at 3.5, 5.5 and 8.5 bar IMEP
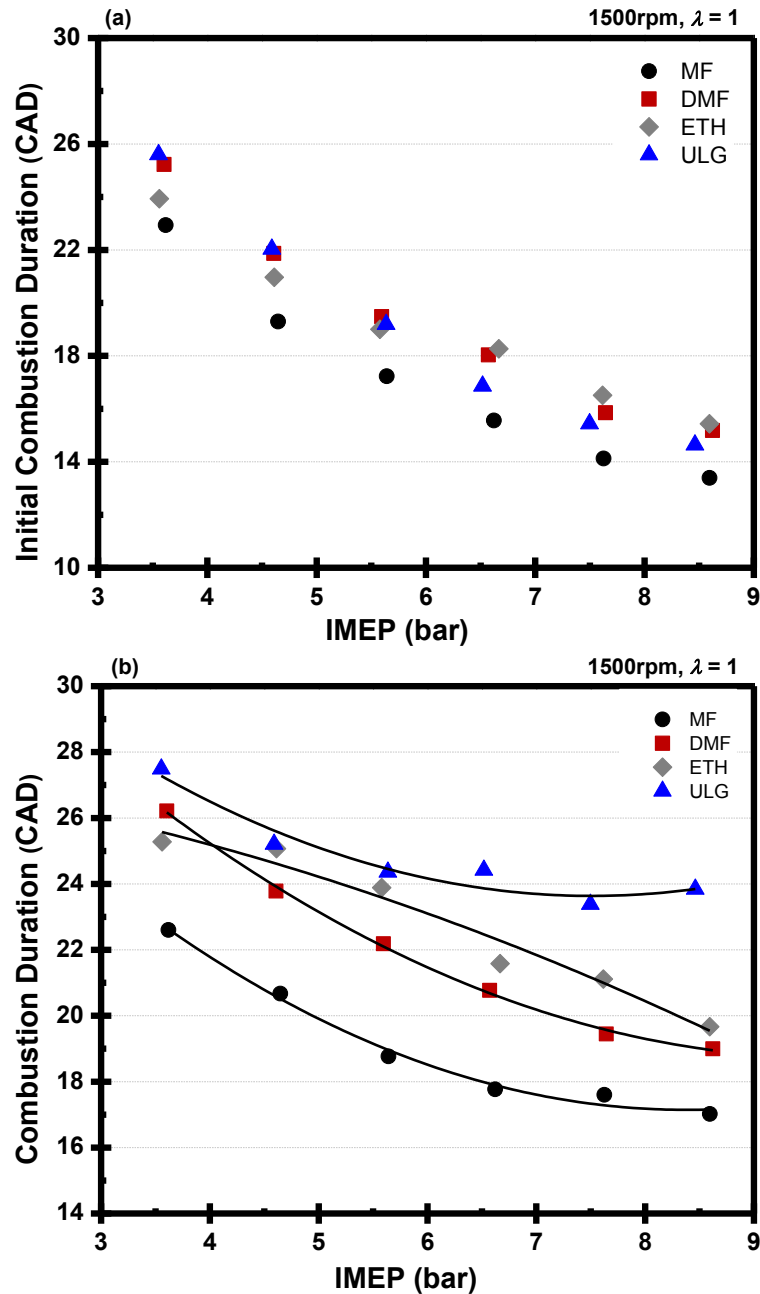
Figure 4-4: Combustion phase for MF and other three fuels at 3.5-8.5bar IMEP
(a) ICD, (b) CD

The combustion initiation durations (CID), which is defined as the engine crank angle interval between ignition timing and 5% MFB crank angle position, are presented in Figure 4-4 (a). The CID of MF combustion is always the shortest among all the tested fuels. The difference between MF and gasoline regarding CID becomes closer as engine load increases, which is because of their increased differences in fuel-optimized

MBT/KLSA timings. Advanced spark timing tends to increase CID due to a lower fuel and air mixture pressure and temperature at the time of ignition. Due to ethanol's outstanding heat of vaporization and octane rating, the difference in CID between MF and ethanol is increased with engine load. The difference in CID between MF and DMF maintains consistent (2 CAD) throughout 3.5-8.5 bar IMEP, due to similar octane rating and cooling effect.

Figure 4-4 (b) shows the combustion durations (CD), which is the crank angle interval between 10% MFB and 90% MFB, for MF and other three fuels at 3.5-8.5bar IMEP. When using MF as the engine fuel, its combustion consistently has the shortest CD whilst gasoline has the longest CD. The gap between MF and gasoline in CD increases with engine load. The maximum difference of 7 CAD between MF and gasoline is at 8.5 bar IMEP and the minimum difference of 4 CAD is at 3.5 bar IMEP. The CD for MF at 8.5 bar IMEP is about 3 and 2 CAD shorter than ethanol and DMF, respectively.
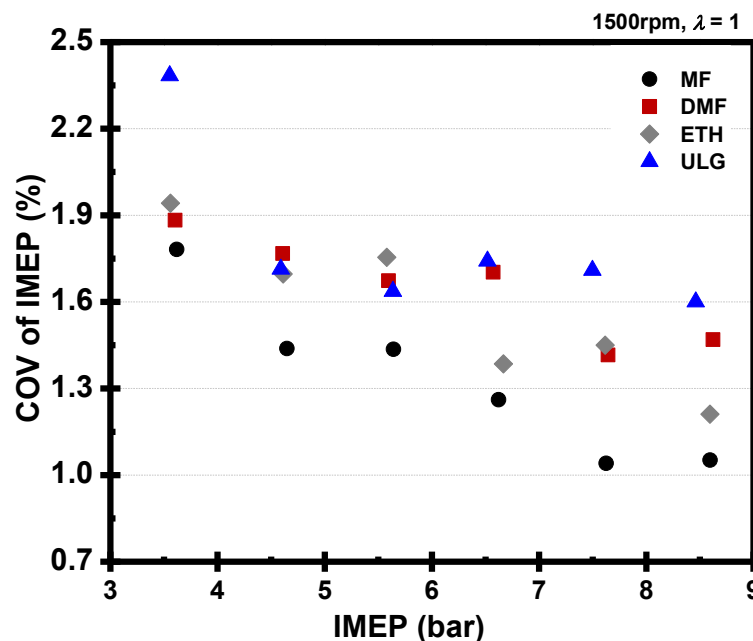
Figure 4-5:   COV of IMEP for MF and other three fuels at 3.5-8.5 bar IMEP

Fast burning rates of oxygenised hydrocarbon have already reported by many publications (Aleiferis et al., 2008, Cairns et al., 2009, Yeliana et al., 2008). This is why

oxygenated fuels such as MF, DMF and ethanol, have a shorter CD than gasoline. The combustion stability, indicated by the COV of IMEP, is shown in Figure 4-5. The combustion stability of MF is the lowest in four tested fuels, indicating that MF has an ideal fuel for lean GDI combustion mode.

4.3.3   In-Cylinder Pressure and Temperature

The in-cylinder pressure for MF and other three fuels at 3.5, 5.5 and 8.5 bar IMEP are shown in Figure 4-6. At 3.5 and 5.5 bar IMEP, MF has the highest in-cylinder pressure in four tested fuels. At 8.5 bar IMEP, MF has similar maximum in-cylinder pressure to bio-ethanol. The pressure profile difference between MF and gasoline are significantly different and sensitive to engine load. At 8.5 bar IMEP, the combustion of gasoline is significantly slower than other fuels, which is because of retarded spark timing, and weak turbulence inside the cylinder at the ignition timing. If compression ratio is optimised for each fuel, it is expected that the combustion of gasoline will be quicker.
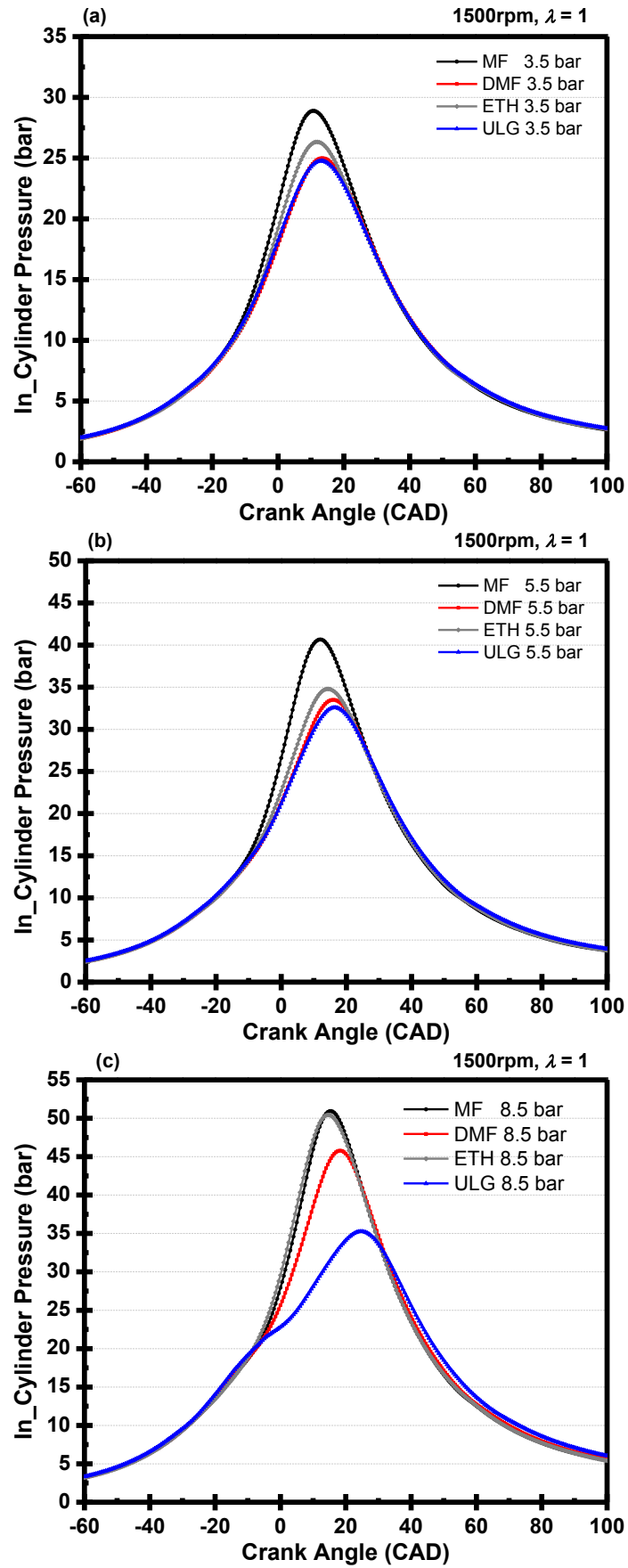
Figure 4-6:   In-cylinder pressure at 3.5, 5.5 and 8.5 bar IMEP for MF and other three fuels

The theoretical in-cylinder temperature of tested fuels at 3.5, 5.5 and 8.5 bar IMEP are shown in Figure 4-7, which are calculated using a 1D Ricardo Wave model, where the difference between experimental and simulated IMEP and maximum pressure is within 2%. Indolene is used to represent gasoline fuel. Unknown properties of MF and DMF, such as the viscosity-temperature behaviour, were copied from indolene. MFB50 and MFB10-90 are used as input parameters in the SI Wiebe combustion function.
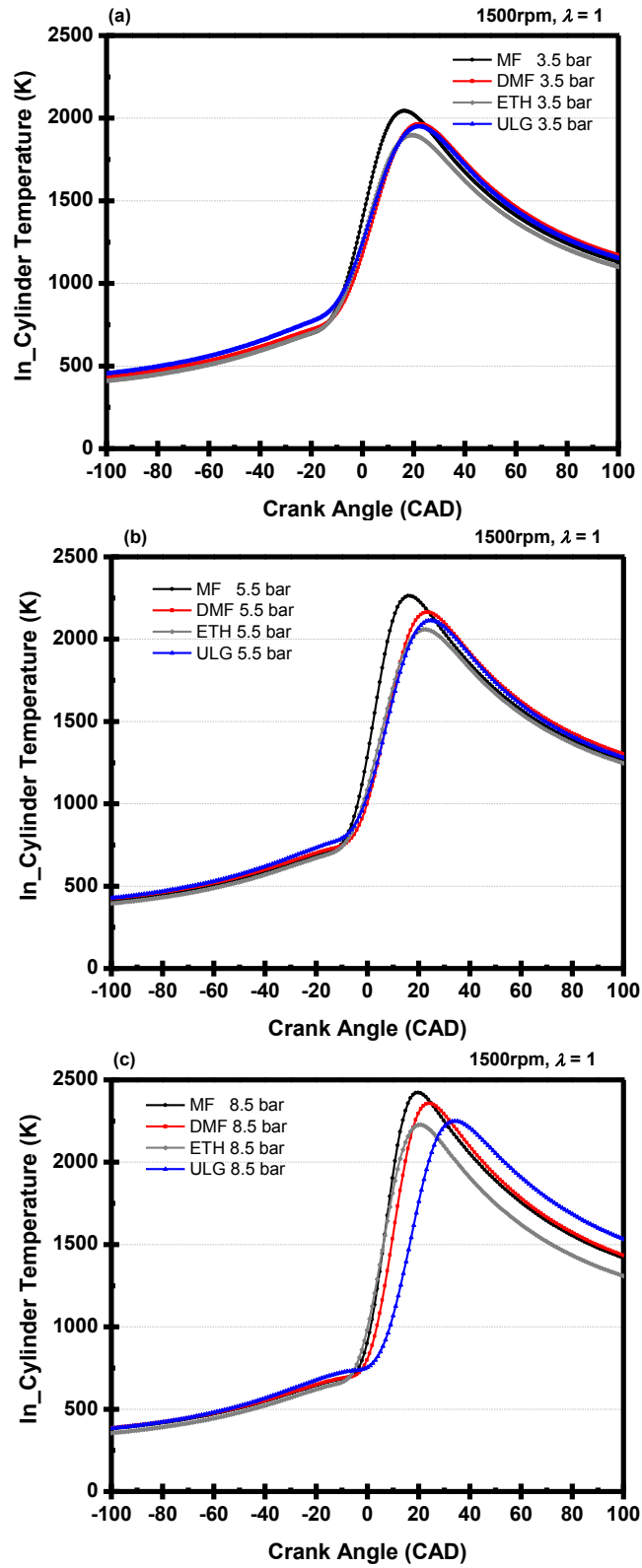
Figure 4-7:   In-cylinder temperature at 3.5, 5.5 and 8.5 bar IMEP for MF and other three fuels

The combustion temperatures of MF at those three loads are significantly higher amongst four tested fuels, especially compared with that of gasoline. This is due to the faster burning rate of MF as well as its advanced spark timing. At 3.5 and 5.5 bar IMEP, the temperature profiles for gasoline, ethanol and DMF are not significantly different however for MF the temperature rise rate is obviously larger. At 8.5 bar IMEP, the temperature rise rate of MF and ethanol are similar however MF combustion leads to higher peak temperature.
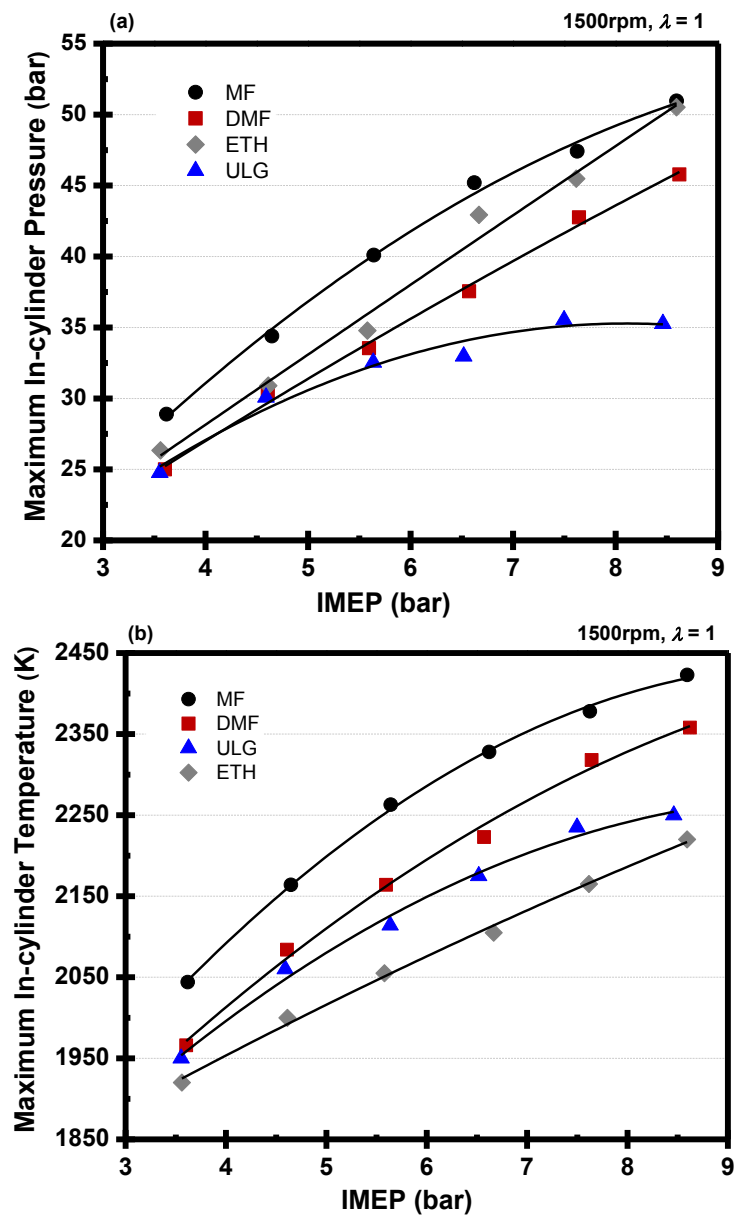
Figure 4-8: Maximum in-cylinder (a) pressures, (b) temperature for MF and other three fuels at 3.5-8.5 bar IMEP

The maximum in-cylinder pressure and temperature for MF and other three fuels at 3.5-8.5 bar IMEP is shown in Figure 4-8. MF combustion consistently leads to the highest in-cylinder peak pressure. Gasoline combustion produces the lowest peak pressure among the four fuels and the maximum in-cylinder pressure peaks at 7.5 bar IMEP. The difference between MF and gasoline in maximum in-cylinder pressure increases with engine load. The maximum in-cylinder pressure of ethanol becomes closer to that of MF as load increases. The difference in combustion duration between MF and DMF is not sensitive to engine load. If fuel-optimised compression ratio is used, it is expected that the peak in-cylinder pressure and temperature for gasoline, DMF and MF will be lower than that presented in in Figure 4-8.

There are two major factors that attribute to the significantly higher peak pressure for MF: fuel-optimized MBT/KLSA timing and faster burning rate. Faster burning rate for MF leads to more heat released around TDC and higher maximum in-cylinder pressure. Although MF and DMF have similar fuel-optimized MBT/KLSA timings, its maximum in-cylinder pressure is consistently higher than DMF due to its faster burning rate. The combination of fuel-optimized MBT/KLSA timing and faster burning rate makes MF have higher peak pressures than gasoline.

The maximum in-cylinder temperature for MF and other three fuels at 3.5-8.5 bar IMEP are shown in Figure 4-8 (b). As load increases maximum in-cylinder temperature increases. MF generates the highest maximum in-cylinder temperature and ethanol the lowest. The maximum in-cylinder temperature, like peak pressure, is sensitive spark timing and burning rate. Although MF has similar fuel-optimized MBT/KLSA timings with DMF, the faster burning rate of MF makes its peak temperature higher than DMF. As burning rate increases, maximum in-cylinder temperature increases. MF has a significant higher

peak temperature than ethanol, because of faster burning rate of MF, and ethanol's significant cooling effect. If fuel-optimised compression ratio is used, it is expected that the peak in-cylinder pressure and temperature for gasoline, DMF and MF will be lower than that presented in Figure 4-8.
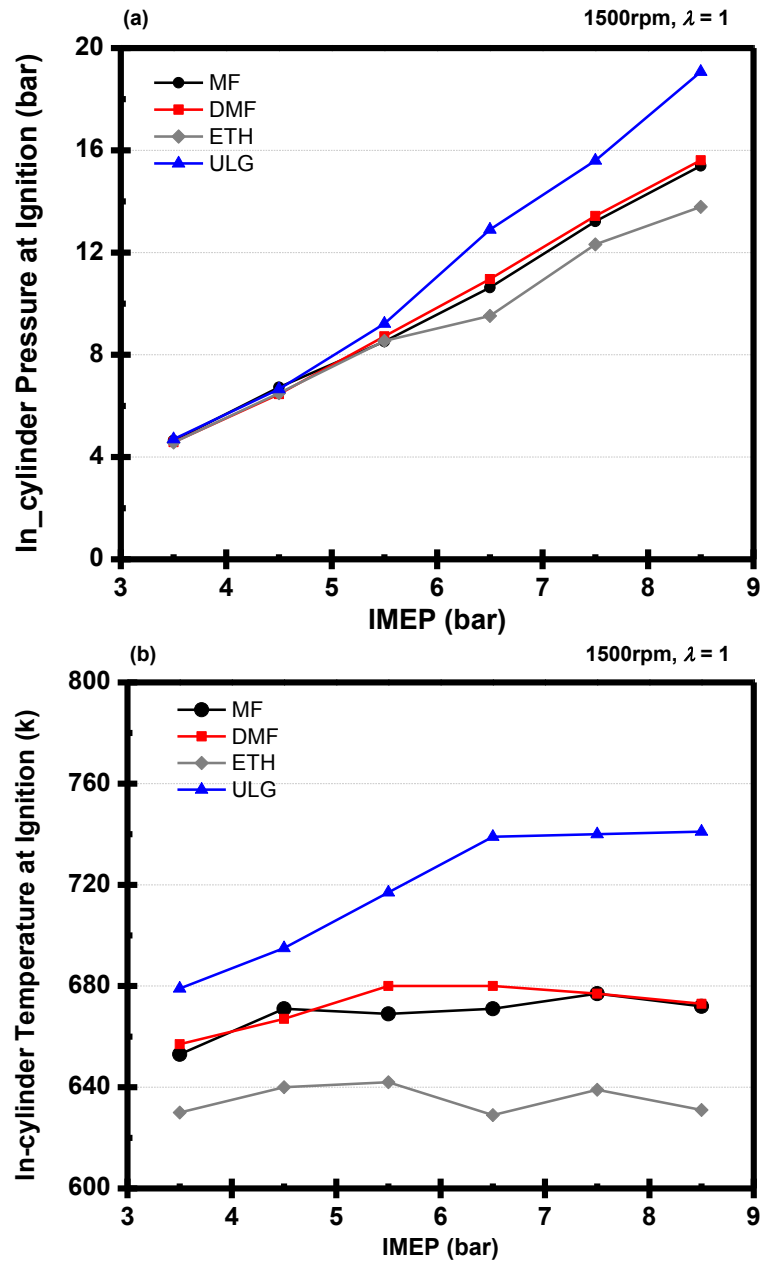
Figure 4-9: In-Cylinder (a) pressure, (b) temperature at ignition event for MF and other three fuels at 3.5-8.5 bar IMEP

The temperature and pressure of in-cylinder mixture charge at the time of ignition for MF and other three fuels at 3.5-8.5 bar IMEP are shown in Figure 4-9. MF consistently has

higher in-cylinder temperature in the event of ignition than ethanol. This is because of the synergy effects of later ignition and lower heat of vaporization of MF. Compared with gasoline, MF has lower in-cylinder temperature in the event of ignition mainly because of more advanced spark timing. DMF and MF shares similar anti-knock ability and heat of vaporization therefore the in-cylinder temperature and pressure at the event of ignition are quite similar.

4.3.4 Indicated Thermal Efficiency

The indicated thermal efficiencies for MF and other three fuels at 3.5-8.5 bar IMEP are shown in Figure 4-10.
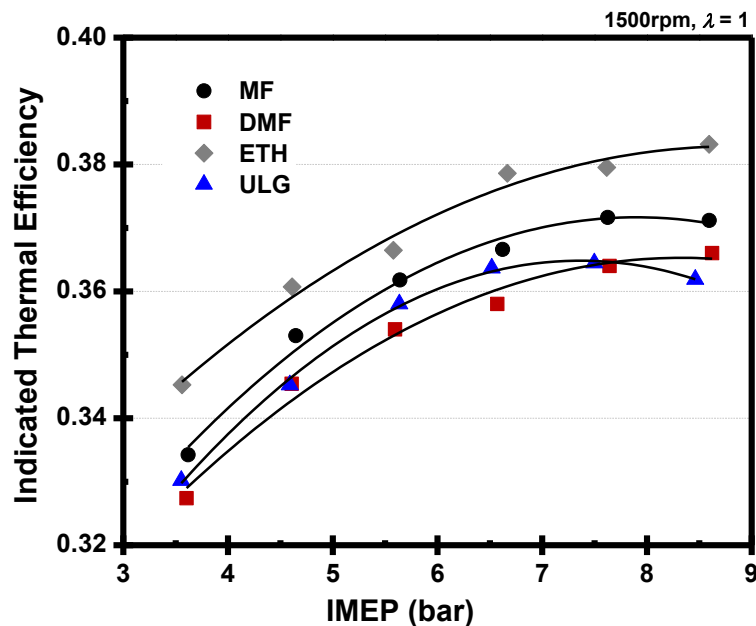
Figure 4-10: Indicated thermal efficiency for MF and other three fuels at 3.5-8.5 bar IMEP

The indicated thermal efficiency of MF is better than gasoline and DMF. Heat loss is the main source of wasted energy during combustion. High in-cylinder temperature leads to more energy loss to the cylinder wall and exhaust, which partially explains indicated the lower thermal efficiency of MF than that of ethanol. On the other hand, ethanol consistently has optimized combustion phase, because its combustion is not limited by

engine knock. For ethanol, the combustion temperature is significantly lower than that of gasoline, and thus the heat transfer to cylinder wall and piston is low. As a consequence, more chemical energy released during combustion of ethanol is converted into effective work to the piston. This is another reason that ethanol has higher indicated efficiencies than MF. It should be noted that the compression ratio of the engine is not optimized. In the 11.5 compression ratio GDI engine, combustion phase is optimal up to 5.5 bar IMEP for gasoline, and up to 6.5 bar IMEP for DMF and MF. If a lower compression ratio GDI engine is used, it is expected that knocking may not occur even at wide open throttle condition. The engine efficiency at the range of 3.5-5.5 bar IMEP for gasoline, DMF and MF in a lower compression ratio GDI engine will be less than that in an 11.5 compression ratio GDI engine. At high engine loads, the engine efficiency may be improved for gasoline, DMF and MF in a fuel-optimised compression ratio, because combustion phase will be optimised and there is high in-cylinder charge turbulence at the timing of ignition. Therefore, for ethanol, a further increase of compression ratio may lead to a higher indicated efficiency. For gasoline, DMF and MF, when compression ratio is decreased, there is a trade-off in the indicated efficiencies between low and medium engine loads, and high engine loads.

4.3.5   Combustion Efficiency

The combustion efficiency, presented in Figure 4-11, describes the completeness of combustion.
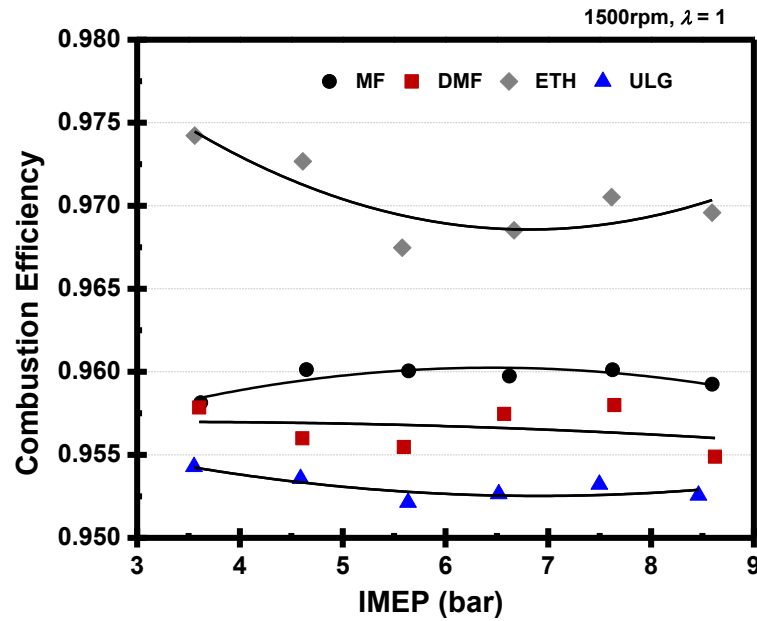
Figure 4-11: Combustion efficiency for MF and other three fuels at 3.5-8.5 bar IMEP

Generally, the combustion efficiency of SI engine is in the range of 92% to 98% (Heywood, 1989). The 2%-8% incomplete combustion is because of the unreleased chemical energy in incompletely combusted products like CO, and unburned HCs. From Figure 4-11, MF has higher combustion efficiency compared to DMF and gasoline whilst ethanol has the highest combustion efficiency. Combustion efficiency is associated with combustion temperature, partially indicated by the maximum in-cylinder temperatures (Figure 4-9 (a)). Higher combustion temperature leads to more complete combustion and HC post-oxidization. Oxygen content is another positive factor effecting combustion efficiency. The oxygen in fuel molecule self-supplied oxygen in combustion, and leads to high combustion efficiency. MF has lower oxygen content than ethanol, explaining that MF has lower combustion efficiency than ethanol.

HCs in the exhaust are not individually measured, and thus the actual hydrocarbon calorific value of the HCs in the exhaust is unknown. An assumption made in the calculation of combustion efficiency is that the calorific value of the unburned HCs is assumed to be equal to the calorific value of fuel, which is based on the fact that most of

the HCs in the exhaust are unburned fuels. In reality, there are other HCs including oxygenated HCs in the exhaust in addition to the unburned fuel. However in this study, quantitative specification of HCs in the exhaust is not carried out, and also the sensitivity of FID detectors varies towards oxygenated HCs, therefore the combustion efficiencies given in this thesis are approximate values.

4.3.6   Indicated Specific Fuel Consumption

The gravimetric indicated specific fuel consumptions (GisFCs) for MF and other three fuels are shown in Figure 4-12 (a). The volumetric indicated specific fuel consumptions (VisFCs) are presented in Figure 4-12 (b).
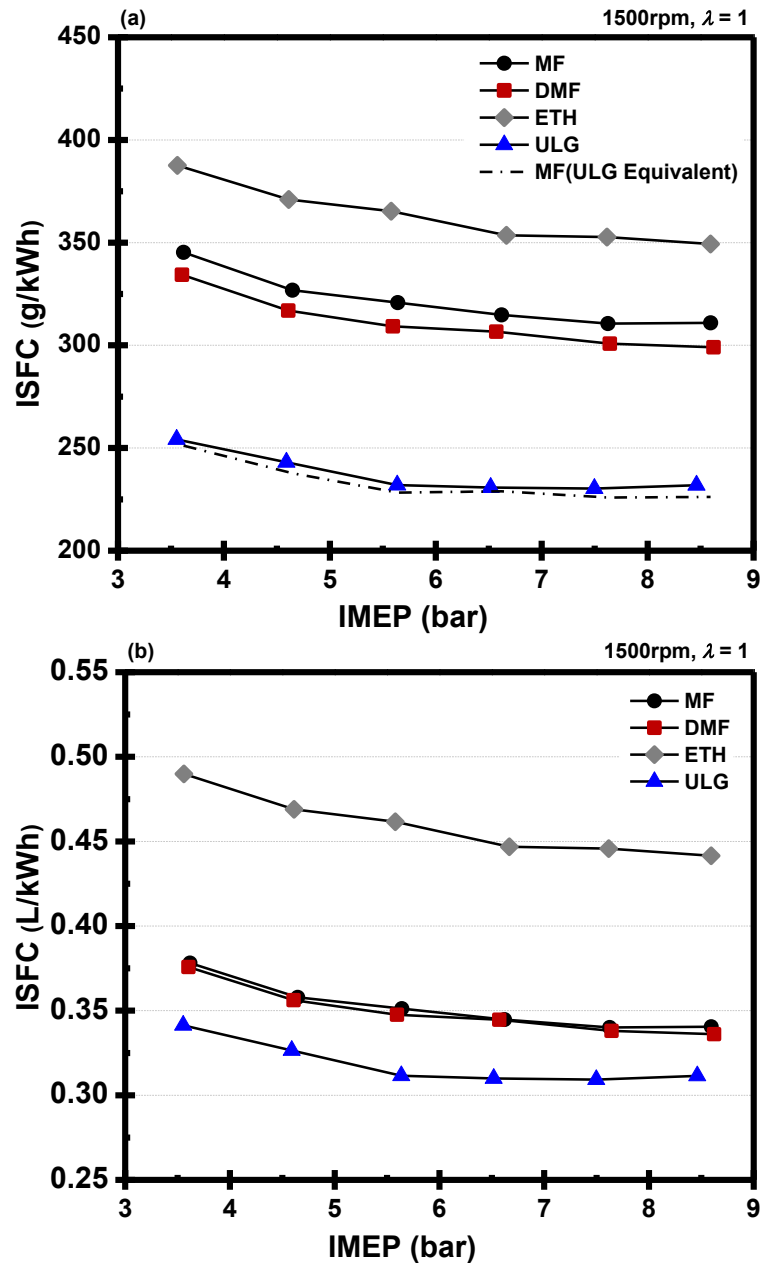
Figure 4-12:   GisFC for MF and other three Fuels at 3.5-8.5 bar IMEP

MF has around 12%-13% lower GisFC than ethanol because of its higher energy content. Even though MF has a 5.4% lower energy density (in mass) than DMF, its higher indicated thermal efficiency makes its volumetric fuel consumption closer to DMF. Due to the higher energy content of gasoline, MF is not competitive to gasoline in terms of GisFC. The dash line in Figure 4-12 (a) shows the gasoline normalized GisFC for MF. It can be

seen that MF has lower gasoline normalized GisFCs due to its higher indicated thermal efficiency. MF is close to gasoline and DMF, and 30% less than ethanol in VisFC.

4.4   Summary

This chapter examines the combustion characteristics of MF, DMF and ethanol in a single cylinder spray guided GDI research engine in the engine load ranging from 3.5 to 8.5 bar IMEP, 1500 rpm engine speed of and stoichiometric combustion. The results are compared with gasoline. The following are the main conclusion of this study:

1.   Regardless of the similar chemical structure, MF shows notably different combustion characteristics to DMF. MF burns fastest rate among the four studied fuels at equivalent engine conditions, which also makes MF generate the highest in-cylinder peak pressure.

2.   MF shows a better anti-knock ability than gasoline, due to its compact molecule structure and faster burning rate, which allows more advanced spark timing. MF a competitive fuel in the application of downsized SI engines.

3.   Due to the combined effect of significant anti-knock ability, fast burning rates, MF has the second highest indicated thermal efficiency among the fuel tested fuels. At 8.5 bar IMEP, the indicated thermal efficiency for MF is 1.4% and 2.7% higher than DMF and gasoline respectively.

4.   Fuel consumptions for DMF and MF are comparable to gasoline, and 30% lower than ethanol, which is mainly due to their high energy content.

It should be pointed out that, since a fixed geometric compression ratio of 11.5 is used, fuels with higher octane rating will experience less engine knocking. Knocking is observed when the GDI engine uses MF, DMF and gasoline. Severe engine knock is detected when gasoline is used. Consequently, spark timing is retarded to an extent that the combustion of gasoline is slow at high engine load due to weak in-cylinder turbulence. Therefore, the effect of compression ratio on combustion of MF, DMF and ethanol remains a subject for future investigation.

CHAPTER 5

5 Emission Characteristics of MF in a GDI Engine Compared with DMF, Ethanol and Gasoline

This chapter details the emission characteristics of a GDI engine fuelled with MF. The results of DMF, gasoline and ethanol results are also presented.

5.1 Introduction

This chapter focuses on the emission characteristics of MF in a DISI research engine. The research interests covered gaseous emissions including NO_x, HC, CO and PM emissions as well as NO_x control strategies. The investigation of carbonyls emissions and key HC speciation was also carried out and presented in this chapter.

Before any bio-fuel being widely promoted, a detailed research focusing on its emissions should be carried out. The regulated gaseous emission from MF combustion were investigated and compared with those of gasoline and ethanol. Currently, little is known about aldehydes emissions and individual HCs from MF combustion, let alone their chemical reaction mechanisms. In recent years, the research evidences show that aldehyde emissions from SI engines especially formaldehyde and acetaldehyde, are highly toxic and harmful to human bronchial epithelial cells (Saladino et al., 1985). Some HCs in the emissions from SI engines such as benzene and toluene are even toxic and can cause cancer (Agency, 1998).

HCs speciation is a fundamental combustion research work. It is usually used to validate the kinetic combustion mechanism. Furthermore, HCs speciation and aldehyde

quantitative measurement are of vital importance in the calibration of FID because the sensitivity of FID differs to individual HCs, especially to the oxygenated HC. As reported by Wallner, FID's response factor towards formaldehyde and acetaldehyde are only 0.2 and 0.6 respectively whilst toluene is 1 (Wallner, 2011, IARC, 2011, CARB, 2010). MF has oxygen element in its molecule therefore it has a profound importance to do fuel-specific FID calibration in order to make reliable and repeatable measurement (Grob, 1985).

5.2 Experimental Procedure

The engine was firstly run for at least 20 minutes, using the PFI injection system. When the coolant and oil temperatures stabilized at 358 K, the engine was considered to be warm and then GDI injection system was switched on to replace the PFI injection system. For all of the tests, the exhaust temperature was monitored as an important indicator of stable test conditions. All of the tests were carried out at ambient air intake conditions (298 ±1 K), at the engine speed of 1500 rpm and stoichiometric air/fuel ratio (AFR). The test conditions are listed in Table 5-1.

Table 5-1: Engine test conditions and test equipment

	Note	**Tested Fuels**	**IMEP (bar)**	**Spark Timing (ɓTDC)**	**Emission measurement equipment**
Gaseous emissions (NO$_x$, HC and CO)		MF, DMF, ULG, ETH	3.5-8.5	KLSA/MBT	Horiba
NO$_x$ Emissions Control	EGR Strategy (cold EGR)	MF, DMF,ULG, ETH	6.5	ULG: 17 MF: 22 ETH: 25	Horiba
	Retarded Spark Timing Strategy			Varied	Horiba
Carbonyls emissions		MF, DMF,ULG, ETH	6.5	KLSA/MBT	HPLC
HC speciation		MF	6.5	KLSA/MBT	GCMS

For each test point, the throttle and injection duration pulse were control simultaneously to reach one desired engine load. The setup of HPLC and GCMS, and the test procedure were all introduced in the introduction chapter.

5.2.1   Aldehydes measurement

Aldehydes were measured using a HPLC (model: Shimadzu LC20). The aldehydes being measured included formaldehyde, acetaldehyde, acrolein, propionaldehyde, methacrolein, benzaldehyde, valeradehyde, m-tolualdehyde and hexaldehyde. The samples were bubbled at 1 L/min for 20 min in an acidified 2,4-dinitrophenylhydrazine (DNPH) reagent (20 mL). The reaction of carbonyls with the DNPH reagent forms DNPH-carbonyl derivatives, which was analysed then by HPLC. The HPLC parameters and column information can be found in the experimental setup chapter.

5.2.2   Hydrocarbon speciation

The samples were delivered to the GCMS (model: Perkin-Elmer Clarus600) though a heated line and injected into the GC column using a six-port injection valve. MS with a porous layer open tubular column was used to identify HCs with carbon number ranging from 3 to 8. This allows unknown compounds to be qualitatively measured. The mass spectrum (mass to charge ratio, or m/z, for each mass) of each peak was identified using a NIST library. Detailed GCMS operation parameters and column information can be found in the experimental setup chapter.

5.3 Gaseous Emissions and NO_x Control Strategies
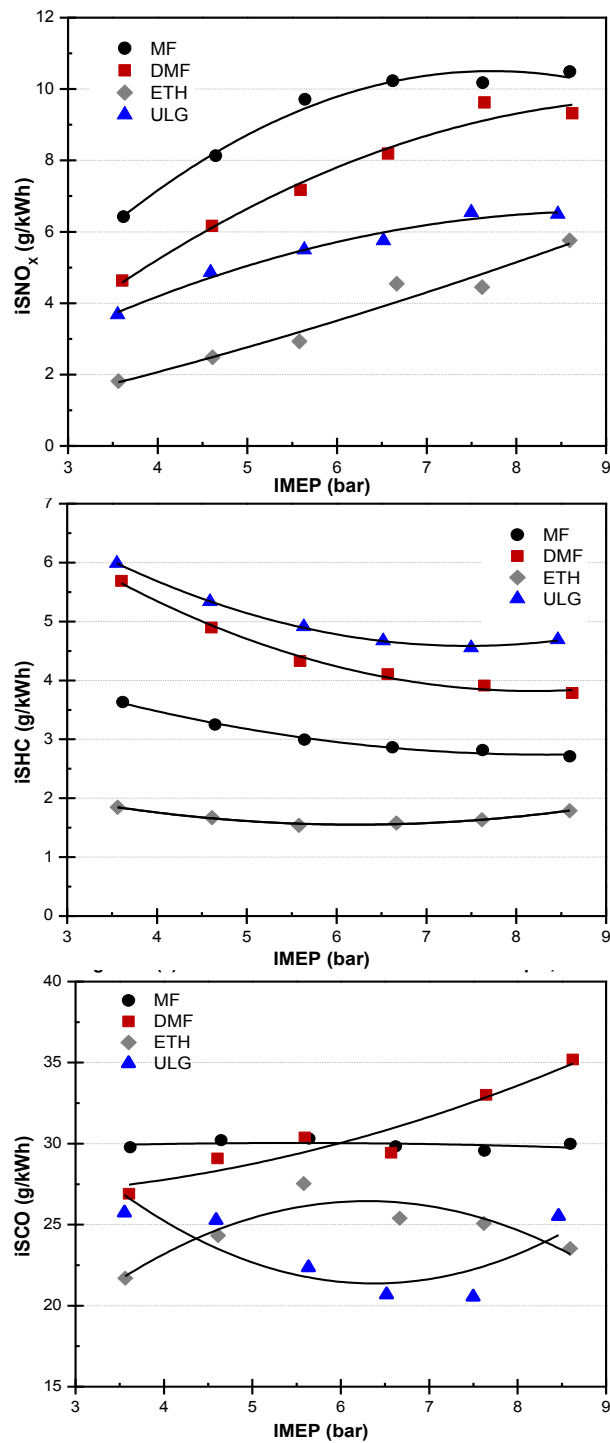
Figure 5-1: Indicated specific gaseous emissions for MF and other three fuels at 3.5-8.5 bar IMEP

Figure 5-1 shows gaseous emissions, including NO_x, HC, and CO. The NO_x formation is primary dependent on the combustion flame temperature (Heywood, 1989), which is clearly observed in Figure 5-1 (a) and Figure 4-8 (b) (maximum in-cylinder

temperature). MF combustion in GDI engine under MBT/KLSA spark timing produces the highest NO_x emissions because of its significant high maximum in-cylinder temperature. The maximum difference in NO_x emissions between MF and other three fuels is at 3.5 bar IMEP, where MF produced 82%, 280% and 40% more NO_x emissions than gasoline, ethanol and DMF, respectively. For all the tested fuels, NO_x emissions increase with engine load, and have a similar tend as the maximum in-cylinder temperatures. NOx emissions are related to the adiabatic flame temperature. The combustion of fuels with a higher H/C ratio tend to have higher adiabatic flame temperature because water has a higher specific heat capacity than CO_2 (Harrington and Shishu, 1973, Daniel et al., 2011).

Figure 5-1 (b) presents the indicated specific hydrocarbon (isHC) emissions for MF and other tests fuels. MF combustion produces significantly lower HC emissions than gasoline and DMF. HC emissions from MF, gasoline and DMF combustion decrease with engine load, which is primary because of the increased in-cylinder temperature as engine load increases. Higher temperature makes the HC oxidization in the exhaust stroke more complete.

Oxygenated fuels tend to produce low HC emissions, which partially explain that MF produces lower HC emissions than gasoline and DMF. However, HC emissions of MF combustion can also be related with HC measurement method. FID method is used for quantitatively measuring HC emissions however, the sensitivity of FID is reduced when oxygenated hydrocarbons are among the sample gas, which is reported by Wallner (Wallner and Miers, 2008) and Price et al (Price et al., 2007b).

Figure 5-1 (c) presents the indicated specific carbon monoxide (isCO) emissions for MF and other tests fuels. In is obvious that MF produces more isCO emissions than ethanol and gasoline. The CO formation is sensitive to the mixture homogeneity and is significantly increased as air/fuel mixture is rich. Although tests are conducted under

stoichiometric combustion, the homogeneity for each fuel/air mixture various due to their difference fuel properties. Spray with a shorter penetration distance leads to less fuel impingement on the piston crown and cylinder liner. Liquid fuel firm on cylinder liner and piston crown is difficult to be fully evaporated. Lower volatility can also reduce the homogeneity of fuel/air mixture. Gasoline produced less isCO emissions than MF, which is because gasoline is relatively easier to form homogenous combustible mixture due to its higher volatility property. On the other hand, ethanol is an oxygenated fuel and thus self-supplies oxygen in the combustion reaction (Dale Turnera et al., 2011).
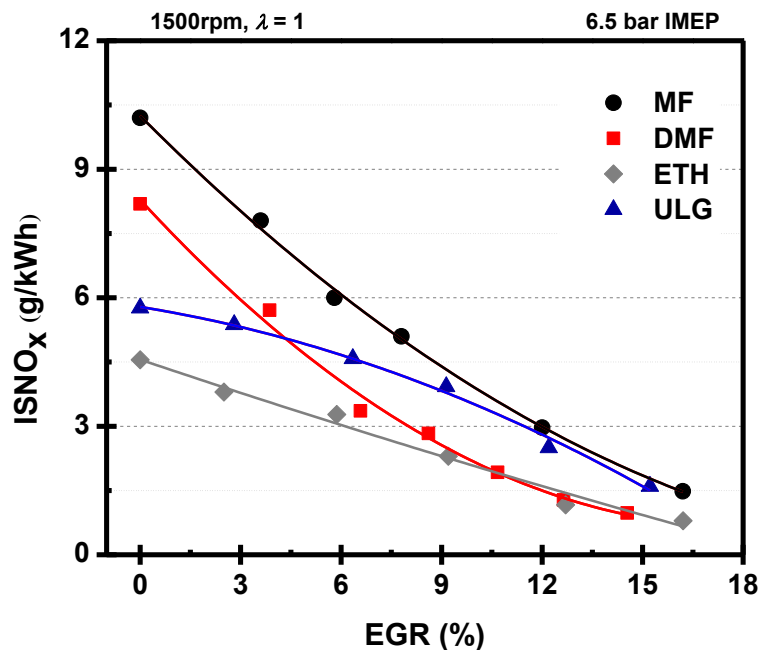
Figure 5-2:   Effect of EGR on the NO_x emissions in a DISI engine fuelled with MF, DMF, gasoline and ethanol at 6.5 bar IMEP

Figure 5-2 shows the effect of EGR on indicated specific NOx emissions from MF, DMF, gasoline and ethanol at 6.5 bar IMEP. Adding EGR is effective method of controlling NO_x emissions mainly due to its notable impact on reducing the combustion flame temperature. With 7.8% and 16.2% EGR, the NO_x emissions from MF combustion could be reduced by 50% and 83% respectively. Even though without adding EGR, NO_x emissions from MF were 77% higher than those from gasoline at 6.5 bar IMEP, the use of

EGR at the range of 12% to 16% made their NO_x emissions at the same level. The use of EGR also reduces the NO_x emissions difference between MF and ethanol.
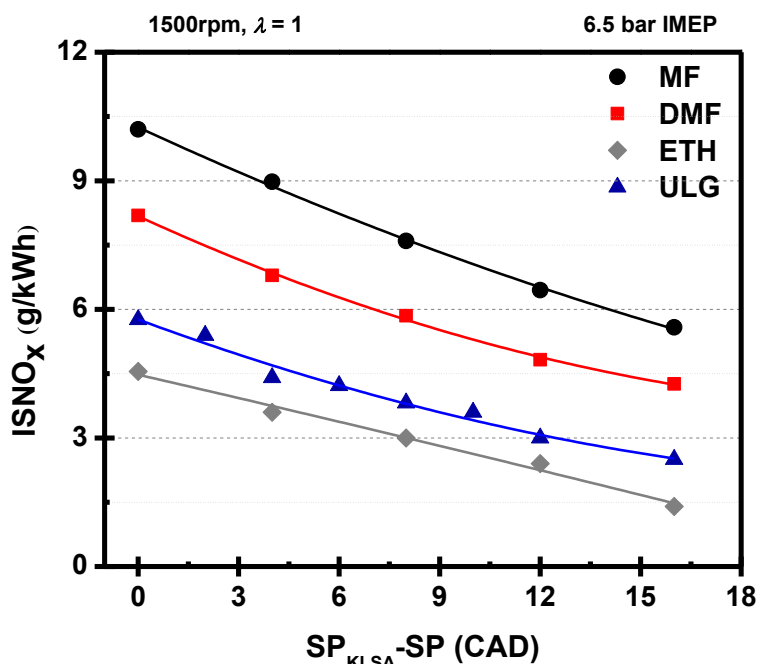
Figure 5-3: Effect of spark timing on the NO_x emissions in a DISI Engine fuelled with MF, DMF, gasoline and ethanol at 6.5 bar IMEP

Figure 5-3 shows the effect of spark timing on indicated specific NO_x emissions from MF, DMF, gasoline and ethanol at 6.5 bar IMEP. The *x* axis represents the number of CAD that spark timing is away from KL_SA spark timing. NO_x emissions are almost negatively linear to the retarded spark timing. With 8 and 16 CAD retarded spark timing, NO_x emissions from MF combustion were reduced by 25% and 45%, respectively. Similar reductions are observed when using gasoline and ethanol as fuels. Unlike the EGR strategy, when using retarded spark timing strategy the NO_x emissions from MF combustion is always higher than those from gasoline and ethanol.

It is concluded that even though MF combustion produces more NO_x emissions than those of gasoline and ethanol, the use of EGR or spark timing strategy would lower down its NO_x emissions to an equivalent level of gasoline and ethanol combustion.

5.4   Aldehyde Emissions
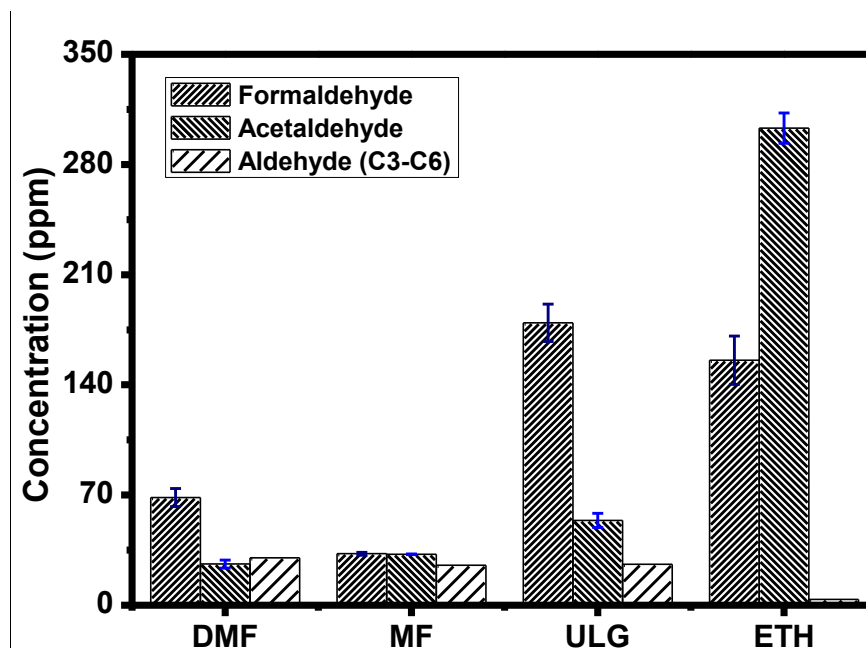
Figure 5-4:   (a) Formaldehyde and acetaldehyde, (b) total C3-C6 aldehyde
emissions for MF and other tested fuels at 6.5 bar IMEP

The aldehyde emissions of MF, DMF, gasoline, and ethanol at 6.5 bar IMEP are
presented in Figure 5-4. Formaldehyde emissions of MF were almost halved compared
with those of DMF, which were lower than those of gasoline, and ethanol. Acetaldehyde
emissions of MF were close to those of DMF and were lower than those of gasoline and
ethanol. The concentrations of aldehydes ranging from C3 to C6 were relatively low
compared with formaldehyde and acetaldehyde. The overall aldehyde emissions of MF (89
ppm) and DMF (104 ppm) were considerably lower than those of gasoline (258 ppm) and
ethanol (462 ppm). The total aldehyde emissions accounted for 4.6%, 4.7%, 9.2% and
25.1% of total HC emissions for MF, DMF, gasoline and ethanol.

5.5   HC Speciation

Figure 5-5, Figure 5-6 and Figure 5-7 show the gas chromatogram of the exhaust from MF combustion. Unburned fuel (MF, 17.29 min) dominated the HC emissions, which is also reported by many researchers (Kar and Cheng, 2009, Zhu et al., 2012). Common heavy HCs such as xylenes (26.10 min, 26.29 min, and 26.90 min for the three forms), toluene (23.05 min), ethylbenzene (23.24 min), and benzene (19.74 min) were detected, as well as the light HC of propene (5.58 min). Oxygenated HCs such as acrolein ($CH_2=CHCHO$, 13.85 min), acetone (CH_3COCH_3, 14.87 min), methyl vinyl ketone ($CH_2=CHCOCH_3$, 18.04 min), acetic acid (CH_3COOH, 18.60 min), propanoic acid (CH_3CH_2COOH, 21.67 min), 3-butenoic acid ($CH_2=CHCH_2COOH$, 24.42 min), and the furan series emissions, including furan (13.38 min), DMF (21.12 min), and furfural (24.75 min) were also detected. Aromatic hydrocarbons are common in the combustion of furan series biofuel flames, for both the premixed flames and engine combustion (Wu et al., 2009a, Wei et al., 2012, Tran et al., 2014, Togbé et al., 2014, Daniel et al., 2012c).
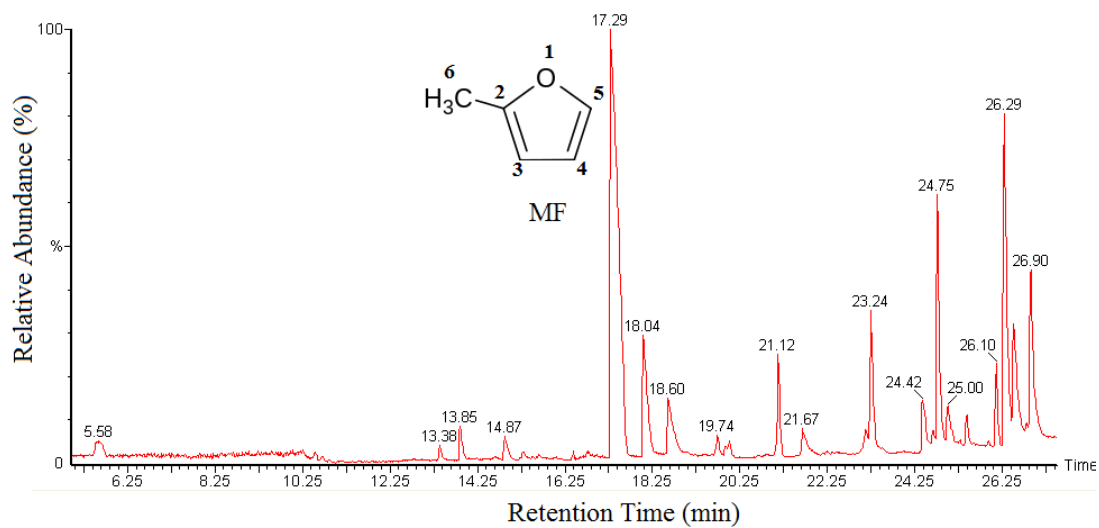
Figure 5-5: Chromatograms of HCs for MF at 6.5 bar IMEP (retention time: 5 to 27.5.5 min)
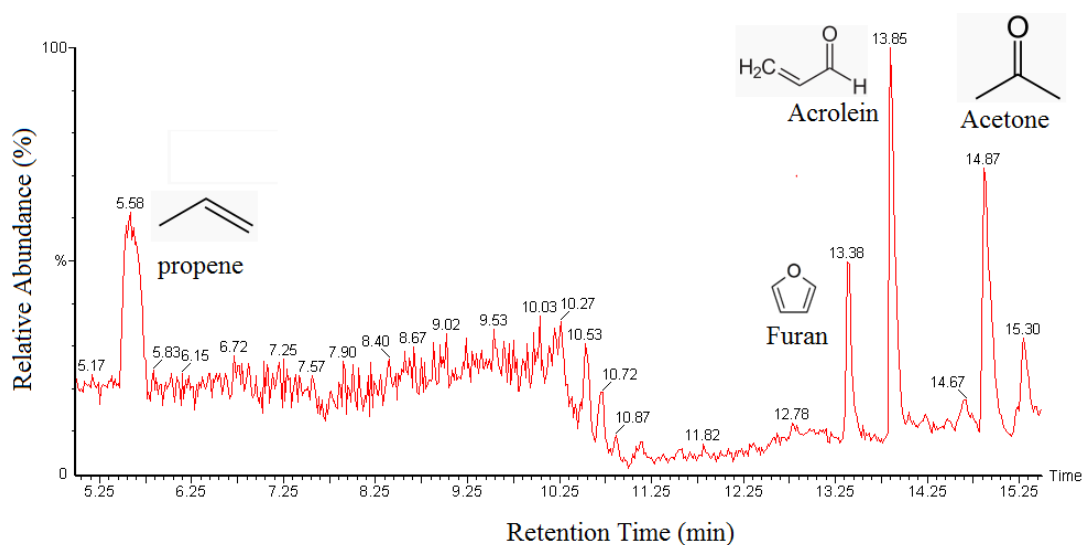
Figure 5-6: Chromatograms of HCs for MF at 6.5 bar IMEP (retention time: 5 to 15.5 min)
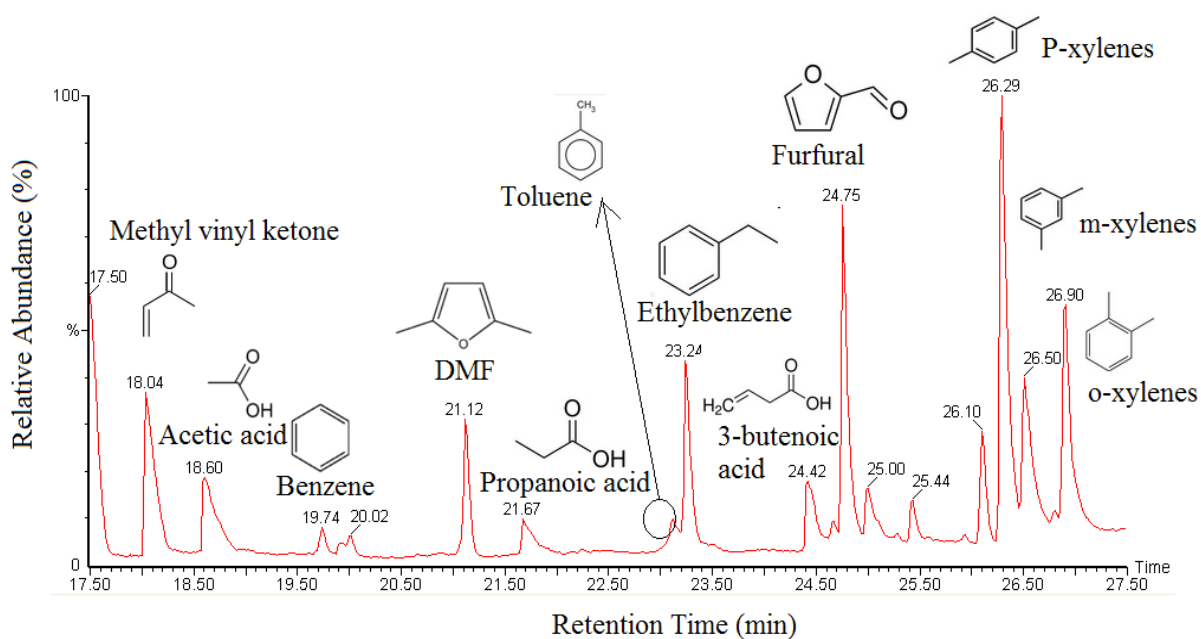
Figure 5-7: Chromatograms of HCs for MF at 6.5 bar IMEP (retention time: 17.5 to 27.5 min)

CHAPTER 6

6 Impact of Fuels on PM Emissions from a GDI Engine under various Injection Pressure and Injector Fouling Conditions

Followed by previous chapter (Chapter 5) which studied the gaseous emissions from GDI engine fuelled with biofuels, this chapter examines the impact of fuels (ethanol and gasoline) on PM Emissions from a GDI Engine under various injection pressure and injector fouling. Experiments were carried out under the operating conditions of stoichiometric combustion, 1500 rpm engine speed and 3.5-8.5 bar IMEP. Two fuels (gasoline and ethanol), four injection pressures ranging from 50 to 172 bar, and three fouled injectors were studied. SMPS was used to measure particle size distributions.

6.1   Introduction

In recent years, PM emissions from the GDI engine, especially the ultrafine particulates, have become a subject of concern. Euro 5b and coming Euro 6 emission standards put pressure on reducing PM emissions from GDI engines. Therefore, it is of vital importance to understand the characterization of particulates as well as the influence of different factors (engine type, fuel properties, and injection system) on their formation/oxidation mechanisms.

Unlike wall-guided GDI engines, spray-guided GDI engines have less fuel impingement on the piston crown; therefore the combustion is less diffusive. The particle emissions vary widely, depending on fuel properties such as aromatic content, volatility and oxygen content (Aikawa et al., 2010, Chen et al., 2012, Di Iorio et al., 2011, Liang et al., 2013, Leach, 2012, Armas et al., 2013, Labecki et al., 2012). A 'PM Index' for predicting

PM emissions from gasoline vehicles was concluded (Aikawa et al., 2010). They calculated the PM Index distribution of 1445 commercially available gasoline fuels from around the world and found that the PM Indices of gasoline fuels sold globally fall in a very wide band. It is well reported that compared to gasoline, pure ethanol produces much less PM emissions in GDI engines (Daniel et al., 2011, Di Iorio et al., 2011, Catapano et al., 2013).

Injection system, such as the injection pressure and injector fouling, is important in determining the engine-out PM characteristics. High DI injection pressure and good injector condition leads to higher spray velocity, shorter injection pulse and smaller droplets which are more widely distributed (Oh et al., 2012, He et al., 2012, Matousek et al., 2013). Injector fouling in GDI engines is a far greater concern than in PFI engines due to the injectors' harsher thermal conditions and its direct impact on the fuel and air mixture process, and combustion (Zhao et al., 1999, Arters and Macduff, 2000, Bardasz et al., 1999, Aradi et al., 2003). Berndorfer et al. (Berndorfer et al., 2013) studied a fouled injector and observed diffusion combustion phenomenon near the injector tip, after the main combustion in a GDI optical engine, leading to high soot and high HC emissions.

There is a need of better understanding PM characteristics in GDI engines, but detailed study of the impact of fuels on PM Emissions from a GDI Engine under various injection pressure and injector fouling is limited, especially concerning the close-space GDI engines. Even through it is clear that gasoline fuel and injection pressure both have significant impact on the particulate emissions in GDI engines, it is not clear which of those two factors is more prominent. Therefore, this paper examines the impact of fuel and injection system on PM emissions in a spray-guided GDI engine. Two fuels (gasoline and ethanol), four injection pressures (50, 100, 150 172 bar) and three injectors (one clean injector and two fouled injectors) were tested. The test conditions were shown in Table 6-1.

Table 6-1:   Engine operating conditions

Factors	Fuel	Injection Pressure (bar)	Injector number	Others
Injection pressure	gasoline	50, 100, 150, 172	# 3 (clean)	IMEP: 3.5-8.5 Lambda: 1 Engine speed: 1500 rpm, Start of injection: 280 ᵇTDC Ignition timing: MBT/KLSA
	ethanol	50, 100, 150	# 3 (clean)	
Injector fouling	gasoline	50, 150	# 1 (8.5%) # 2 (5.3%) # 3 (clean)	
	ethanol	150		

6.2   Impact of Injection Pressure

6.2.1   Gasoline

Figure 6-1 shows on the HC emissions for gasoline at 3.5-8.5 bar IMEP under various injection pressures. Higher injection pressure consistently led to decreased HC emissions within the entire tested load range due to improved spray atomization (He et al., 2012, Matousek et al., 2013).
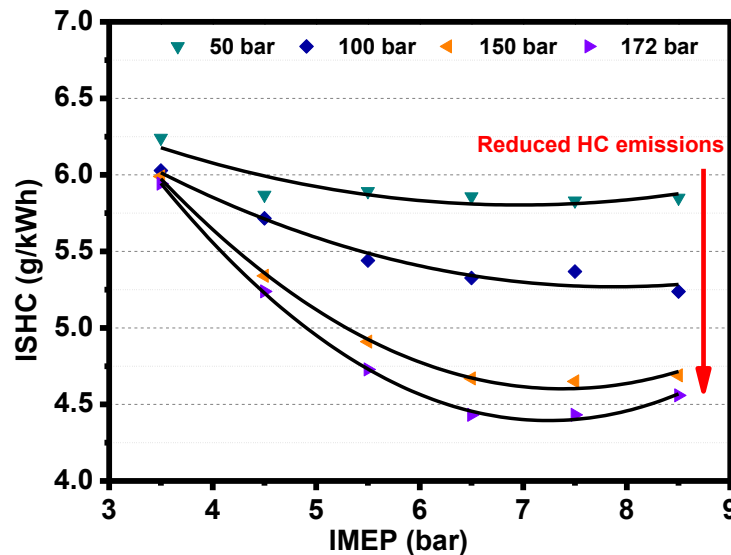
Figure 6-1:   HC emissions in a GDI Engine fuelled with gasoline under various injection pressures

Figure 6-2 shows the effect of injection pressure on particle size distributions in number (a, b and c) and mass (d, e and f) for gasoline at 4.5, 6.5 and 8.5 bar IMEP. At 4.5 bar IMEP, the particulate size distributions in number (Figure 6-2 (a)) and mass (Figure 6-2 (d)) had mono-peak shapes under 100-172 bar injection pressure, indicating that most of the particles were nuclei HCs and there were limited soot emissions. At 6.5 bar IMEP, the differences in particulate size distributions in number (Figure 6-2 (b)) were limited, however there were obvious differences in particulate size distributions in mass (Figure 6-2 (e)). At 8.5 bar IMEP, both the particulate size distributions in number (Figure 6-2 (c)) and mass (Figure 6-2 (f)) demonstrated dual-modal shapes and had completely different characteristics under various injection pressures.
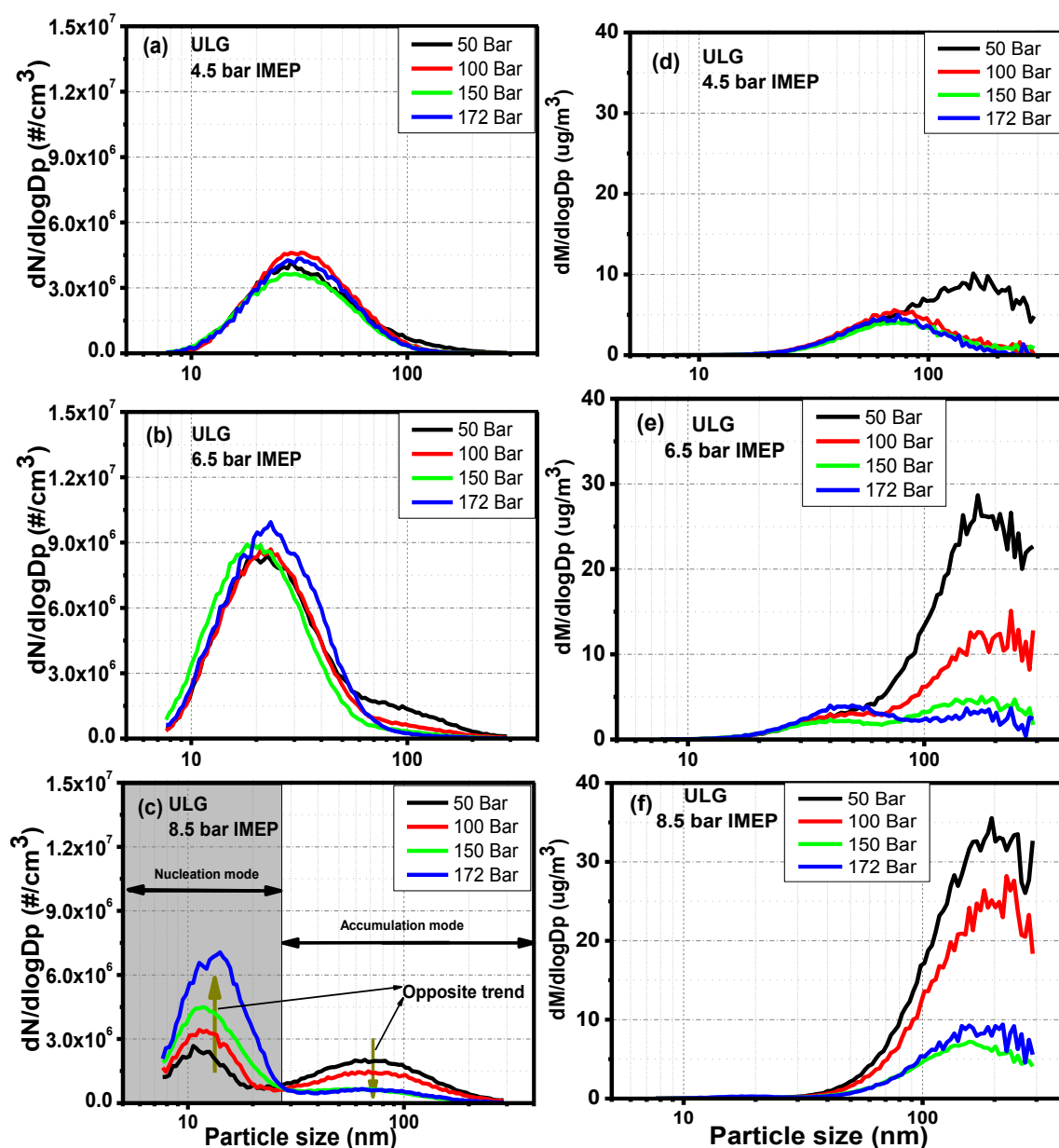
Figure 6-2: Particle size distributions in number (a, b and c) and mass (a, b and c) in GDI engine fuelled with gasoline under various injection pressures

Particle size distributions are composed of particles with different nature: (a) nuclei HCs which mainly compose the nucleation mode, and (b) soot agglomerates with HCs condensed or adsorbed on their surface, which compose the accumulation mode (Kittelson, 1998). Injection pressure affects particle size distributions through its impacts on both HCs and soot formation and the interactions between them. The interactions could be clearly observed in the particle size distributions in number at 8.5 bar IMEP (Figure 6-2 (c)). An

increased injection pressure resulted in increased PN in the nucleation mode. However, at 8.5 bar IMEP, higher injection pressure contributed to lower HC emissions (Figure 6-1), and lower soot emissions as indicated by the lower PN at the accumulation mode. The opposite trend is because soot not only directly determines the accumulation mode, but also has an indirect impact on the nucleation mode (Kittelson, 1998). High injection pressure reduced the soot formation and thus the available soot surface area for the HC adsorption or condensation, favouring hydrocarbon nucleation (Kittelson, 1998). Since the nucleation mode is the main contributor of PN emissions and the accumulation mode is the main contributor of PM emissions, it can be seen that there is an apparent trade-off in the PM and PN emission in the GDI engine at high injection pressures. This example reflects the complexity of particle emission analysis, necessitating separating/identifying of particles based on the particle nature.

The separation of particles from GDI engines into the nucleation and accumulation mode is not straightforward. Previous research shows that majority of particulates from GDI engines is composed of volatile material (unburnt HCs and lubricant) while soot only accounts for a small fraction (2%-29%), varying significantly on engine operating conditions (Price et al., 2007a).

There is no standard method to separate the nucleation and accumulation mode based on the particle nature, due to the complexity of particulate formation in the combustion process and evolution in the exhaust system. In most publications, particles were not classified into different modes, and analysis was done on total particle number and mass (He et al., 2012, Maricq et al., 1999, Farron et al., 2011, Myung et al., 2012, Ojapah et al., 2013). In some publications (Daniel et al., 2012a, Daniel et al., 2013, Daniel et al., 2011), particle size was used to separate PM modes, with 50-100 nm corresponding to the accumulation

mode and 0-50 nm corresponding to the nucleation mode, as originally proposed by Kittelson (Kittelson, 1998). Eastwood suggested that the nucleation mode is in the size range of less than100 nm and the accumulation mode is in the range of 100-900 nm (Eastwood, 2007). Obviously, particle size only partially reflects the particle nature; therefore we consider more interesting try to separate particulate by nature rather than just by size.

In this study, PM modes are separated based on the inflection point of the net particle size distribution using a Matlab script developed by the University of Castilla-La Mancha, which is also used in (Armas et al., 2011). This Matlab script has its limitation that it is only able to separate the PM modes if PM size distributions have dual-modal shapes with clear separated peaks or lightly/medium overlapped peaks. The PM size distribution is the sum of the nucleation and accumulation modes. For PM size distributions that are able to be separated by this Matlab script, an assumption is made that PM size distributions for the nucleation and accumulation mode are normal distributions. The left-side of the first peak of the PM size distribution is mostly from the nucleation mode and the right-side of the second peak is mostly from the accumulation mode. The separation point and lognormal fitted distributions are based on the criteria to minimise the difference between the distribution resulting to add the two fitted log-normal distributions (i.e. nucleation and accumulation) and the actual one.

At low engine loads, the nucleation mode in the particle size distribution overlaps largely with the accumulation mode, making the separation impossible. Only in some cases such as Figure 6-2 (c)), a dual-mode shape with a light overlap is observed and the separation can be easily made, which is presented in Figure 6-3 (a). In this operating condition, the high soot concentration increased the weight of PN in the accumulation mode and reduced that in the nucleation mode, which led to two clearly separated modes.

However, when soot formation is low, separation based on the particle size distributions expressed in number becomes difficult (e.g. 50 bar injection pressure and 6.5 bar IMEP, Figure 6-3 (b)).

Another approach to identify PM modes is proposed here. As the accumulation mode is the primary source of PM emissions, particle size distributions in mass could help to separate the modes. At 6.5 bar IMEP and high injection pressure, the particle size distribution expressed in mass had a dual-modal shape with a slight overlap (Figure 6-3 (c)). In this engine condition, there was a relatively low soot formation and lower HC emissions, compared with those of the lower injection pressure.
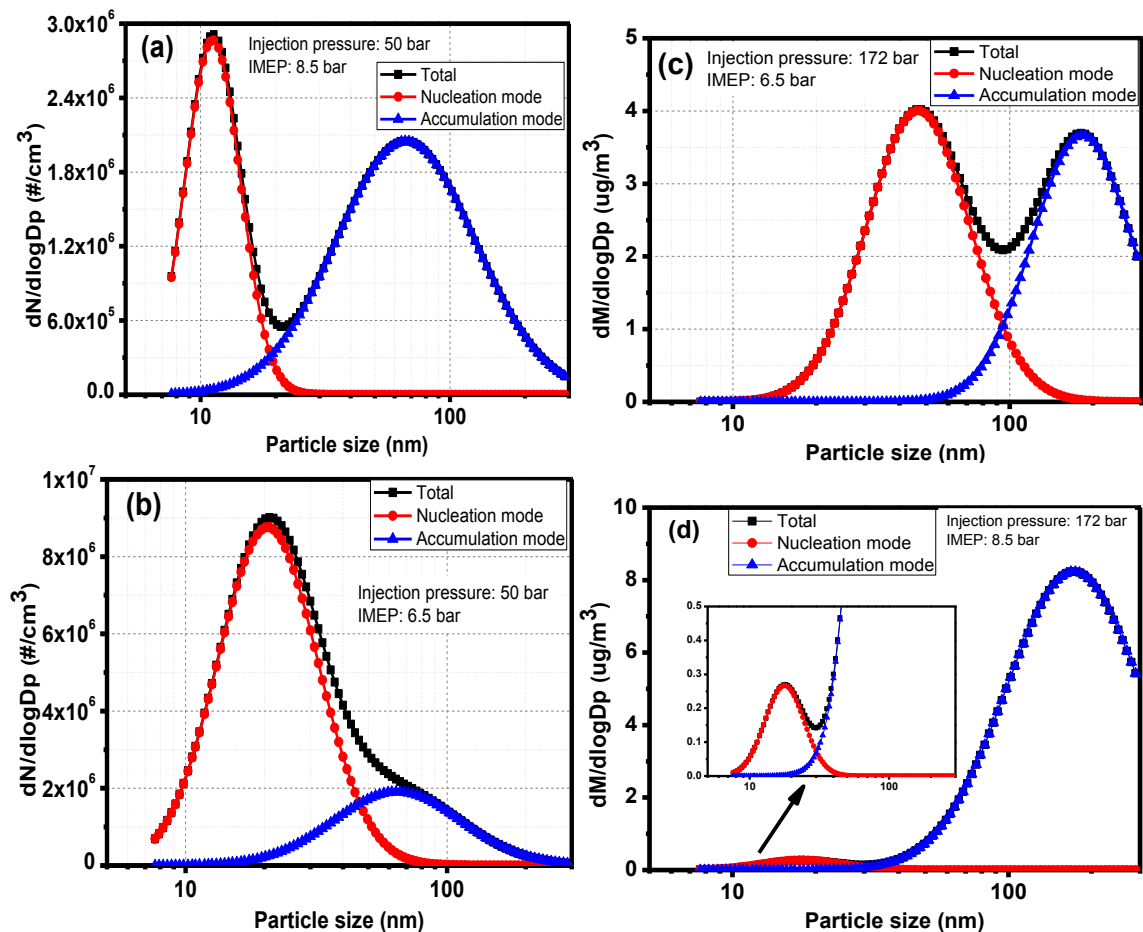
Figure 6-3: PM mode separations based on particle size distributions expressed in number (a, b) and mass (c, d)

Table 6-2 and Table 6-3 listed the possibility of particle mode separation based on particle size distributions in number and mass respectively. It can be concluded that high soot formation at high engine loads was the key for separation based on the particle size distribution in number, while at medium level of soot formation (such as 6.5 bar IMEP), the separation based on the particle size distribution in mass is possible.

Table 6-2:   Possibility of PM mode separation based on number distributions

		IMEP (bar)					
		3.5	**4.5**	**5.5**	**6.5**	**7.5**	**8.5**
	50	-	-	-	+	++	++
Injection	100	-	-	-	+	++	++
Pressure	150	-	-	-	-	+	++
	172	-	-	-	-	+	++

- Refers to the case of impossible mode separation
+ Refers to the case of possible mode separation however with some challenges such as in Figure 6-3 (b)
++ Refers to the case of very clear mode separation such as Figure 6-3 (a)

Table 6-3:   Possibility of PM mode separation based on mass distributions

		IMEP (bar)					
		3.5	**4.5**	**5.5**	**6.5**	**7.5**	**8.5**
	50	-	-	-	+	-	-
Injection	100	-	-	-	+	-	-
Pressure	150	-	-	-	+	+	-
	172	-	-	-	+	++	+

- Refers to the case of impossible mode separation
+ Refers to the case of possible mode separation however with some challenges such as in Figure 6-3 (d)
++ Refers to the case Refers to the case of very clear mode separation such as Figure 6-3 (c)
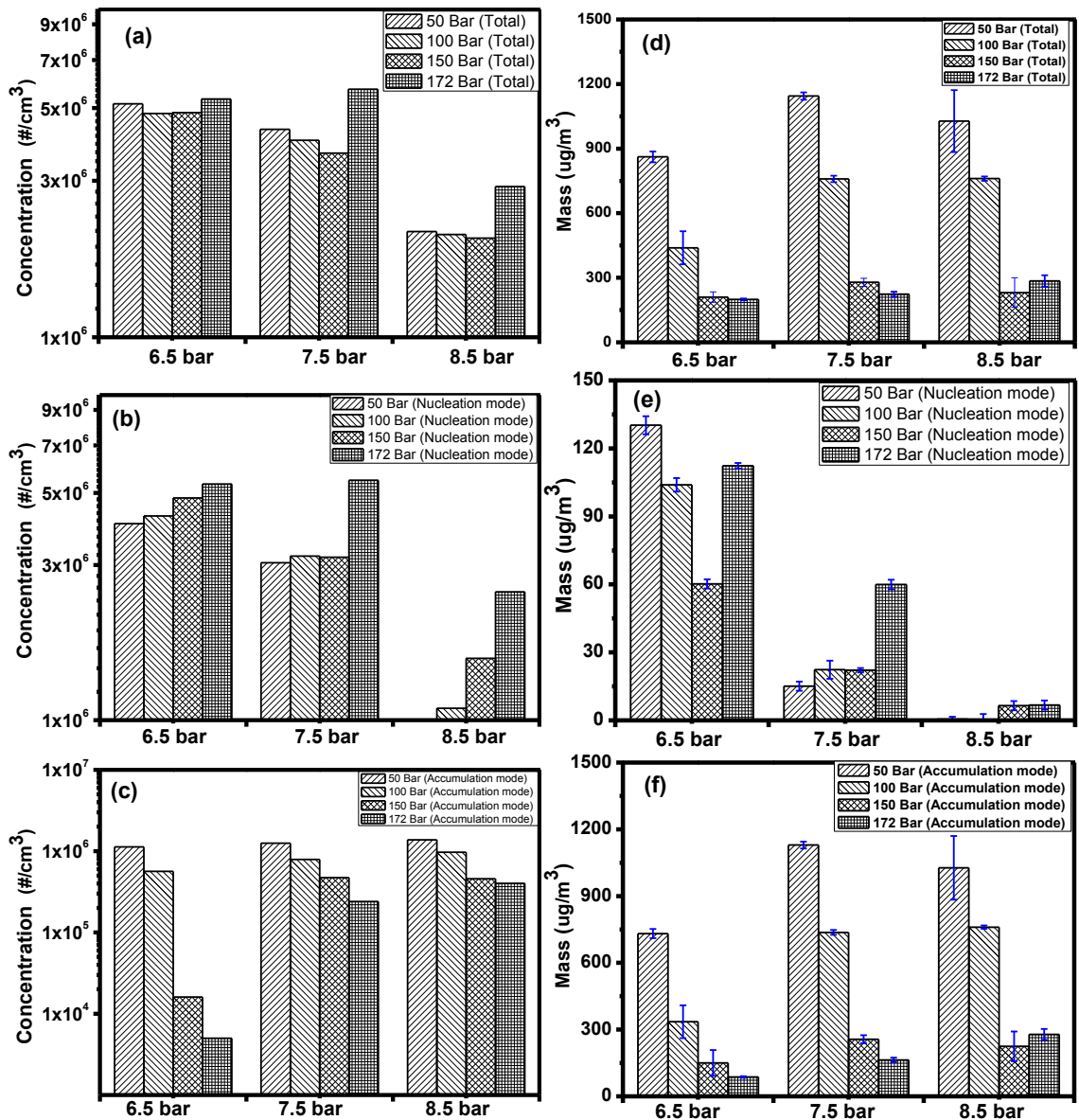
Figure 6-4:   PN (a, b and c) and PM (d, e and f) emissions in GDI engine fuelled with gasoline under various injection pressure

Table 6-2 and Table 6-3 listed the possibility of particle mode separation based on particle size distributions in number and mass respectively. It can be concluded that high soot formation at high engine loads was the key for separation based on the particle size distribution in number, while at medium level of soot formation (such as 6.5 bar IMEP), the separation based on the particle size distribution in mass is possible.

Table 6-2 and Table 6-3 listed the possibility of particle mode separation based on particle size distributions in number and mass respectively. It can be concluded that high soot formation at high engine loads was the key for separation based on the particle size distribution in number, while at medium level of soot formation (such as 6.5 bar IMEP), the separation based on the particle size distribution in mass is possible.

Table 6-2 and Table 6-3, it is possible to calculate PM mass and PN in the nucleation and accumulation mode independently, the result of which is presented in Figure 6-4. Increased injection pressure led to reductions of both PM and PN emissions in the accumulation mode. However, high injection pressure seemed to have a negative effect on PN emissions in the nucleation mode. The injection pressure of 172 bar consistently led to increased PN emissions in the nucleation mode compared to other tested injection pressures. This could be related to the reason mentioned earlier: low soot formation led to less soot surface available for HCs to be condensed or adsorbed on.

6.2.2   Ethanol

Figure 6-5 shows the effect of injection pressure on HC emissions for ethanol at 3.5-8.5 bar IMEP. Unlike from gasoline combustion, HC emissions from ethanol combustion were not sensitive to injection pressure. The explanation is that ethanol has one oxygen in its molecule, which gives it produce less soot compared with gasoline, due to more complete combustion (Di Iorio et al., 2011, Chen et al., 2012). On the other hand, even though low injection pressure led to more fuel impingement on the piston and cylinder liner, ethanol evaporated more easily due to its lower boiling point compared with gasoline. Figure 6-6 shows particulate size distributions in number (a and b) and in mass (c and d) for ethanol at

117

4.5 and 8.5 bar IMEP under various injection pressure. For all tested load and injection pressure conditions of ethanol, the particle size distributions consistently demonstrated mono-peaks, with the majority of particles in the diameters between 30 and 50 nm, suggesting that the soot formation in ethanol combustion is limited.
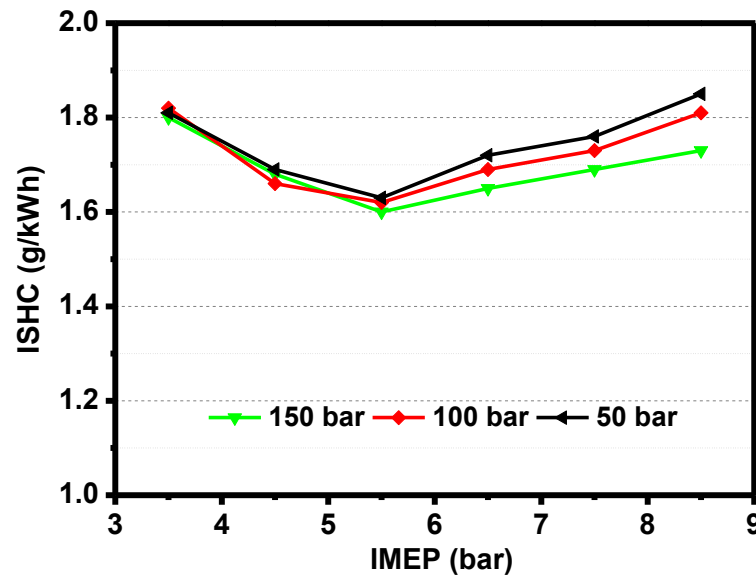
Figure 6-5: Effect of injection pressure on HC emissions in a GDI engine fuelled with ethanol
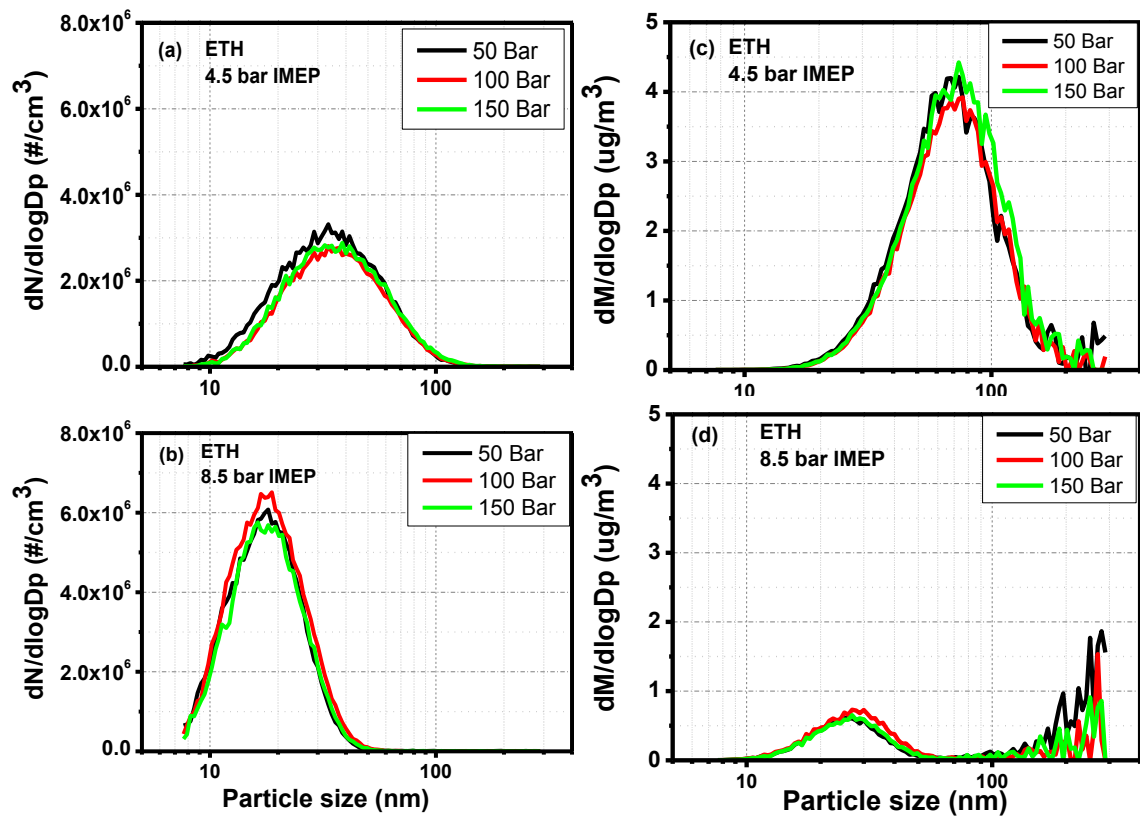
Figure 6-6: Effect of injection pressure on particle size distributions in number (a, b) and mass (c, d) in a GDI engine fuelled with ethanol
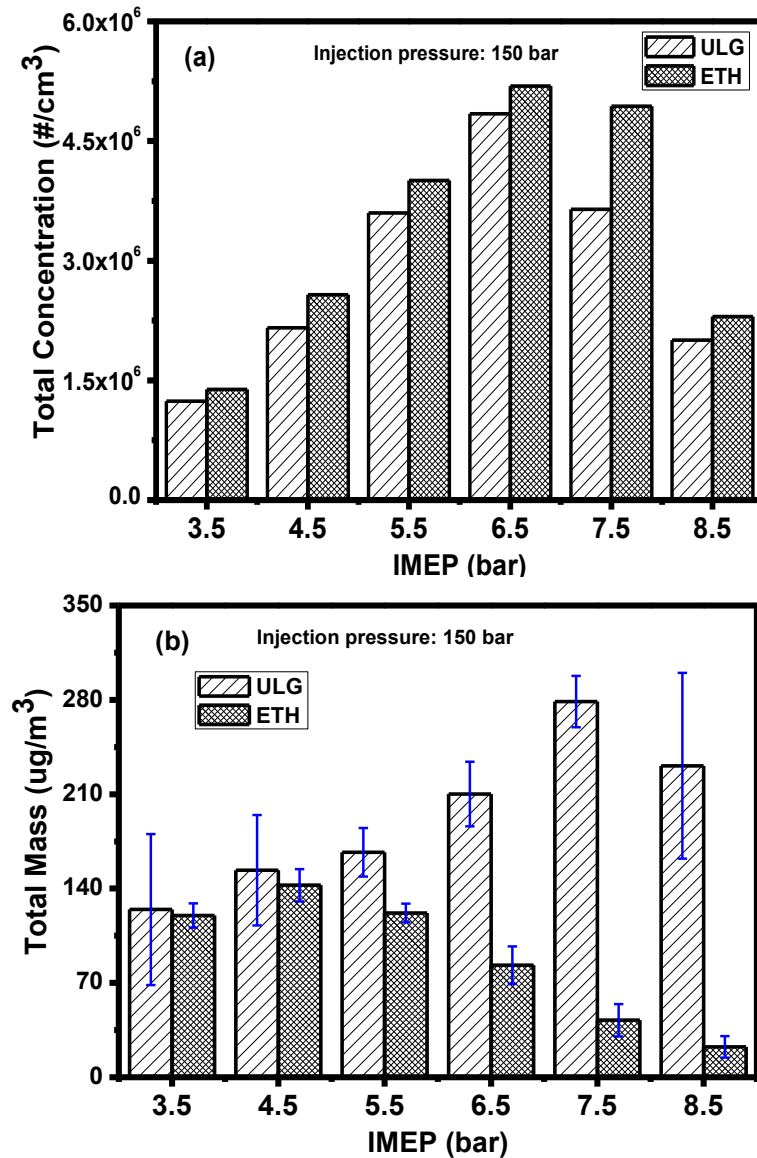
Figure 6-7: Comparison of (a) PN and (b) PM emissions from a GDI engine fuelled with gasoline and ethanol

Figure 6-7 shows the comparison of PM mass and PN emissions from gasoline and ethanol combustion under 150 bar injection pressure. Compared with PM mass emissions, PN emissions are less sensitive to fuel. The differences made by gasoline and ethanol in PN emissions are in the range of 6-16% whilst the difference in the PM mass emissions is about 3% at low load (3.5 bar) and up to 900% at high load (8.5 bar). The reason why ethanol has lower PM emissions compared to gasoline is due to ethanol's oxygen content and high volatility. Higher PN emissions from ethanol compared to gasoline is because of the

following two reasons. Firstly, while soot as nuclei provides the surface on which unburnt HC is adsorbed or condensed, ethanol has reduced soot particles and therefore most of the HC is formed from the particles in nucleation mode, which is the main contributor to the ethanol PN emissions. Secondly, the ethanol adsorbed on the soot has higher volatilities, compared to typical HCs in gasoline, and thus the PN emissions from ethanol combustion are higher.

6.3   Impact of Injector Fouling

6.3.1   Injector and Flow Rate Test

Three GDI injectors supplied by Bosch were studied, including two fouled ones that were used in previous engine testing at the University Birmingham. Various fuels were used for several months at the engine load of 3.5 to 8.5 bar IMEP. Carbon deposits were built up inside the injector nozzle and also on the injector tip. Flow rate bench, with an injection pressure of 150 bar and iso-octane as the test fuel, was used to characterise injector fouling. Injection pulse widths ranging from 0.3 to 6 ms were selected, and the fuel from 1000 injections was collected and weighted by a balance with a resolution of 0.1 g. Each injection width was repeated at least three times. Figure 6-9 shows the averaged results. Injector 1 and 2 had a flow rate loss of 8.5% and 5.3% respectively. Injector 3 is a clean injector. After the flow rate test, the injectors were used in the GDI engine and PM emissions were measured by SMPS.
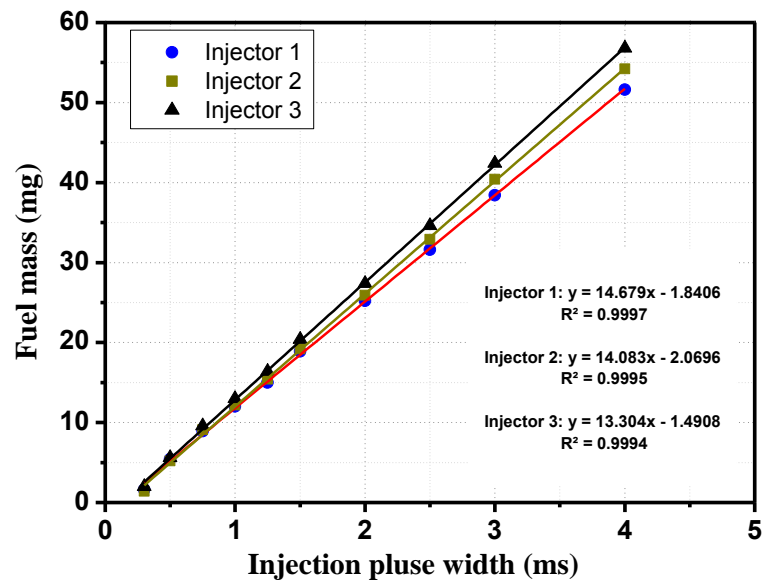
Figure 6-8:   Injector flow test for Injector 1-3
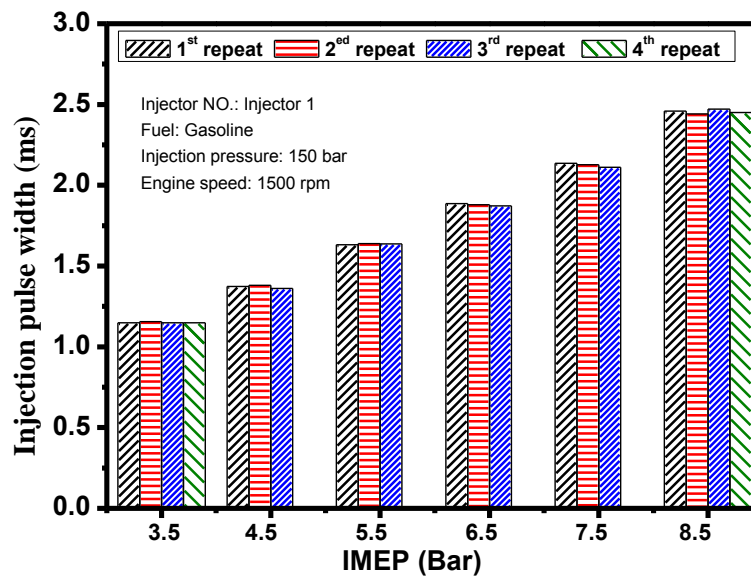
Figure 6-9:   Injection pulse widths for Injector 1 at 3.5-8.5 bar IMEP

It is essential to make sure that the injector condition is consistently throughout PM measurement, and thus the possibility that injector deposits are washed away or further accumulated during the experiment has been considered. The variation in injection pulse width for a certain injection quantity was used as a simple indicator of the variation of injector condition. The engine test designed for the study of the effect of a fouled injector on

PM emissions lasted 3 hours for each injector. Each engine operating point for every injector was repeated for at least three times and the injection pulse width was recorded. There was no evidence that injector 1 and 2 experienced any noticeable change during the PM measurement in this study. Figure 6-9 shows the injection pulse width of injector 1 throughout the PM measurement. It is clear that the injection pulse width in the 3 tests had very good repeatability and therefore, it is believed that the injector conditions throughout the experimental study were consistent.

In summary, although injectors were not fouled using a systematic fouling engine testing cycle, fouled injectors were accurately characterised, and their conditions stayed consistent throughout the entire PM measurement.

6.3.2   Gasoline
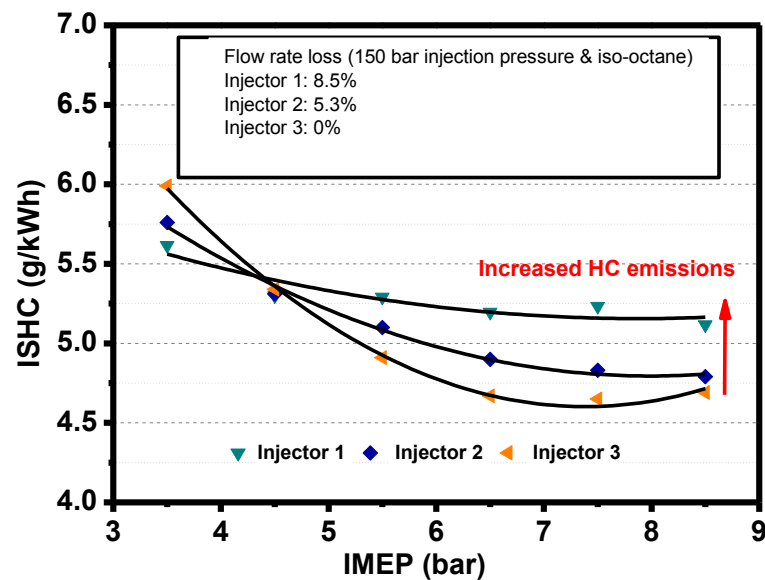
Figure 6-10:   HC emissions for gasoline at 150 bar injection pressure when using GDI injector 1, 2 and 3 (engine speed=1500 rpm, λ=1)

Figure 6-10 presents HC emissions for gasoline at 3.5-8.5 bar IMEP at 150 bar injection pressure when using GDI injector 1, 2 and 3. Compared with the clean injector

(#3), the fouled injector (#1) yielded approximately 10% higher HC emissions at the engine load range of 5.5-8.5 bar IMEP. Similar results are also reported in other publications (Joedicke et al., 2012, Sandquist et al., 2001). This is possibly linked to the increased fuel impingement due to longer injector pulse width resulting from injector fouling. The fuel film continues to evaporate during the combustion stroke and therefore diffusive combustion occurs, which leads to high HC and soot formation. Another reason is possibly related to the gasoline adsorbed on carbon deposits near the injector tip. The adsorbed gasoline contributes to the diffusive combustion after the main combustion, which is reported in (Berndorfer et al., 2013) using optical diagnostics. The distorted spray which leads to imperfect air/fuel mixture preparation is also another reason for high HC emissions (Zhao et al., 1999, Arters and Macduff, 2000, Bardasz et al., 1999, Aradi et al., 2003).

Figure 6-11 shows the impact of injector fouling on the particulate size distributions in number (a, b and c) and mass (d, e and f) for gasoline at 4.5, 6.5 and 8.5 bar IMEP under 150 bar injection pressure. The clean injector (#3) consistently had better particulate size distributions in number and mass. At 4.5 and 6.5 bar IMEP, it is clear that the fouled injector (#1) produced significantly higher particulate size distributions in number. At 8.5 bar IMEP, the benefit of the clean injector (#3) regarding particulate size distributions in mass is obvious.
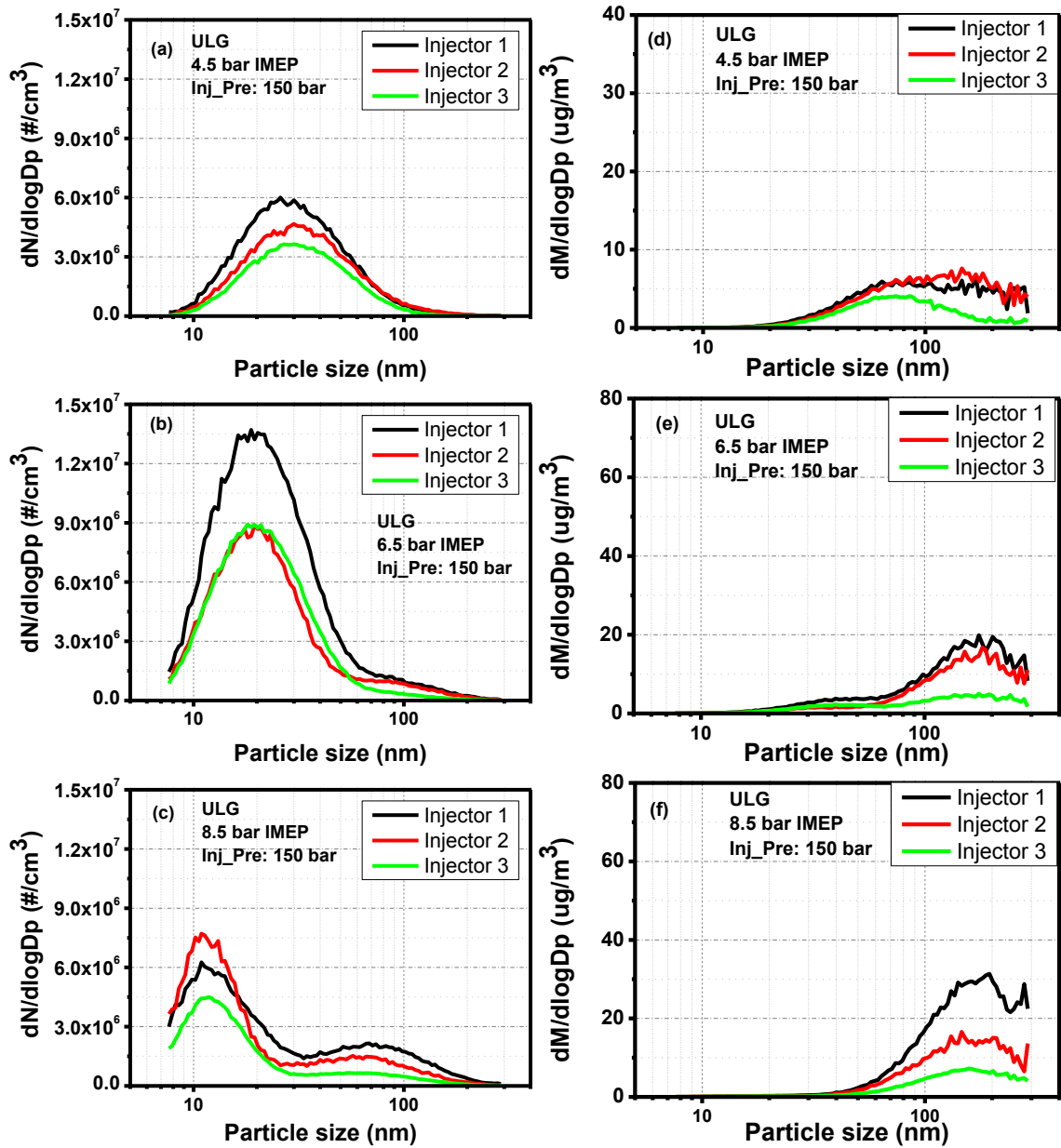
Figure 6-11: Particle size distributions in number (a, b and c) and mass (d, e and f) in a GDI engine fuelled with gasoline at 150 bar injection pressure when using GDI injector 1, 2 and 3 (engine speed=1500 rpm, λ=1)
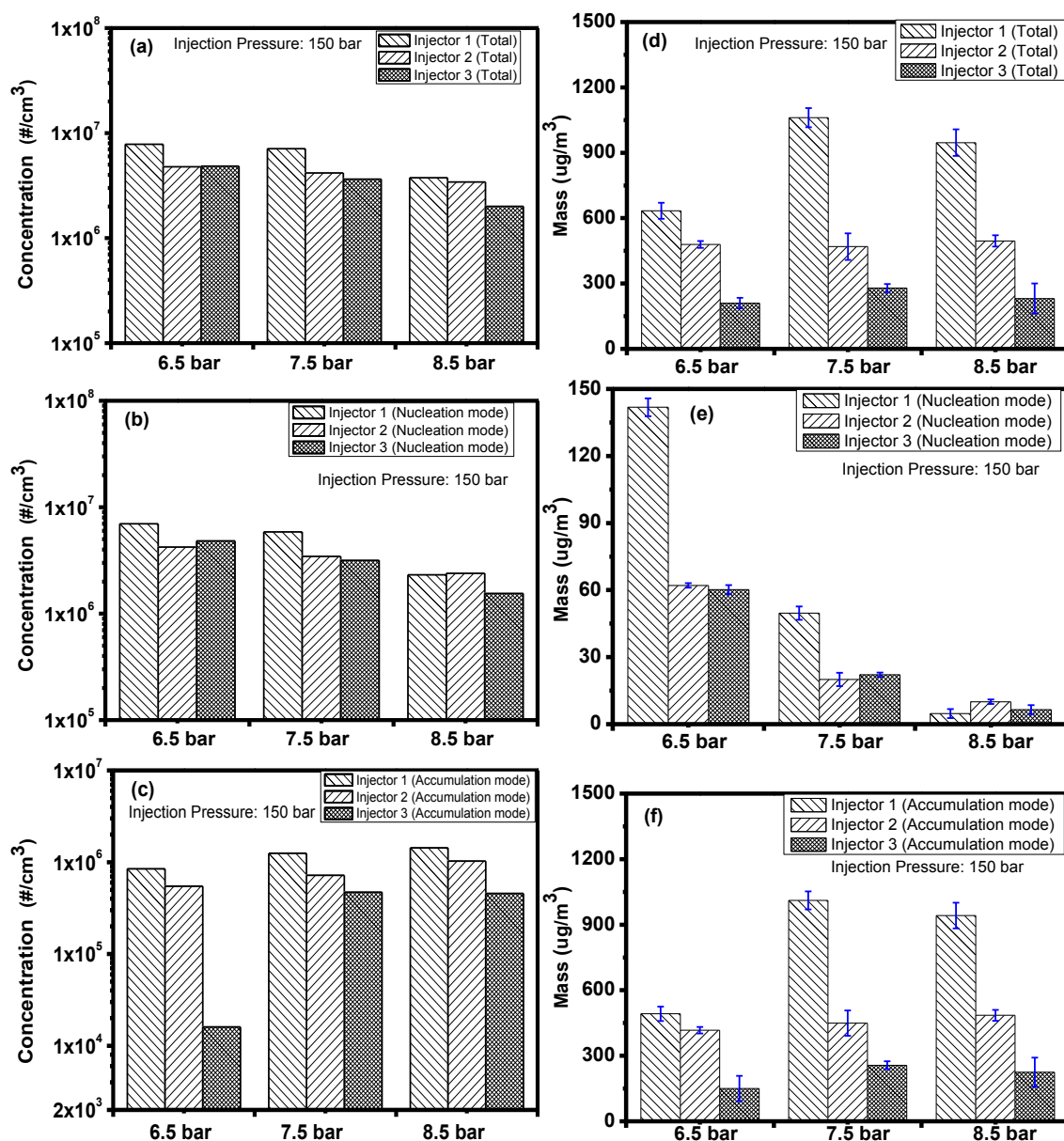
Figure 6-12: PN (a, b and c) and PM (d, e and f) emissions in GDI engine fuelled with gasoline at 150 bar injection pressure when using GDI injector 1, 2 and 3

The particulates at 6.5-8.5 bar IMEP were separated into the nucleation and accumulation modes, using the same method described in the section 3.1.1. Figure 6-12 presents the impact of injector fouling on PM and PN emissions at 6.5-8.5 bar IMEP at 150 bar injection pressure. At all tested engine loads, the clean injector 3 (#3) consistently led to the lowest PM and PN emissions. The high PM and PN in the accumulation mode for the fouled injector is the direct indicator of high soot formation, which is a result of diffusive

126

combustion. Increased fuel impingement, gasoline adsorption on the deposit on the injector tip, and distorted spray all contribute to the diffusive combustion. The maximum difference was observed at the highest engine load 8.5 bar IMEP, in which the PN emissions of the clean injector (#3) were nearly 53% and 58% of those of the fouled injectors (#1) and (#2) respectively.

Figure 6-13 shows combustion parameters such as peak in-cylinder pressure, combustion initiation duration (CID), and combustion duration for injector (#1) and (#3) at 3.5-8.5 bar IMEP and 150 bar injection pressure. The CID is defined as the crank angle interval between the start of spark discharge and 5% mass fraction burned (MFB). The combustion duration is defined as the crank angle interval between 10% and 90% of MFB.

Unlike PM emissions, those combustion parameters are not significantly sensitive to the fouled injectors, therefore, only results from injectors (#1) and (#3) are presented. It is clear that for the fouled injector (#1) the peak pressure is slightly increased by up to 0.7 bar for the engine load range of 3.5-8.5 bar IMEP, resulting from its slightly longer combustion duration (by up to 0.5 CAD). However, there is almost no difference in CID between injectors (#1) and (#3).
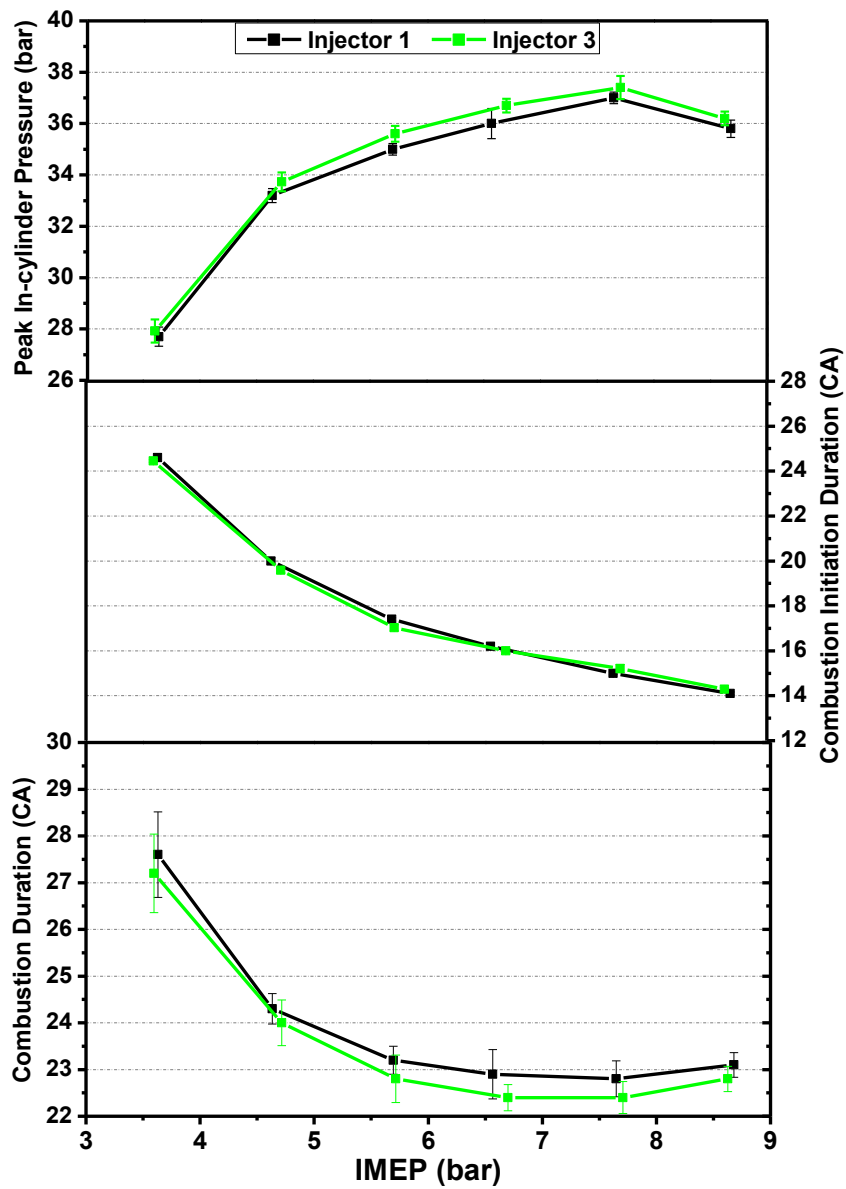
Figure 6-13: Peak in-cylinder pressure, combustion initiation duration (CID), and combustion duration for injectors (#1) and (#3) in a GDI engine fuelled with gasoline at 150 bar injection pressure
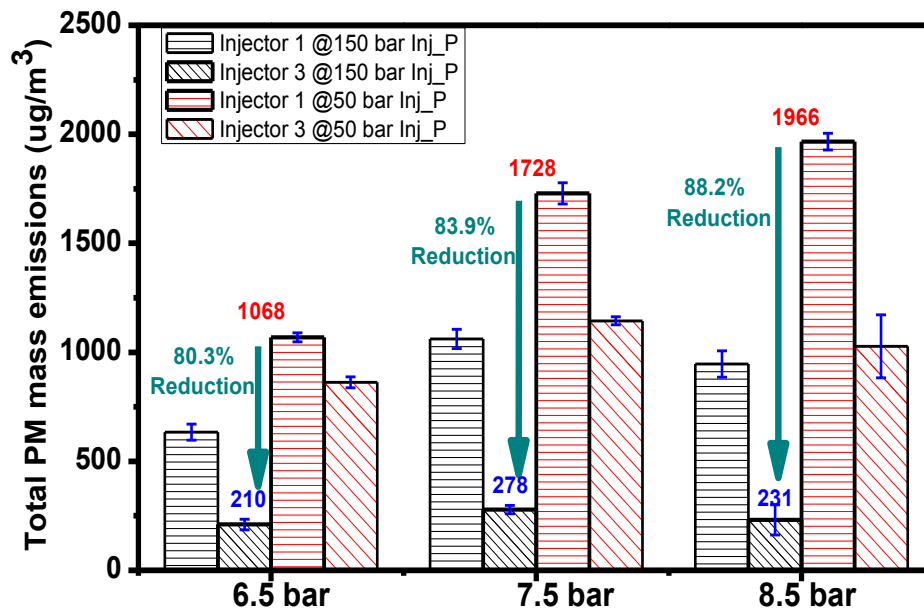
Figure 6-14: Comparison of total PM emissions for injectors 1 and 3 under 150 and 50 bar injection pressure at 6.5-8.5 bar IMEP

Figure 6-14 shows the comparison of PM and PN emissions for injectors (#1) and (#3) under 150 and 50 bar injection pressure at 6.5-8.5 bar IMEP. Compared with the fouled injector (#1) at 50 bar injection pressure (the worst injection system), the clean injector (#3) at 150 bar injection pressure (the best injection system) led to a reduction of the PM emission by 80.3-88.2%. This demonstrates how much difference the condition of the injection system can make to the particle emissions from the gasoline engine.

It is known that variations of fuel specifications on the market lead to variations of PM emissions from gasoline fuelled vehicle engines (Khalek et al., 2010, Leach, 2012, Aikawa et al., 2010). Aikawa et al. proposed a 'PM index' for predicting the PM emissions for gasoline vehicles ((Equation 6-1) (Aikawa et al., 2010).

$$I\,(VP, DBE) = \sum_{i=1}^{n}(DBE_i + 1)/(VP\_443\,K)_i)] \times W_{ti} \qquad \text{(Equation 6-1)}$$

Here, *VP_443 K* means vapour pressure of a single component *i* at the temperature of 443 K. W_{ti} means the weight fraction of the single component *i*. DBE represents the double bond equivalent ((Equation 6-2).

$$DBE = (2C - H + 2)/2 \qquad \text{(Equation 6-2)}$$

More detailed information about the 'PM Index' is available in (Aikawa et al., 2010). Aikawa et al. calculated the PM Index distribution for 1445 worldwide commercially available gasoline fuels (Fig.12 in (Aikawa et al., 2010)) and found that the PM Indices for the gasoline fuels sold globally fell in a very wide band, ranging from 0.67 to 3.86. If excluding the top and bottom 10% of the data, the PM Indices for the remaining 80% fuels fall into the range of 1 to 2.2. Based on the PM Index model, the fuel with the PM index value of 1 reduces the PM emissions by 54.5% compared to the fuel with a PM index value of 2.2. Given the results in the present study using a different injection system, it appears that the difference in PM emissions made by the injection system cleanliness can be more important than that made by the gasoline fuel composition.

6.3.3   Ethanol

Figure 6-15 presents HC emissions for ethanol at 150 bar injection pressure using injector 1 and 3. It is clear that the fouled injector (#3) did not have a significant negative impact on HC emissions from the ethanol fuelled GDI engine. Figure 6-16 shows the the particulate size distributions in number (a and b) and mass (c and d) for ethanol at 4.5 and 8.5 bar IMEP at 150 bar injection pressure using injector 1 and 3. Again, injector fouling had a limited impact on the particulate size distributions in both number and mass. It is almost certain that fuel impingement and fuel adsorption on the deposit near the injector tip

is increased due to injector fouling; however the results show that, unlike gasoline, HC and soot formation is not increased when using ethanol is because ethanol evaporates more easily and diffusive combustion is not increased as much as the case of gasoline. On the other hand, compared to the diffusive combustion of gasoline, the diffusive combustion of ethanol leads to lower HC and soot formation due to the oxygen content within the ethanol molecule.
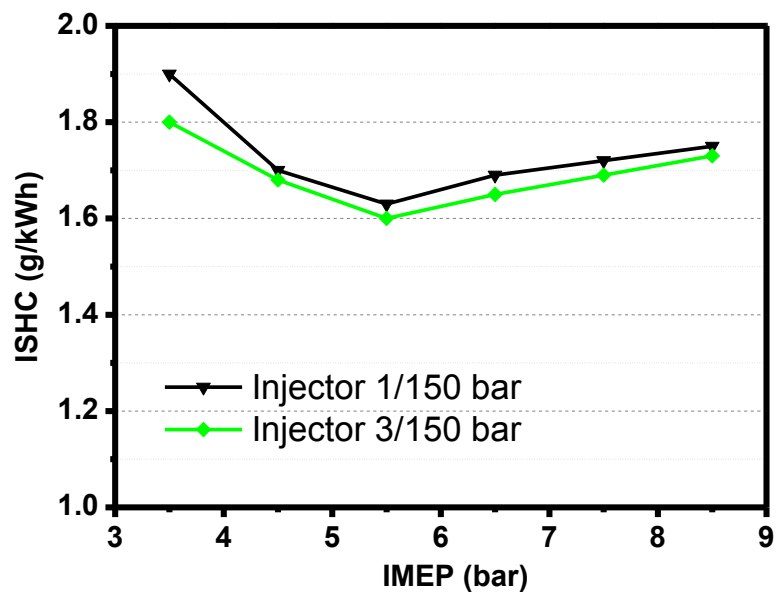
Figure 6-15: Effect of injector fouling on HC emissions for ethanol at 150 bar injection pressure
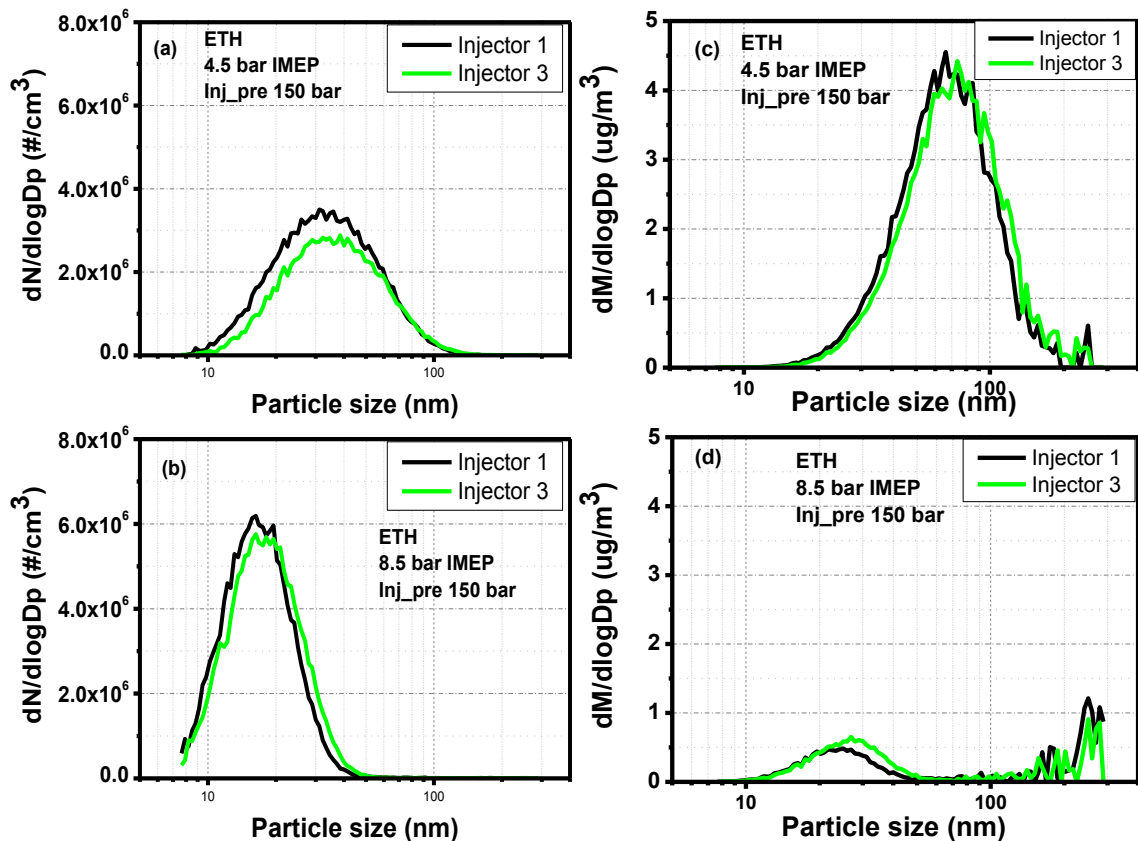
Figure 6-16: Effect of injector fouling on particle size distribution in number (a and b) and mass (c and d) in a GDI engine fuelled with ethanol at 150 bar injection pressure

6.4   Conclusions

The impact of fuels (ethanol and gasoline) on PM Emissions from a GDI Engine under various injection pressure and injector fouling was studied in this chapter. Experiments were carried out under the operating conditions of stoichiometric combustion, 1500 rpm engine speed and 3.5-8.5 bar IMEP. Two fuels (gasoline and ethanol), four injection pressures ranging from 50 to 172 bar, and three fouled injector were studied. SMPS was used to measure particle size distributions. The following is the main conclusions of this study.

1.   Compared with gasoline, ethanol combustion produced much less PM mass emissions, especially at high engine load, which is mainly because of its significantly lower soot formation resulting from its 34% oxygen content in its molecule. However, PN

emissions from ethanol combustion were higher than those from gasoline combustion. This is because, unlike gasoline, most of unburnt HCs from ethanol formed the condensed nano-particles in the nucleation mode, and only a small fraction of unburnt HC is attached or adsorbed on the limited soot surface.

2.   High injection pressure improves the particle emissions from a GDI engine fuelled with gasoline, because of better spray atomization. By increasing the injection pressure from 50 bar to 150 bar, PM and PN emissions were decreased by up to 22% and 78% respectively. However, increasing the injection pressure further to 172 bar, PN emissions were increased because of a significant increase in the nucleated HC particles. It seems that there is a trade-off between the PM and PN emissions from GDI engines at certain engine conditions.

3.   Injector fouling should be considered carefully in the combustion system design in the close-concept GDI engines. Fouled GDI injector affects PM emissions increasing both HC and soot formation, resulting from the diffusive combustion due to fuel impingement and fuel adsorption on the deposit near the injector tip. Fouled injectors could increase PM mass emissions by up to ten times as shown in this study. Unlike in the case of gasoline, PM emissions from ethanol combustion are not sensitive to the injection system. The HC and soot formation are not evidently increased when low injection pressure and fouled injectors are used, which is because ethanol evaporates more easily and thus experiences less diffusive combustion.

Furthermore, it is hypothesised that the differences in PM emissions made by injection system (pressure and injector fouling) are more significant than the differences made by the composition of commercial gasoline fuels on the market. The data from Honda shows that the PM Index of 80% of worldwide commercially available gasoline fuels is within the

range of 1 to 2.2, indicating a difference of up to 54.5% in the corresponding PM emissions.

The difference made in PM emissions by the injection system is up to 88% in this study. In

the real filed, injector fouling can be much worse than the fouled injectors used in this study.

However, this hypothesis needs further and comprehensive investigation.

CHAPTER 7

7 PM Composition and Soot Oxidation for PM Emissions from a GDI Engine Fuelled with DMF, Ethanol and Gasoline

Followed by the previous chapter (Chapter 6), investigating the impact of fuel and injection system on PM emissions from a GDI engine, this chapter exams the study of PM composition and soot oxidation for PM emissions from a GDI engine fuelled with DMF, ethanol and gasoline. Information of PM composition and soot oxidation is also important for the design of high efficient GPFs and improving GPFs' durability.

The GDI engine was operated at fixed 1500 rpm engine speed with rich combustion and late fuel injection strategy, representing one of the worst scenarios of PM emissions in GDI engines. A TGA method was optimized and then used for analysing PM from GDI engines. A kinetic model was used to interpret the data from TGA and quantitatively describe the soot oxidation reactivity.

7.1 Introduction

The previous chapter investigated gasoline's and ethanol's PM emissions under different injection systems. Results shows that, compared to gasoline, ethanol produces less PM emissions, which are also less sensitive to fuel injection system. Therefore, it would be interesting to study PM composition, as well as soot oxidation from PM produced in GDI engines. On the other hand, research evidence shows that PM emissions produced from lean combustion GDI vehicles are similar to or even more than those from compression ignition engines equipped with DPFs (Mathis et al., 2005, Andersson et al., 2008). The stringent PM regulations may not be satisfied by pushing the boundary of

engine optimization, and/or using green fuels alone. There is a potential that, in the future, GPFs will be applied on GDI engines, just like DPFs on diesel engines. Many investigations have been done on the GPFs (Richter et al., 2012, Chan et al., 2013, Kim et al., 2013). To improve durability of GPFs, a better knowledge of soot oxidation characteristics is required.

The detailed specification of Perkin Elmer TGA used in this study can be found in Chapter 2. TGA is a widely applied in the study of PM emissions from diesel engines. The sample atmosphere can be any gas, depending on the research objective. For example, when PM sample is placed and heating up in the N_2/Argon gas atmosphere, the volatilities in PM sample will evaporate. When air or oxygen is used as gas atmosphere, soot will react with the gas.

TGA is relatively easy to operate; however, there are several key factors with respect to the instrument and sample that are critical to the TGA reliability and repeatability of measurement. These factors include the balance, furnace, temperature, sample mass, sample atmosphere gas flow rate and heating ramps. The balance, furnace and temperature are independent to sample and can be calibrated according to standard operation procedures. Optimising soot sample mass is important, because not enough soot samples may lead to inaccurate results whilst too much sample will lead to the oxidation process largely controlled by diffusive oxidation. The heating ramp setting in the TGA is also significantly important because it affects the accuracy of the results (Rodríguez-Fernández et al., 2011). A lower heating ramp can improve the accuracy and reliability of results but the test can be very long. Therefore in this study an optimised sample mass and heating ramp are investigated. Then this optimized TGA method was used to the study of study of the impact of fuel and engine load on PM composition and soot oxidation for PM emission

produced from the combustion of gasoline, ethanol, E25 and DMF in the GDI engine. The

engine test conditions are listed in Table 7-1.

Table 7-1:   Engine test conditions

	Fuel	IMEP (bar)	λ	Engine speed (rpm)	Start of Injection (SOI) (˚bTDC)
TGA method development	Gasoline	8.5	0.9	1500	100
Effect of fuel	Gasoline, DMF, E25, Ethanol	8.5	0.9	1500	100
Effect of engine load	Gasoline, DMF	5.5 and 8.5	0.9	1500	100

7.2   Arrhenius-type Reaction Model

The data produced by TGA was quantitatively analysed and described by a general

reaction model, called Arrhenius-type reaction model. It is widely used in many other

literatures in modelling the soot oxidation process (Rodríguez-Fernández et al., 2011, Yang

et al., 2010, Karin et al., 2011, Mendiara et al., 2007, Stratakis and Stamatelos, 2003). The

mathematical expression of this Arrhenius-type reaction model is presented as below.

$$-\frac{dm}{dt} = k_c m^n p_{O_2}{}^r = A * exp\left(\frac{-E_a}{RT}\right) * m^n * p_{O_2}{}^r \qquad \text{(Equation 7-1)}$$

where m represents mass; t, represents time; k_c represents the oxidation rate constant; A

represents exponential factor; E_a represents activation energy of soot oxidation; p_{O_2}

represents the partial pressure of oxygen; n and r are the reaction orders of sample and

oxygen, respectively; R, the universal gas constant; and T, the temperature. In most of the

cases, for the purpose of simplification, the reaction orders, n and r, are set as unity

(Rodríguez-Fernández et al., 2011, Yang et al., 2010).

$$\ln\left(-\frac{1}{m}\frac{dm}{dt}\right) = -\frac{E_a}{R}\frac{1}{T}+\ln\left(Ap_{O_2}\right) \quad \text{(Equation 7-2)}$$

When logarithms are taken in both left and right side of the (Equation 7-1, a derived new equation ((Equation 7-2) can be used to calculate the activation energy. In (Equation 7-2, a line can be derived with *1/T* as x and $\ln\left(-\frac{1}{m}\frac{dm}{dt}\right)$ as y. The slope of this line equals to $-E_a/R$.

7.3   TGA Method Development
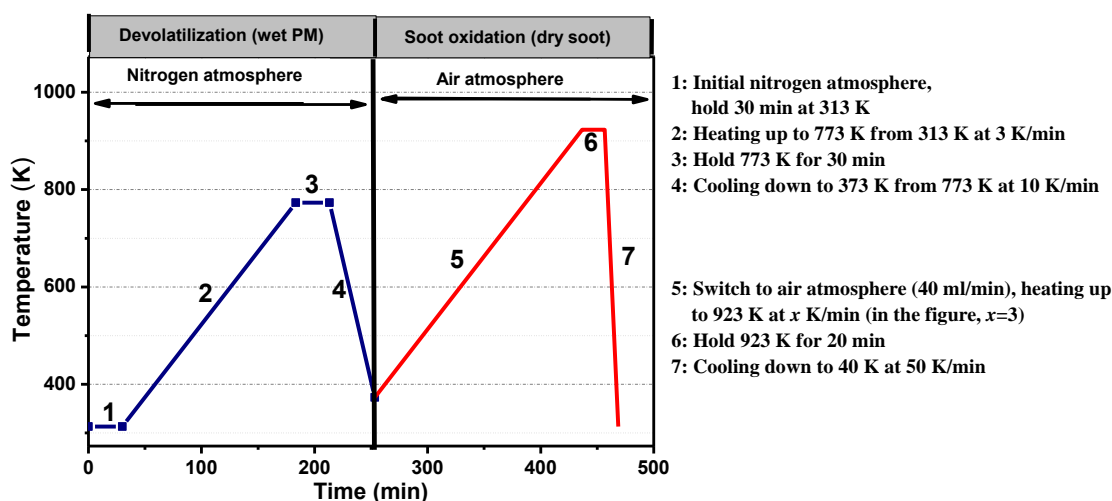
Figure 7-1:   TGA method

Figure 7-1 illustrated the TGA method. Because the PM collected on the filter contains volatile materials adsorbed/condensed on the soot, it was important to remove all of the volatile material before the oxidation process. Steps 1-3 in Figure 7-1 presents this devolatilization treatment, which includes heating PM sample in a N_2 atmosphere up to 773 K at the rate of 3 K/min, and then maintaining at 773 K for 30 min to ensure a complete removal of volatile materials. The devolatilization profiles of PM became flat after maintaining 773 K for 30 min under an N_2 atmosphere. Oxygen-free nitrogen was selected to ensure that no soot will be oxidized during the devolatilization treatment. The mass of volatile materials is the weight difference before and after the devolatilization treatment.

Step 4 was designed to cool furnace down to 373 K. In step 5, air is used as the sample atmosphere. Step 6 was added to make sure that soot was completely oxidized by heating up the sample up to 923 K. The temperature of 923 K is chosen because of two considerations. First of all, filter should not be melted. Secondly, soot has to be fully oxidized. The temperature of 923 K satisfies both considerations. The mass of soot in the PM sample is the sample mass loss before and after the oxidization process.

7.3.1   Effect of Heating Ramp

Soot samples of approximately 0.1 mg were used in the investigation of heating ramp on soot oxidation. Figure 7-2 shows the soot weight profiles at various heating ramp. It is clear that soot oxidation process was highly sensitive to heating ramp. When using high heating ramp (larger than 5 K/min) Soot, which can be oxidized in low temperatures, was only partially oxidized because of the over-high heating ramp and was continued to be oxidized at higher temperature range. When the heating ramp was slowed to 3-5 K/min, the differences between the soot weight profiles were insignificant.
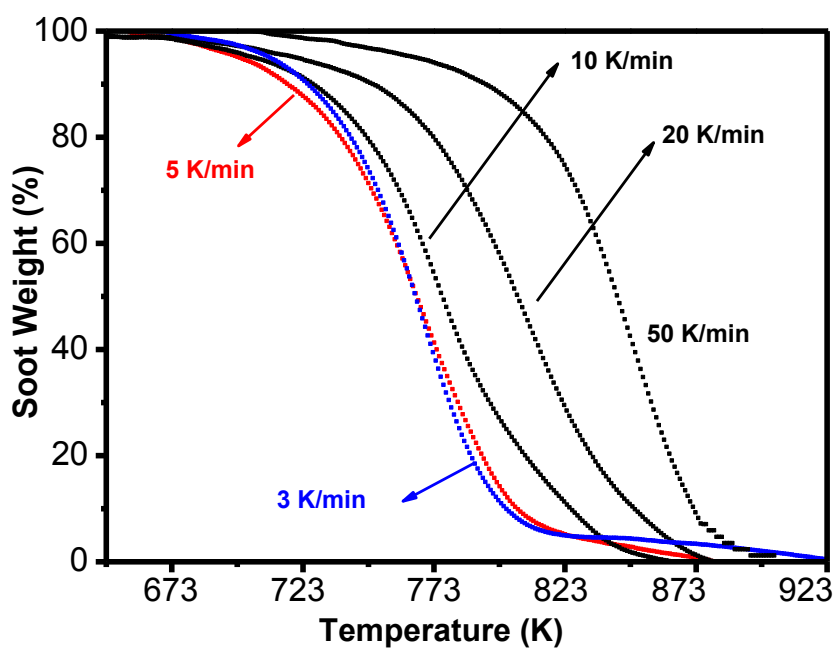
Figure 7-2:   Soot weight profile at various heating ramps
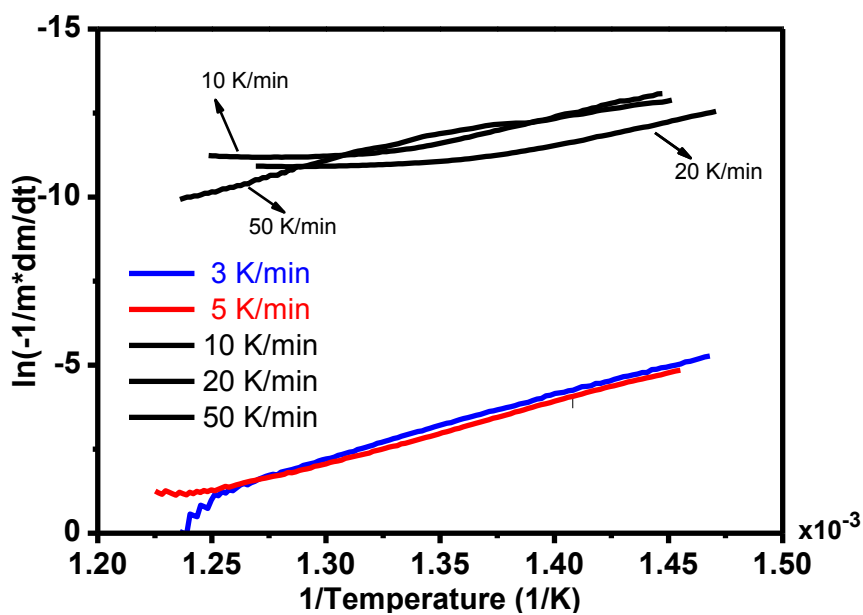
Figure 7-3:   Kinetic model at various heating ramps

Table 7-2:   Reactive energy at various heating ramps

Heating ramp (K/min)	Ea (kJ/mol)	R^2
3	153.0	0.9901
5	145.0	0.993
10	84.0	0.8993
20	67.1	0.8903
50	114.5	0.9754

Figure 7-3 shows the kinetic model using different heating ramp setting in TGA. Table 7-2 lists the activation energy calculated from the slop of lines shown in Figure 7-3. It is clear that, for the 3-5 K/min heating ramp, the linearity of the lines ((Equation 7-2), as indicated by R^2, is high, with the calculated activation in a small range of 145 and 153kJ/mol.

7.3.2   Effect of Soot Mass

Soot samples of 0.025-0.111 mg were collected and analysed. The optimized heating ramp of 3 K/min was used. A high sample mass increases the result accuracy, however an excessive sample mass leads to diffusive reactions due to the deep sample layer is potentially inaccessible to the oxidation (Rodríguez-Fernández et al., 2011). Figure 7-4 shows soot derivative weight profiles at various soot mass. Figure 7-5 shows the effect of soot mass on two oxidation parameters, the activation energy and maximum mass loss rate temperature (MMLRT). MMLRT is the temperature that leads to the highest sample weight loss rate. For a sample with a mass larger than 0.04 mg, the activation energies are between 146 and 152.4 kJ/mol and the MMLRTs are between 490 and 494 K. Even though it seems that soot sample as low as 0.025 mg leads to good results of soot oxidation, soot of more than 0.040 mg is recommended.
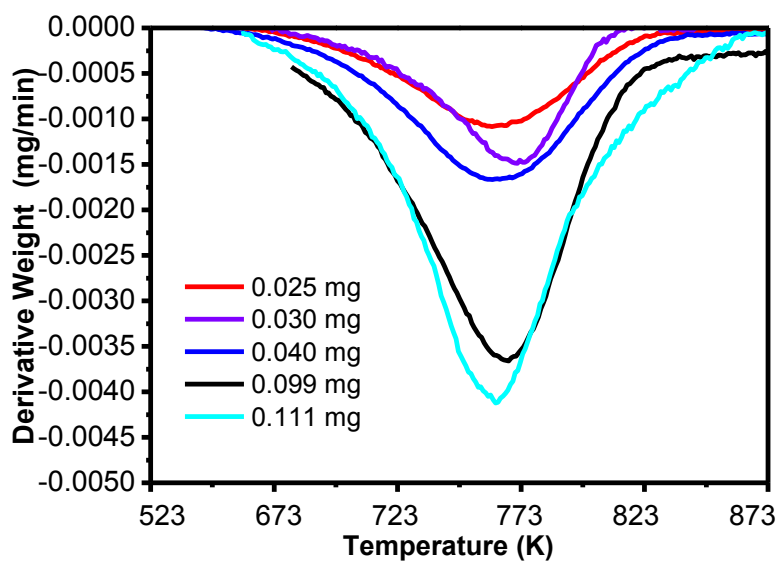
Figure 7-4:   Soot derivative weight profiles at different sample mass
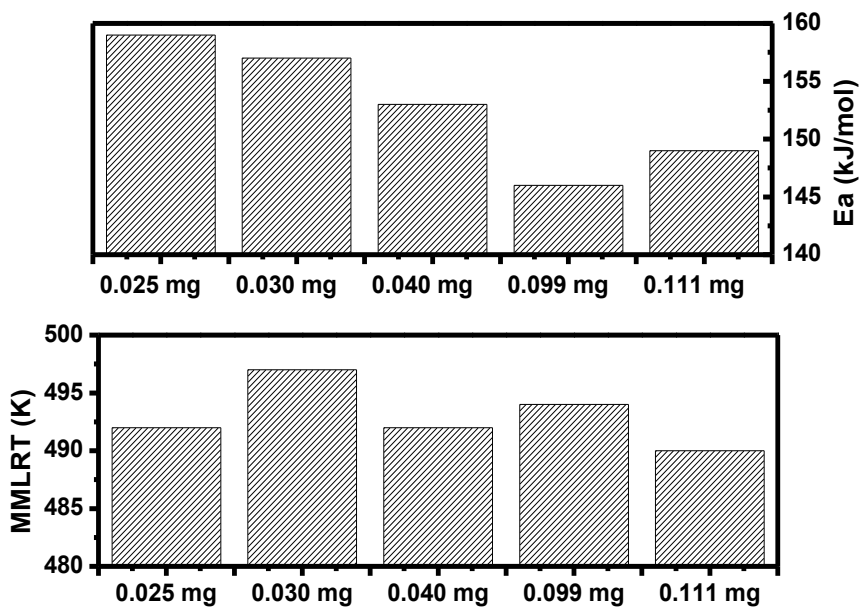
Figure 7-5:   Activation energy and MMLRT at different sample mass

7.4   TGA Method Application

7.4.1   Effect of Fuel

Figure 7-6 shows the PM composition for the four tested fuels. 'ULG' and 'ETH' in the figure are short for gasoline and ethanol respectively. The volatile components (HCs, lubricant etc.) in the PM were classified into two ranges: low volatility (313-573 K) and high volatility (573-773 K) (Price; et al.). PM produced from the engine combustion is primary composed of particles with different nature: a) condensed HCs and b) soot agglomerates with HC adsorbed/condensed on its surface (Kittelson, 1998). Based on the results form Figure 7-6, it is clear volatile materials accounts for the most of PM mass.
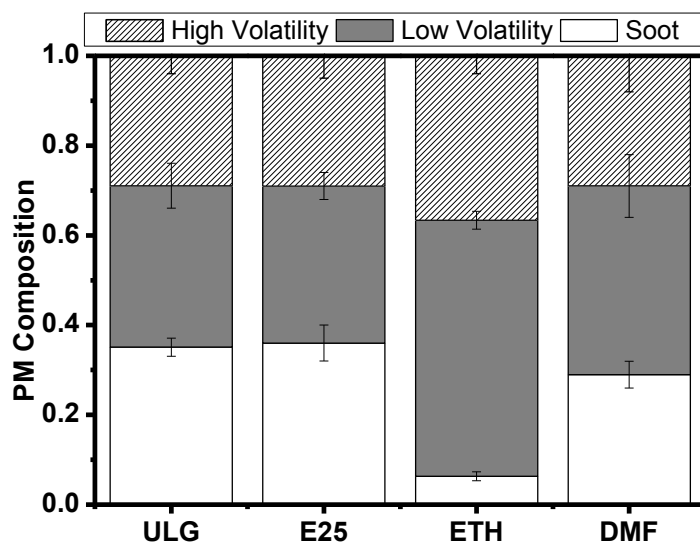
Figure 7-6:   PM composition for PM from gasoline, DMF, E25 and ethanol combustion

Soot fraction in PM composition is strongly affected by fuel properties. For PM produced from ethanol combustion, 6.3% of PM mass was soot. The reason is that in the molecule of ethanol, there is an oxygen atom, which makes ethanol have 34.8% oxygen content. Ethanol combustion produces lower soot formations than gasoline due to more oxygen available for combustion (Di Iorio et al., 2011, Chen et al., 2012). For PM produced from DMF combustion, soot accounted for 29% of PM mass, which was much

higher than PM produced from ethanol combustion because of its less oxygen content. The elemental soot in PM produced from gasoline and E25 combustion are similar (36%). Ethanol combustion produces significant lower HC and PM emissions than gasoline (Wang et al., 2013a, Di Iorio et al., 2011). Therefore, it is highly possible that gasoline in E25 is the primary source to the HC and soot emissions. In other words, PM produced from E25 combustion is mainly due to its 75% gasoline; therefore it explains that no significant difference in PM composition is observed in PM produced from E25 and gasoline. Ethanol and light HCs of gasoline in the blended fuel E25 form an azeotropic mixture which evaporates easily and produces limited PM emissions (Di Iorio et al., 2011, Catapano et al., 2013). The heavy HC compounds remaining on piston, valve and cylinder liner create extremely ideal environment for the soot formation, which potentially explain that soot fraction for PM produced from E25 combustion is a bit higher than that for gasoline, which complies with the literature (Khalek et al., 2010, Di Iorio et al., 2011, Catapano et al., 2013). It has to be noted that the tests carried out in this study in under rich combustion and late injection, representing the one of the worst cases of PM emissions in GDI engines. It lean, homogenous combustion is applied, it is expected that soot will account far less than 36% at the same engine load (8.5 bar IMEP). The PM composition of PM emissions from GDI engines is significantly different to that from diesel engines; therefore the method or strategy for mitigating or adapting PM emissions in GDI and diesel engines is not expected to be the same. In GDI engines, by reducing volatile materials in the PM emissions, it is possible to greatly reduce the PM emissions.
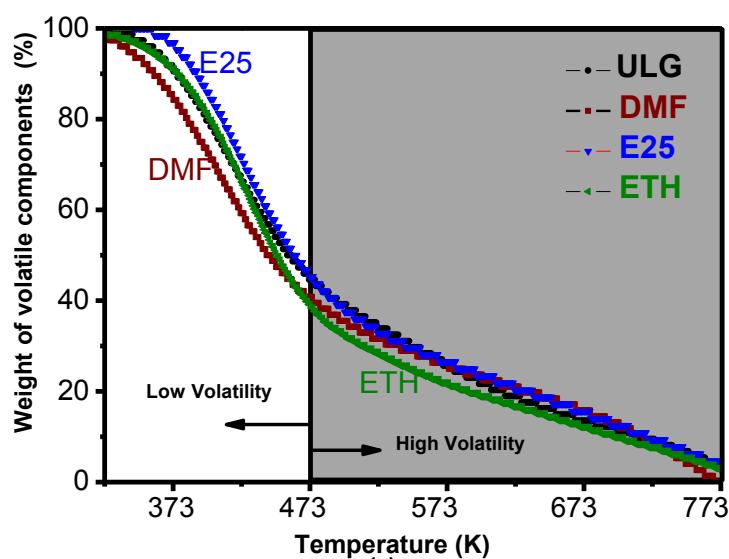
Figure 7-7: Devolatilization profiles for PM from gasoline, DMF, E25 and ethanol combustion
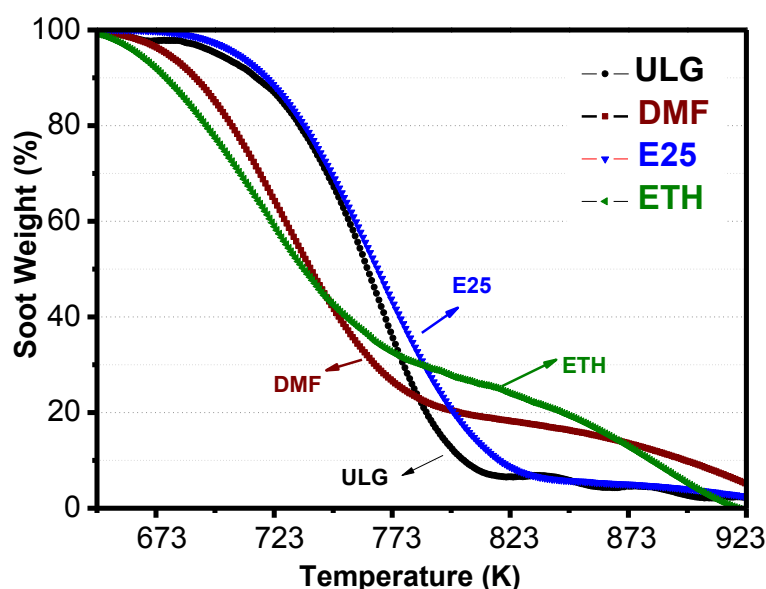
Figure 7-8: Soot oxidization profiles for PM from gasoline, DMF, E25 and ethanol combustion

Figure 7-7 shows the normalized volatility weight profiles for various fuels in the devolatilization process. No obvious differences in the volatility weight profiles amongst all the tested fuels were observed. For DMF and ethanol, the low volatility fraction was approximately 60% whilst for gasoline and E25 it was approximately 55%. The normalized soot weight profiles for PM produced from various fuels during the oxidization process are presented in Figure 7-8. The soot oxidization profiles are significantly sensitive

to fuel, and oxidization of soot produced from DMF and ethanol combustion started at a

lower temperature than soot produced from gasoline and E25 combustion.
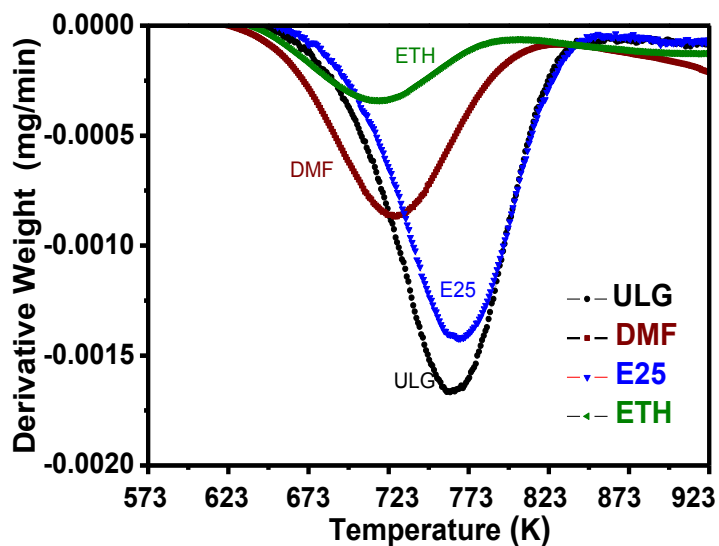
Figure 7-9:   Soot oxidization derivative weight profiles for PM from gasoline, DMF, E25 and ethanol combustion
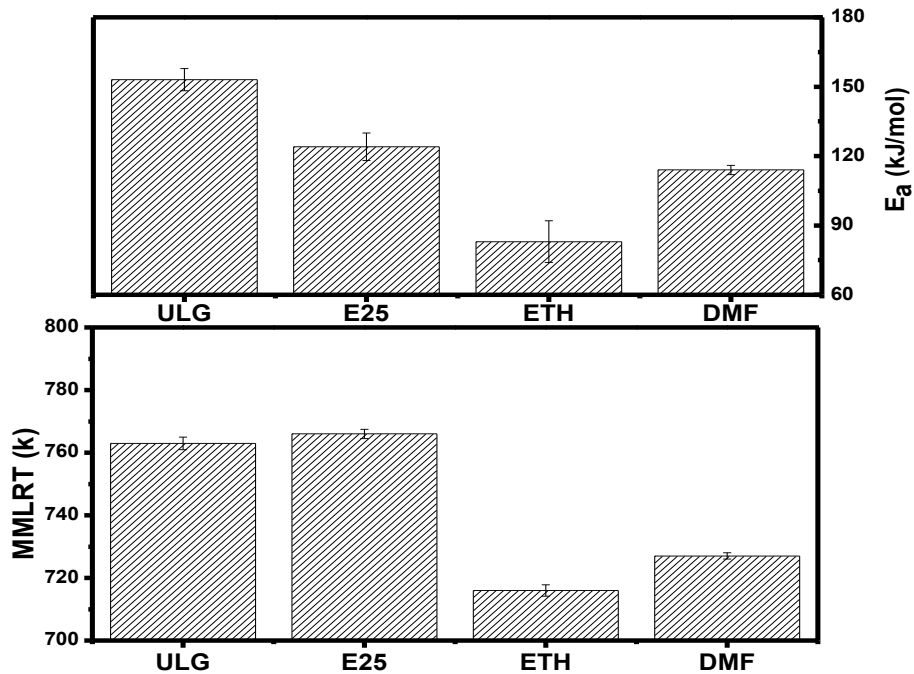
Figure 7-10:   Activation energy and MMLRT for PM from gasoline, DMF, E25 and ethanol combustion

Figure 7-9 presents the soot derivative weight profiles for soot generated from the combustion of gasoline, ethanol, E25 and DMF. The area integrated of soot derivative weight profile and *x* axial is proportional to the soot mass. From Figure 7-9 it is clear that E25 combustion produced less soot than gasoline. DMF led to less soot emissions than gasoline and E25 but not as low as ethanol. Figure 7-10 presents the calculated activation energies and MMLRTs for soot generated from the combustion of gasoline, ethanol, E25 and DMF. It is clear that the activation energy for the soot produced from gasoline combustion in the GDI engine was the highest (153 kJ/mol), and for soot from ethanol combustion it is the lowest (83 kJ/mol). By adding 25% ethanol into the gasoline (E25), the activation energy was reduced from 153 to 124 kJ/mol. For PM produced from DMF combustion, the activation energy (109 kJ/mol) was between those of gasoline and ethanol. The differences in activation energies between fuels were statistically significant. Soot from gasoline and E25 have similar MMLRT, which was higher than those for soot produced from DMF and ethanol combustion.

In summary, soot from ethanol combustion was the most easily oxidized, indicating that it was easy to regenerate the particle filters in GDI engines fuelled with ethanol. Soot generated from the combustion of gasoline was not easy to be oxidized; however, by adding 25% ethanol into gasoline, the soot had a reduction in the oxidation activation energy. The reactivity order for soot from four tested fuel are: ethanol>DMF>E25>gasoline.

Based on the literature on the study of soot from diesel engines, it could be hypothesised that the high reactivity of soot from DMF and ethanol combustion could be due to two primary factors: size of primary and agglomerated particles, and soot oxidization mode.

(a)   Smaller primary and agglomerated particles with higher surface/volume ratio, are more easily oxidized. From the literature, the combustion of oxygenated fuels tends to produce smaller primary particles (Herreros, 2009). Research evidence at the University of Birmingham also confirmed that the combustion of DMF and ethanol produces smaller particles (Daniel et al., 2011). This partially explains the higher oxidization rate of soot produced from DMF and ethanol combustion compared to that of the soot produced from gasoline combustion.

(b)   Studies on the effect of various functional groups on soot oxidation reactivity are available (Bacho et al., 2009, Yehliu et al., 2012, Müller et al., 2005), although the findings are not conclusive. Soot from the combustion of oxygenated fuels tends to have oxygenated functional groups associated with internal burning in the oxidation process, the rate of which is 10 times higher than that of the normal surface burning (Song et al., 2006). Therefore it is envisaged that DMF and ethanol generated soot will experience internal burning. However the effect of oxygenated surface functional groups on soot reactivity was not clear, and the relative amount of aliphatic C-H groups on the soot surface affects the soot oxidation reactivity (Wang et al., 2013b); therefore it requires more investigation.

7.4.2   Effect of Engine Load

PM emissions generated from ethanol combustion at 5.5 bar IMEP were very low and it is significantly difficult to collect enough sample without damaging the filters. Therefore the results for ethanol at 5.5 bar IMEP are not available.
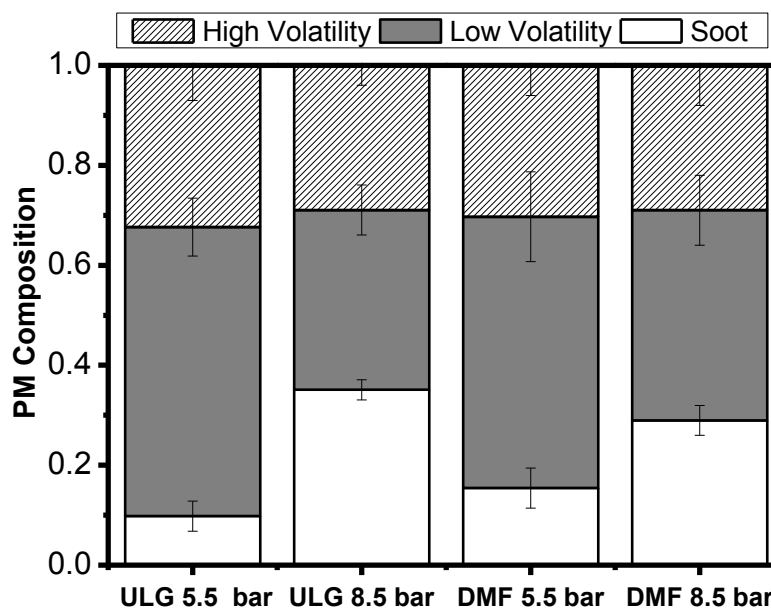
Figure 7-11: PM composition for PM produced from gasoline and DMF combustion at 5.5 and 8.5 bar IMEP

Figure 7-11 shows the PM composition for PM produced from gasoline and DMF combustion at 5.5 and 8.5 bar IMEP. It can be seen that the soot fraction is increased, which is more obvious for PM produced from gasoline combustion. In the precious study at the University of Birmingham, it has been reported that as engine load increased, HC emissions were reduced due to more HC being post-oxidized at high temperature (Wang et al., 2013a). The soot formation increases with engine load due to more fuel wetting in the cylinder liner and on the piston crown. The combined effect of reduced HC emissions and increased soot formation leads to higher soot fraction in PM composition at higher engine load. Soot fraction accounted for 15.4% and 28.9% of PM produced form DMF combustion at 5.5 and 8.5 bar IMEP respectively. However, soot fraction was 9.8% and 35.1% of PM mass at 5.5 and 8.5 bar IMEP respectively. It is clear that soot fraction in gasoline-generated PM changes at 5.5 and 8.5 bar IMEP is more than that in DMF-generated PM. DMF has one oxygen atom in its molecule, which leads to less PM

emissions than gasoline. Therefore, as the engine load is increased, there is more soot

formation from gasoline combustion than that of DMF combustion.
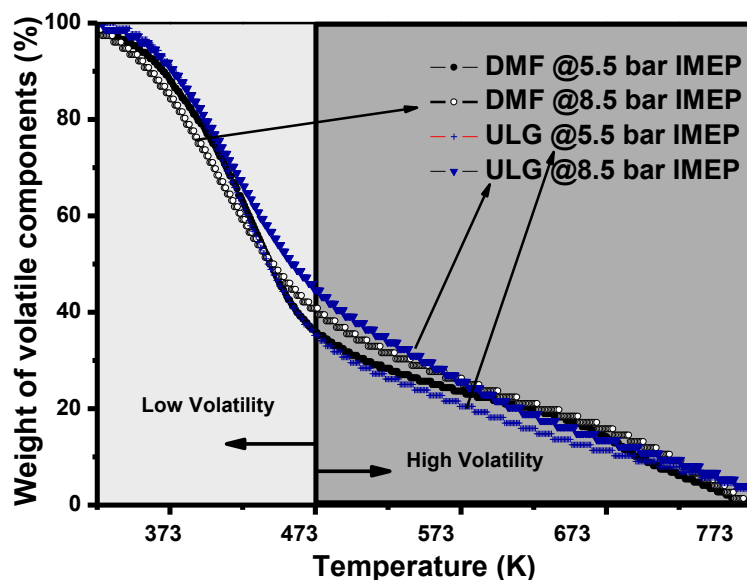
Figure 7-12: Devolatilization profiles for PM from gasoline and DMF combustion at 5.5 and 8.5 bar IMEP
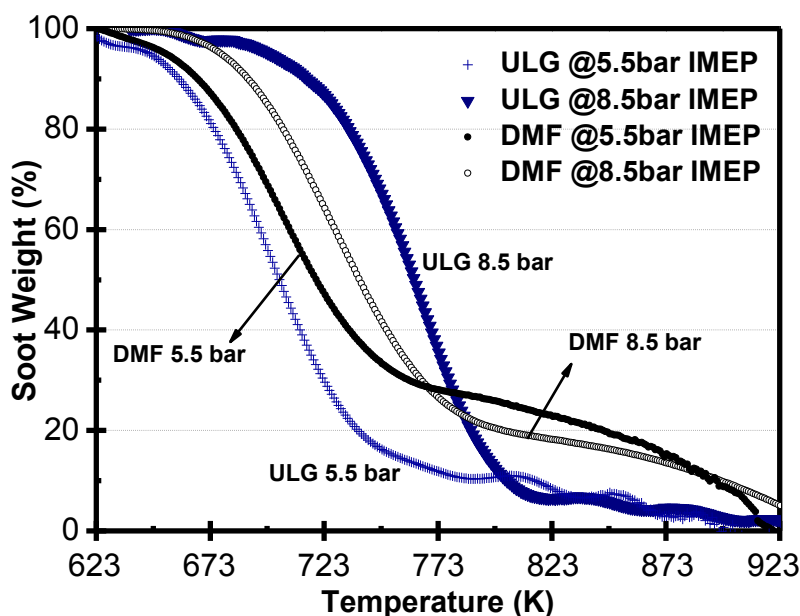
Figure 7-13: Soot oxidation profiles for PM from gasoline and DMF combustion at 5.5 and 8.5 bar IMEP

Figure 7-12 shows the PM devolatilization profiles at 5.5 and 8.5 bar IMEP. The

sensitivity of PM devolatilization profile to engine load was limited. Figure 7-13 represents

soot oxidation profiles at 5.5 and 8.5 bar IMEP. The soot oxidation profile for soot from gasoline combustion moved to high temperature range as the engine load is increased from 5.5 to 8.5 bar IMEP. For DMF generated soot, the shift in soot oxidation profiles was not as obvious as that from gasoline combustion.

Figure 7-14 presents the soot derivative weight profiles for PM generated from DMF and gasoline combustion at 5.5 and 8.5 bar IMEP. For gasoline combustion at 8.5 bar IMEP, net soot formation was increased, indicated by the area enveloped by the soot derivative weight profiles and x axial. Soot produced from DMF combustion also increased at 8.5 bar IMEP compared with that at 5.5 bar IMEP, however at a low rate than that in gasoline combustion. Figure 7-15 illustrated MMLRT and activation energies for PM generated from gasoline and DMF combustion at 5.5 and 8.5 bar IMEP. For soot produced from DMF combustion, there was a 20 K difference in MMLRT between the engine load of 5.5 and 8.5 bar IMEP, however the difference was 70 K for that of gasoline-generated soot. The activation energy for soot produced from DMF combustion was 109 and 114 kJ/mol at 5.5 and 8.5 bar IMEP respectively, indicating that more energy (4.6%) was required to for the oxidization reaction as engine load was increased from 5.5 to 8.5 bar IMEP. However for soot produced from gasoline combustion, reaction energy is increased more, from 131 to 153 kJ/mol at 5.5 to 8.5 bar IMEP respectively.
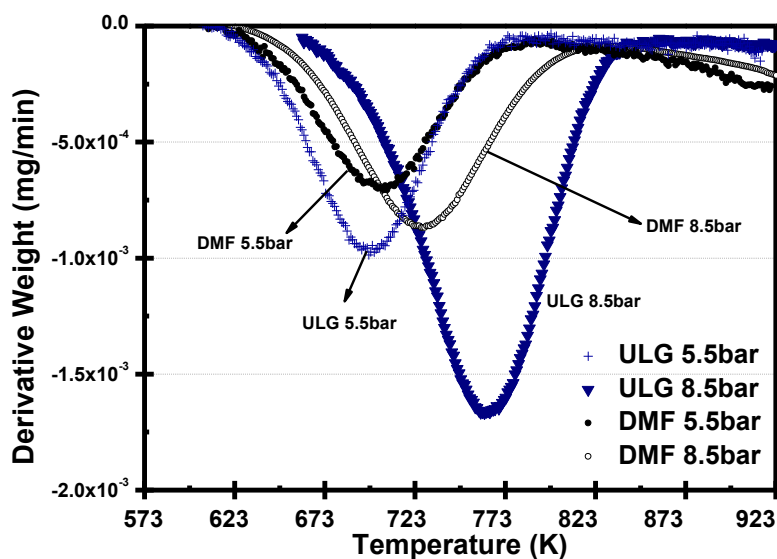
Figure 7-14: Soot oxidization derivative weight profiles for PM from gasoline and DMF at 5.5 and 8.5 bar IMEP
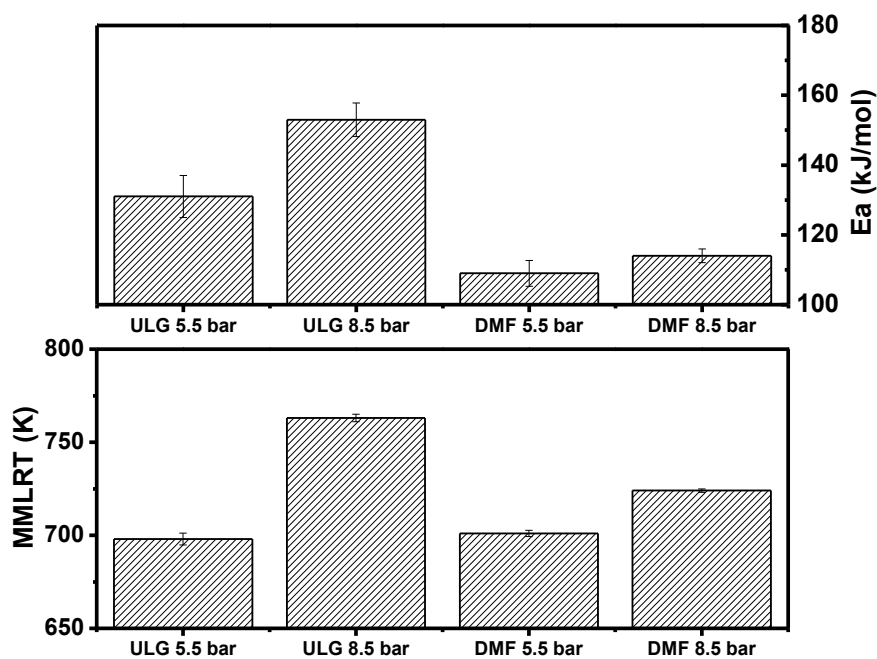
Figure 7-15: Activation energy and MMLRT for PM from gasoline and DMF at 5.5 and 8.5 bar IMEP

The oxidation reaction for soot produced in DMF and gasoline combustion became difficult when soot was produced at higher engine load, the reasons for which are soot nano-structure, primary and agglomerated particle size.

(a) **Soot nano-structure.** Soot nano-structure has a close impact on the ratio of active edge carbon atoms to inactive basal carbon atoms, which affects the reactivity of soot oxidation process. Soot structure has been investigated using equipment such as XRD and HR-TEM (Yehliu et al., 2012, Müller et al., 2005, Zhu et al., 2005). The order of soot structure is indicated by crystalline length, crystalline height and fringe length, and tortuosity. It has been found that particles with a less ordered nano-structure (Müller et al., 2005, Yehliu et al., 2012)), tend to have a higher oxidation reactivity. Soot produced from higher combustion temperatures in diesel engines tends to have higher ordered structures (Zhu et al., 2005, Lee et al., 2002). The data from the present work also shows that the soot produced at high engine load with high combustion temperature requires more energy to be oxidized.

(b) **Size of primary and agglomerated particles**. More soot was formed at 8.5 bar IMEP compared to 5.5 bar IMEP engine load, which is a result of higher rate of soot production and growth at higher temperature in the combustion chamber. On the other hand, at 8.5 bar IMEP, more fuel is injected into the cylinder and thus there are more locally rich areas in the combustion chamber. The increased fuel impingement at high engine load enhances soot formation and growth. Both locally rich areas and fuel impingement results in larger primary particles (Lapuerta et al., 2007) and agglomerates, reducing the particle surface/volume ratio and thus soot reactivity, which explains that the soot produced at 8.5 bar IEMP required more energy and higher temperature in the oxidation process than soot produced at 5.5 bar IMEP. From Figure 7-15 (a), it is also clear that the effect of engine load on the net soot production in DMF combustion is lower than that in gasoline combustion. It is expected that the change in the size of primary and

agglomerated particles from DMF combustion at 5.5 and 8.5 bar IMEP is smaller than that from gasoline combustion.

7.5   Conclusions

A TGA method was optimized and applied in the investigation of PM composition and soot oxidation characteristics for PM emissions produced from a GDI engine. Gasoline, ethanol, E25 and DMF were tested. The engine was operated at 1500 rpm with a rich combustion and late fuel injection strategy.

1.   A heating ramp of 3-5 K/min and a soot sample of larger than 0.040 mg are proven to lead to repeatable results for the oxidation of PM from a GDI engine.

2.   PM emissions from the GDI engine mainly comprised of volatile components (over 60%). The research carried out by the University of Oxford shows that, during cold start, a second generation (spray-guided) GDI engine fuelled with gasoline produced PM with around 2-29 wt% of elemental soot (Price et al., 2007a). Even through the engine condition in the author's work is late injection, rich fuel/air ratio and warm condition, differencing from the cold start condition used by Price et al (Price et al., 2007a), both results show that PM composition from the second generation GDI engine are dominated by volatile components.

3.   Soot produced from the combustion of oxygenated fuels such as ethanol and DMF are easier to be oxidized compared to soot from gasoline combustion, indicated by the lower MMLRT and oxidation activation energies. Blending ethanol into gasoline will produce soot that is much easier to be oxidized.

4.   The activation energies and temperature required for soot oxidation are increased with engine load. For soot produced form gasoline combustion, its oxidization

behaviour is more sensitive to engine load than the soot generated from the combustion of DMF.

More study is needed to be carried out to further understand the faster oxidation rates of soot produced from the combustion of oxygenated fuels in GDI engines. The study on particulate morphology, nano-structure and soot surface functional groups are helpful to understand the soot oxidation process.

CHAPTER 8

8   Summary and Future Work Suggestions

This PhD thesis was about the application of bio-fuel (DMF, MF and ethanol) in a single cylinder DISI research engine. Research interests cover combustion characteristics and emissions, especially PM emissions. The combustion analysis accounts for one experimental chapter and emissions account for three chapters. The key conclusions of this thesis are presented, followed by further work suggestions.

8.1   Summary

The engine tests are conducted in a 4-valve, 4-stroke single-cylinder close-space concept (spray-guided) DISI research engine with a fixed compression ratio of 11.5:1. The main summaries are presented separately according to the chapter orders.

Chapter 4:   Combustion characteristics and fuel combustions of MF in a DISI engine

In the single cylinder DISI engine with a fixed compression ratio of 11.5:1, MF demonstrates competitive or better combustion characteristics compared to gasoline, and widely used ethanol, which agrees with the finding from first MF engine publication (Thewes et al., 2011). MF has a better anti-knock ability compared to gasoline, making it a competitive fuel in the application of downsized SI engines. Due to synergy effects of higher octane rating and fast burning rate, MF combustion has higher indicated thermal efficiency than gasoline. Compared with DMF, MF has notably robust combustion characteristics although they have similar molecule structures. Last but not the least; MF

has low fuel consumptions than ethanol because of its higher energy content. The fuel consumption is of interest because it is relevant to the range of distance a driver can drive before the top-up fuel tank becomes empty.

The first MF engine report suggested that MF allowed for a compression ratio increase of more than 3.5 units compared to RON 95 gasoline, which led to up to 9.9% higher efficiency at full load at 2000 rpm in a boosted single cylinder DISI engine (Thewes et al., 2011). In this thesis, the compression ratio is not optimized for each individual fuel. For ethanol, a geometric compression ratio higher than the current one (11.5:1) can be used due to its high octane rating. For DMF and MF, engine knocking is observed at engine loads higher than 6.5 bar. If a lower compression ratio is used, the combustion phase can be optimized, with the crank angle position of 50% MFB at the range of 8~10 °aTDC. The combustion phase of gasoline is the least optimized especially at 8.5 bar IMEP, since retarded spark timings are required in order to avoid engine knock.

Chapter 5:   Emission characteristics of MF in a DISI engine

In the single cylinder DISI engine with a fixed compression ratio of 11.5, MF combustion yields much less HC emissions compared to gasoline combustion. Due to its higher in-cylinder temperatures, MF generated significantly higher NO_x emissions compared to gasoline and ethanol. NO_x emissions from MF combustion can be addressed by using EGR or retarded spark timing strategies. Aldehyde emissions from MF combustion are significantly lower than those of gasoline and ethanol. GC/MS detected signals of cancerigenic products such as toluene, benzene and furan in the MF exhaust sample however their concentrations are very low compared with the main MF signal.

Chapter 6:   Impact of Fuels on PM Emissions from a GDI Engine under various Injection Pressure and Injector Fouling conditions

Fuel, injection pressure and injector fouling have direct links to spray patterns such as spray angle, droplet diameter and penetration distance which are closely related to the air/fuel mixture preparation in DISI engines and thus PM emissions. In this work, the impact of fuels on PM Emissions from a GDI engine under various injection pressure and fouled injectors was studied. The experiments were conducted in a DISI research engine (λ=1, engine speed=1500 rpm, load=3.5-8.5 bar IMEP). Two fuels (gasoline and ethanol), four injection pressures (50, 100, 150, 172 bar) and three injectors (one clean and two fouled injectors with 5.3% and 8.5% fuel flow rate loss) were tested.

The results showed that, PM emissions from DISI engines vary significantly to fuel. Gasoline combustion yields 4-30 times higher PM mass-based and 25%- 40% higher PM number-based emissions compared with those of ethanol combustion. Ethanol combustion produces almost no soot formation and most of particles emitted are volatile organics. PM emissions from the combustion of gasoline and ethanol respond differently towards injection pressure and injector fouling. For gasoline fuelled DISI engines, injection system has an essential impact of the PM emissions: high injection pressure (150 bar) and clean injectors (no injector deposit) both are the keys for low PM emissions. Unlike gasoline, PM emissions from ethanol operated DISI engines are not sensitive to the injection system: low injector pressure and injector fouling have very almost no impacts on PM emissions.

Chapter 7:   PM Composition and Soot Oxidation for PM emissions from a GDI Engine

A TGA method was optimized and applied in the study PM composition (soot and volatility) and soot oxidization characteristics. The GDI engine was operated at fixed 1500 rpm engine speed with rich combustion and late fuel injection strategy, representing one of the worst scenarios of PM emissions in GDI engines. The results show that PM produced from gasoline, E25 and DMF are mainly volatile materials, and soot only accounts for up to 35% of PM mass at 8.5 bar IMEP under rich combustion and late injection operating condition. Ethanol combustion produces PM with only 6.3% elemental soot. Soot oxidation is sensitive to fuel and engine load. Unlike gasoline, ethanol combustion produces soot which is easily oxidized, showed by the less energies and low temperature required for oxidization. Activation energy for the oxidation of soot produced from gasoline combustion is highly sensitive to engine load, which is not the case for soot from DMF combustion.

The research carried out by the University of Oxford shows that, during cold start, a second generation (spray-guided) GDI engine fuelled with gasoline produced PM with around 2-29 wt% of elemental soot (Price et al., 2007a). Even though the engine condition in the author's work is late injection, rich fuel/air ratio and warm condition, differing from the cold start condition used by Price et al (Price et al., 2007a), both results show that PM composition from the second generation GDI engine are dominated by volatile components.

8.2   Future Work

The following are some suggestions for future work.

Combustion characteristics of MF, DMF, bio-ethanol, and gasoline in a GDI engine using fuel-optimized compression ratio

In an internal combustion engine, high compression ratio leads to high engine efficiency; however the increase of compression ratio is partially limited by the octane rating of fuel. It would be interesting to compare the combustion characteristics of MF, DMF and gasoline in a GDI engine using fuel-optimized compression ratio. The ranking of octane rating for those four fuels are: ethanol > DMF≈MF > gasoline; therefore it is expected that the ranking of fuel-optimized compression ratios for those four fuels are: ethanol > DMF≈MF > gasoline.

However, it has to be noted that, for gasoline, DMF and MF, when compression ratio is decreased from 11.5:1, there is a trade-off in indicated efficiencies between low and medium engine loads, and high engine loads. Any decrease in compression ratio will lead to low indicated efficiencies at low and medium engine loads, and will lead to potentially increased indicated efficiencies at high engine loads, only if the benefits of increased burning speed due to the increased in-cylinder turbulence during the combustion process outweighs the negative effect resulting from a reduced compression ratio.

Use of MF and DMF in a boosted downsized GDI engine

It would be interesting to use MF and DMF in a downsized engine to fully exploit its high octane rating property. Engine downsizing is a hot topic in recent years, which usually requires turbo-charging and/or supercharging technologies. However engine knock and

pre-ignition is one of the key challenges to the application of engine downsizing. High octane rating fuels like MF provide a good solution to this issue.

PM emissions from GDI engines

• PM measurement in GDI engines is significantly difficult and not comparable due to the lack of repeatability and lack of standard test setup; therefore more work is needed to be done to standardize the PM measurement setup.

• PM emissions from GDI engines are fundamentally different from those of diesel engines, in which majority of mass are composed of volatilities. Research about the effects of TWC and HC trappers on PM emissions could be interesting since most of PM mass is contributed by volatilities.

• Further investigation about the impacts of fuel properties such as vapor pressure, molecule structure on PM emissions should be conducted.

• The study of PM morphology and structure are helpful for a better understand of the fundamental knowledge of soot oxidation in GDI engines.

Impact of MF and DMF on DI injector plugging

GDI injector plugging is an important issue in the application of DISI engines, Injector plugging are shown to reduce injector fuel flow rates and in some cases degrade the spray quality leading to alterations of spray angle, droplet diameter and penetration distance. All of these deviations have negative impacts on the desired air/fuel mixture preparation which is critical to the combustion process in DISI engines. Severe injector deposit issues can cause vehicle drivability problems and misfire especially at light throttle operation conditions. HC, CO and PM emissions may be increased due to injector deposit formation.

The deposit formation mechanism in GDI injector is less understood and requires further study. Previous studies on the GDI injector fouling show that the use of ethanol can help to reduce injector deposit formation. The impact of MF and DMF on injector plugging needs to be investigated in detail, before they are widely promoted as renewable biofuels.

Quantitative HC speciation using GC-MS

Individual HC emissions from MF combustion could be done by using GC-MS. A standard calibration gas containing all HC emissions in the MF and DMF combustion could be used for the quantitative measurement.

LIST OF REFERENCE

ACSS 2013. Particulate Emissions from Petrol-Engined Light-Duty Vehicles taken from the European Fleet. Presented in Cambridge Particle Meeting.

AGARWAL, A. K. 2007. Bio-fuels (Alcohols and Biodiesel) Applications as fuels for Internal Combustion Engines. Progress in Energy and Combustion Science, 33, 233-271.

AGENCY, U. S. E. P. 1998. Carcinogenic Effects of Benzene: An Update. National Center for Environmental Assessment, EPA/600/P-97/001F.

AGENCY, U. S. E. P. 2009. Integrated Science Assessment for Particulate Matter. Final Report, EPA/600/R-08/139F.

AGENT, U. S. E. P. 2005. Final Rule: Revision to the Requirements on Variability in the Composition of Additives Certified Under the Gasoline Deposit Control Program.

AIKAWA, K., SAKURAI, T. & JETTER, J. J. 2010. Development of a Predictive Model for Gasoline Vehicle Particulate Matter Emissions. SAE Int. J. Fuels Lubr., 3, 610-622.

AL-QURASHI, K. & BOEHMAN, A. L. 2008. Impact of exhaust gas recirculation (EGR) on the oxidative reactivity of diesel engine soot. Combustion and Flame, 155, 675-695.

ALEIFERIS, P. G., MALCOLM, J. S., TODD, A. R., CAIRNS, A. & HOFFMANN, H. 2008. An optical study of spray development and combustion of ethanol, iso-octane and gasoline blends in a DISI engine. SAE International 2008-01-0073.

ALEIFERIS, P. G., PEREIRA, J. S., AUGOYE, A., DAVIES, T. J., CRACKNELL, R. F. & RICHARDSON, D. 2010. Effect of fuel temperature on in-nozzle cavitation and spray formation of liquid hydrocarbons and alcohols from a real-size optical injector for direct-injection spark-ignition engines. International Journal of Heat and Mass Transfer, 53, 4588-4606.

ALTIN, O. & ESER, S. 2004. Carbon deposit formation from thermal stressing of petrolelum fuels. Prepr. Pap.-Am. Chem. Soc., Div. Fuel Chem, 49, 765.

ANDERSON, R., YANG, J., BREHOB, D., YI, J., HAN, Z. & REITZ, R. 1997. Challenges of stratified charge combustion. Direkteinspritung im Ottomotor.

ANDERSSON, J., COLLIER, A., GARRETT, M. & WEDEKIND, B. 1999. Particle and Sulphur Species as Key Issues in Gasoline Direct Injection Exhaust. Nippon Kikai Gakkai.

ANDERSSON, J., KEENAN, M. & ÅKERMAN, K. 2008. GDI Particles – Legislation, Current Levels and Control. Presented in Cambridge Particle Meeting.

ANON 2002. Bosch Motronic MED7 Gasoline Direct Injection. Volkswagen Self-Study Program.

ARADI, A. A., COLUCCI, W. J., SCULL, H. M. & OPENSHAW, M. J. 2000a. A Study of Fuel Additives for Direct Injection Gasoline (DIG) Injector Deposit Control. SAE International 2000-01-2020.

ARADI, A. A., EVANS, J., MILLER, K. & HOTCHKISS, A. 2003. Direct Injection Gasoline (DIG) Injector Deposit Control with Additives. SAE International 2003-01-2024.

ARADI, A. A., HOTCHKISS, A., IMOEHL, B., H. SAYAR & AVERY, N. L. 2000b. The Effect of Fuel Composition, Engine Operating Parameters and Additives on Injector Deposits in a High-Pressure Direct injection Gasoline (DIG) Research Engine. Aachen Colloquium – Automobile and Engine Technology, 187 - 211.

ARADI, A. A., HOTCHKISS, A., IMOEHL, B., SAYAR, H. & AVERY, N. L. 1999. The Effect of Fuel Composition, Engine Operating Parameters and Additives on Injector Deposits in a High-Pressure Direct injection Gasoline (DIG) Research Engine. SAE International 1999-01-3690.

ARCOUMANIS, C., GAVAISES, M. & NOURI, J. M. 2008. The role of cavitation in automotive fuel injection systems. In Proceedings of the 8th International Symposium on Internal Combustion Diagnostics, AVL, Baden-Baden, Germany.

ARMAS, O., GARCÍA-CONTRERAS, R. & RAMOS, Á. 2013. Impact of alternative fuels on performance and pollutant emissions of a light duty engine tested under the new European driving cycle. Applied Energy, 107, 183-190.

ARTERS, D. C., BARDASZ, E. A., SCHIFERL, E. A. & FISHER, D. W. 1999. A Comparison of Gasoline Direct Injection Part I - Fuel System Deposits and Vehicle Performance. SAE International 1999-01-1498.

ARTERS, D. C. & MACDUFF, M. J. 2000. The Effect on Vehicle Performance of Injector Deposits in a Direct Injection Gasoline Engine. SAE International 2000-01-2021.

ASHIDA, T., TAKEI, Y. & HOSI, H. 2001. Effects of Fuel Properties on SIDI Fuel Injector Deposit. SAE International 2001-01-3694.

ATSUMI, S., HANAI, T. & LIAO, J. C. 2008. Non-fermentative pathways for synthesis of branched-chain higher alcohols as biofuels. Nature, 451, 86–89.

Reference

BACHO, P. S. V., SOFIANEK, J. K., GALANTE-FOX, J. M. & MCMAHON, C. J. 2009. Engine Test for Accelerated Fuel Deposit Formation on Injectors Used in Gasoline Direct Injection Engines. SAE International 2009-01-1495.

BARDASZ, E. A., ARTERS, D. C., SCHIFERL, E. A. & RIGHI, D. W. 1999. A Comparison of Gasoline Direct Injection and Port Fuel Injection Vehicles: Part II - Lubricant Oil Performance and Engine Wear. SAE International 1999-01-1499.

BARKER, J., RICHARDS, P., SNAPE, C. & MEREDITH, W. 2009. A Novel Technique for Investigating the Nature and Origins of Deposits Formed in High Pressure Fuel Injection Equipment. SAE International 2009-01-2637.

BARNES, K., BYFLEET, W. D., KING, S., MACH, H., TILLING, N. J., RUSSELL, T. & SENGERS, H. P. 2005. Fuel additives and the environment. Technical Committee of Petroleum Additive Manufacturers in Europe.

BERG, C. & LICHT, F. O. 2011. World fuel ethanol analysis and outlook. Ministry of Economy, Trade and Industry.

BERNDORFER, A., BREUER, S., PIOCK, W. & BACHO, P. V. 2013. Diffusion Combustion Phenomena in GDi Engines caused by Injection Process. SAE International 2013-01-0261.

BHARDWAJ, O. P., KREMER, F., PISCHINGER, S., LÜERS, B., KOLBECK, A. F. & KOERFER, T. 2013. Impact of Biomass-Derived Fuels on Soot Oxidation and DPF Regeneration Behavior. SAE Int. J. Fuels Lubr., 6, http://dx.doi.org/10.4271/2013-01-1551.

BIKA, A. S., FRANKLIN, L. & KITTELSON, D. B. 2011. Hydrogen assisted combustion of ethanol in Diesel engines. http://www.me.umn.edu/centers/cdr/reports/agexpoposter.pdf.

BRACE, C., ROSE, A. & AKEHURST, S. 2011. Continusely variable supercharger drive: an evaluation of the performance benefits. IMechE, Engine downsizing conference, London.

BOONE, W. P., HUBBARD, C. P., SOLTIS, R. E., DING, Y. & CHEN, A. 2005. Effect of MMT® Fuel Additive on Emission System Components: Detailed Parts Analysis from Clear- and MMT®-Fueled Escort Vehicles from the Alliance Study. SAE International 2005-01-1108.

BROGAN, M. S., SWALLOW, D., BRISLEY, R. J., MATTHEY, J., WORTH, D. & YANG, K. 2000. A New Approach to Meeting Future European Emissions Standards with the Orbital Direct Injection Gasoline Engine. SAE International 2000-01-2913.

CAIRNS, A., STANSFIELD, P., FRASER, N. & BLAXILL, H. 2009. A study of gasoline–alcohol blended fuels in an advanced turbocharged DISI engine. SAE International 2009-01-0138.

CARB 2010. Tables of Maximum Incremental Reactivity (MIR) Values, California Code of Regulations. California Air Resources Board.

CARLISLE, H. W., FREW, R. W., MILLS, J. R., ARADI, A. A. & AVERY, N. L. 2001. The Effect of Fuel Composition and Additive Content on Injector Deposits and Performance of an Air-Assisted Direct Injection Spark Ignition (DISI) Research Engine. SAE International 2001-01-2030.

CASPER, J. K. 2007. Energy: Powering the Past, Present, and Future, Chelsea House Publishers.

CATAPANO, F., DI IORIO, S., LAZZARO, M., SEMENTA, P. & VAGLIECO, B. M. 2013. Characterization of Ethanol Blends Combustion Processes and Soot Formation in a GDI Optical Engine. SAE International 2013-01-1316.

CHAN, T. W., MELOCHE, E., KUBSH, J., BREZNY, R., ROSENBLATT, D. & RIDEOUT, G. 2013. Impact of Ambient Temperature on Gaseous and Particle Emissions from a Direct Injection Gasoline Vehicle and its Implications on Particle Filtration. SAE Int. J. Fuels Lubr., 6, http://dx.doi.org/10.4271/2013-01-0527.

CHAN, T. W., MELOCHE, E., KUBSH, J., ROSENBLATT, D., BREZNY, R. & RIDEOUT, G. 2012. Evaluation of a Gasoline Particulate Filter to Reduce Particle Emissions from a Gasoline Direct Injection Vehicle. SAE Int. J. Fuels Lubr., 5, 1277-1290.

CHARLTON, A., LEA-LANGTON, A., LI, H., ANDREWS, G., TOMLIN, A. & ROUTLEDGE, M. 2011. Particle characteristics and DNA damage induced by exhaust particulate matter collected from a heavy duty diesel engine using biofuelsAlexander. Presented in Cambridge Particle Meeting.

CHEN, L., STONE, R. & RICHARDSON, D. 2012. A study of mixture preparation and PM emissions using a direct injection engine fuelled with stoichiometric gasoline/ethanol blends. Fuel, 96, 120-130.

CHINA, P. & RIVERE, J.-P. 2003. Development of a Direct Injection Spark Ignition Engine Test for Injector Fouling. SAE International 2003-01-2006.

D'AMBROSIO, S. & FERRARI, A. 2012. Diesel Injector Coking: Optical-Chemical Analysis of Deposits and Influence on Injected Flow-Rate, Fuel Spray and EnginePerformance. Journal of engineering for gas turbines and power, 134, doi:10.1115/1.4005991.

DALE TURNERA, HONGMING XU, ROGER F CRACKNELLB, VINOD NATARAJANC & WYSZYNSKIA, M. 2011. Combustion Performance of Bio-Ethanol at Various Blend Ratios in a Gasoline Direct Injection Engine. Fuel, 90, 1999-2006.

DANIEL, R., TIAN, G., XU, H. & WU, X. 2012a. Spark Timing Sensitivity of Gasoline, Ethanol and 2,5-Dimethylfuran in a DISI Engine. Fuel, 99, 72-82.

DANIEL, R., TIAN, G., XU, H., WYSZYNSKI, M. L., WU, X. & HUANG, Z. 2011. Effect of spark timing and load on a DISI engine fuelled with 2,5-dimethylfuran. Fuel, 90, 449-458.

DANIEL, R., WANG, C., XU, H. & TIAN, G. 2012b. Split-Injection Strategies under Full-Load Using DMF, A New Biofuel Candidate, Compared to Ethanol in a GDI Engine. SAE International.

DANIEL, R., WEI, L. X., XU, H. M., WANG, C. M., WYSZYNSKI, M. L. & SHUAI, S. J. 2012c. Speciation of Hydrocarbon and Carbonyl Emissions of 2,5-Dimethylfuran Combustion in a DISI Engine. Energy & Fuels, 26, 6661-6668.

DANIEL, R., XU, H., WANG, C., RICHARDSON, D. & SHUAI, S. 2012d. Combustion performance of 2,5-dimethylfuran blends using dual-injection compared to direct-injection in a SI engine. Applied Energy, 98, 59-68.

DANIEL, R., XU, H., WANG, C., RICHARDSON, D. & SHUAI, S. 2013. Gaseous and particulate matter emissions of biofuel blends in dual-injection compared to direct-injection and port injection. Applied Energy, 105, 252-261.

DEC, J. E. 2009. Advanced compression-ignition engines—understanding the in-cylinder processes. Proceedings of the Combustion Institute, 32, 2727-2742.

DELPHI 2012. Worldwide Emissions Standards - Passenger Cars and Light Duty Vehicles.

DEMIRBAS, A. 2007. Progress and recent trends in biofuels. Progress in Energy and Combustion Science, 33, 1-18.

DI IORIO, S., LAZZARO, M., SEMENTA, P., VAGLIECO, B. M. & CATAPANO, F. 2011. Particle Size Distributions from a DI High Performance SI Engine Fuelled with Gasoline-Ethanol Blended Fuels. SAE International 2011-24-0211.

DRAKE, M. C., FANSLER, T. D., SOLOMON, A. S. & SZEKELY, G. A. 2003. Piston Fuel Films as a Source of Smoke and Hydrocarbon Emissions from a Wall-Controlled Spark-Ignited Direct-Injection Engine. SAE International 2003-01-0547.

DUMONT, R. J., CUNNINGHAM, L. J., OLIVER, M. K., STUDZINSKI, M. K. & GALANTE-FOX, J. M. 2007. Controlling Induction System Deposits in Flexible Fuel Vehicles Operating on E85 SAE International 2007-01-4071.

DUMONT, R. J., EVANS, J. A., FEIST, D. P., STUDZINSKI, W. M. & CU SHING, T. J. 2009. Test and Control of Fuel Injector Deposits in Direct Injected Spark Ignition Vehicles. SAE International 2009-01-2641.

EASTWOOD, P. 2007. Particulate Emissions from Vehicles, John Wiley & Sons, Inc.

ENGLISH, A. 2008. Ford Model T reaches 100. The Telegraph.

FARRON, C., MATTHIAS, N., FOSTER, D., ANDRIE, M., KRIEGER, R., NAJT, P., NARAYANASWAMY, K., SOLOMON, A. & ZELENYUK, A. 2011. Particulate Characteristics for Varying Engine Operation in a Gasoline Spark Ignited, Direct Injection Engine. SAE International 2011-01-1220.

FATOURAIE, M., WOOLDRIDGE, M. & WOOLDRIDGE, S. 2013. In-Cylinder Particulate Matter and Spray Imaging of Ethanol/Gasoline Blends in a Direct Injection Spark Ignition Engine. SAE Int. J. Fuels Lubr., 6, 1-10.

FERNANDES, H., BRAGA, L. C., MARTINS, A. R., BRAGA, S. L. & BRAGA, C. V. M. 2013. Fuel Sulfate Content Influence in the Formation of Inorganics Components Deposits in the Engine Injectors with Technologies of Gasoline Direct Injection. SAE International 2012-36-0314.

FLEMING, J. E., HETRICK, R. E., PARSONS, M. H., SHEERAN, W. M. & ZHANG, X. 2000. Carbonaceous deposit-resistant coating for fuel injectors. United States Patent No. 6145763 patent application.

FRAIDL, G. K., PIOCK, W. F. & WIRTH, M. 1996. Gasoline Direct Injection: Actual Trends and Future Strategies for Injection and Combustion Systems. SAE International 960465.

GILLES-BIRTH, I., BERNHARDT, S., SPICHER, U. & RECHS, M. 2005. A Study of the In-Nozzle Flow Characteristic of Valve Covered Orifice Nozzles for Gasoline Direct Injection. SAE International 2005-01-3684.

GILOT, P., BONNEFOY, F., MARCUCCILLI, F. & PRADO, G. 1993. Determination of kinetic data for soot oxidation. Modeling of competition between oxygen diffusion and reaction during thermogravimetric analysis. Combustion and Flame, 95, 87-100.

GOETTEMOELLER, J. & GOETTEMOELLER, A. 2007. Sustainable Ethanol: Biofuels, Biorefineries, Cellulosic Biomass, Flex-Fuel Vehicles, and Sustainable Farming for Energy Independence, Prairie Oak Publishing.

GREEN, A. C., DAVID, M., LAMBERT, D. & NANDY, M. 2001. Injection nozzle. Delphi Technologies Inc. Patent EP1081374 A2 patent application.

GREIF, D., BERG, E. V., TATSCHL, R., CORBINELLI, G. & D'ONOFRIO, M. 2005. Integrated cavitating injector flow and spray propagation simulation in DI gasoline engine. SAE International 2005-24-085.

GROB, R. L. 1985. Modern Practice of Gas Chromatography, John Wiley and Sons, Inc.

HARRINGTON, J. A. & SHISHU, R. C. 1973. A single-cylinder engine study of the effects of fuel type, fuel stoichiometry, and hydrogen-to-carbon ratio and CO, NO, and HC exhaust emissions. SAE International 730476.

HE, X., IRELAND, J. C., ZIGLER, B. T., RATCLIFF, M. A., KNOLL, K. E., ALLEMAN, T. L. & TESTER, J. T. 2010. The Impacts of Mid-level Biofuel Content in Gasoline on SIDI Engine-out and Tailpipe Particulate Matter Emissions. SAE International 2010-01-2125.

HE, X., RATCLIFF, M. A. & ZIGLER, B. T. 2012. Effects of Gasoline Direct Injection Engine Operating Parameters on Particle Number Emissions. Energy and Fuels, 26, 2014−2027.

HERBSTMAN, S. & VIRK, K. 1991. Use of Dispersants/Detergents in Diesel Injector Keep Clean and Clean Up Studies. SAE International 912330.

HERREROS, J. M. 2009. Fuel effects in size, morphology and microstructure of diesel particulate matter. PhD thesis, University of Castilla-La Mancha (Spain).

HEYWOOD, J. B. 1989. Internal combustion engine fundamentals, McGraw-Hill: New York.

HILDEN, D. 1988. The Relationship of Gasoline Diolefin Content to Deposits in Multiport Fuel Injectors. SAE International 881642.

HU, E., HU, X., WANG, X., XU, Y., DEARN, K. D. & XU, H. 2012. On the fundamental lubricity of 2,5-dimethylfuran as a synthetic engine fuel. Tribology International, 55, 119-125.

HOCHHAUSER, A. M. 2009. Review of Prior Studies of Fuel Effects on Vehicle Emissions. SAE Int. J. Fuels Lubr., 2, 541-567.

HUGHMARK, G. A. & SOBEL, B. A. 1980. A Statistical Analysis of the Effect of MMT Concentration on Hydrocarbon Emissions. SAE International 800393.

IARC 2011. Agents Classified by the IARC Monographs. International Agency for Research on Cancer.

IMOEHL, W., GESTRI, L., MARAGLIULO, M., DEL-FRATE, L., KLEPATSCH, M. & WILDESON, R. 2012. A DOE Approach to Engine Deposit Testing used to Optimize the Design of a Gasoline Direct Injector Seat and Orifice. SAE Int. J. Fuels Lubr. 2012-01-1642.

IMOEHL, W. J. 2004. Method of optimizing direct injector tip position in a homogeneous charge engine for minimum injector deposits. Siemens Vdo Automotive Corporation Patent US6832593 B2 patent application.

IODICE, P. & SENATORE, A. 2013. Influence of Ethanol-gasoline Blended Fuels on Cold Start Emissions of a Four-stroke Motorcycle. Methodology and Results. SAE International 2013-24-0117

ITO, Y., SHIMODA, T., AOKI, T., SHIBAGAKI, Y., YUUKI, K., SAKAMOTO, H., VOGT, C., MATSUMOTO, T., HEUSS, W., KATTOUAH, P., MAKINO, M. & KATO, K. 2013. Advanced Ceramic Wall Flow Filter for Reduction of Particulate Number Emission of Direct Injection Gasoline Engines. SAE International 2013-01-0836.

JACKSON, N. S., STOKES, J. & LAKE, T. H. 1997a. Stratified and homogeneous charge operation for the direct injection gasoline engine--high power with low fuel consumption and emissions. SAE International 970543.

JACKSON, N. S., STOKES, J. & WHITAKER, P. A. 1997b. A gasoline direct injection (GDI) powered vehicle concept with 3 litre/ 100 km fuel economy and EC stage 4 emission capability. Proceedings of the EAEC 6th European Congress.

JOEDICKE, A., KRUEGER-VENUS, J., BOHR, P., CRACKNELL, R. & DOYLE, D. 2012. Understanding the Effect of DISI Injector Deposits on Vehicle Performance. SAE International 2012-01-0391.

KALGHATGI, G. T. 1995. Combustion Chamber Deposits in Spark-Ignition Engines: A Literature Review. SAE International.

KANO, M., SAITO, K., BASAKI, M., MATSUSHITA, S. & GOHNO, T. 1998. Analysis of Mixture Formation of Direct Injection Gasoline Engine. SAE International 980157.

KAR, K. & CHENG, W. 2009. Speciated Engine-Out Organic Emissions from PFI-SI Engine Operating on Ethanol/Gasoline Mixtures. SAE International 952443.

KARIN, P., KOONSOMBATKUL, O. & CHAROENPHONPHANICH, C. 2011. Oxidation Behaviors of Gasohol Deposit. The second TSME international conference on mechanical engineering. TSME-ICOME.

KATASHIBA, H., HONDA, T., KAWAMOTO, M., SUMIDA, M., FUKUTOMI, N. & KAWAJIRI, K. 2006. Improvement of center injection spray guided DISI performance. SAE International Improvement of center injection spray guided DISI performance.

KHALEK, I. A., BOUGHER, T. & JETTER, J. J. 2010. Particle Emissions from a 2009 Gasoline Direct Injection Engine Using Different Commercially Available Fuels. SAE Int. J. Fuels Lubr., 3, 623-637.

KIM, C., TSEREGOUNIS, S. I. & SCRUGGS, B. E. 1987. Deposit Formation on a Metal Surface in Oxidized Gasolines. SAE International 872112.

KIM, Y., KIM, Y., JUN, S., LEE, K. H., REW, S., LEE, D. & PARK, S. 2013. Strategies for Particle Emissions Reduction from GDI Engines. SAE International 2013-01-1556.

KING, J. 2011. Application of synergistic technologies to achieve high levels of gasoline engine downsizing. IMECE: Engine Downsizing Seminar.

KINOSHITA, M., SAITO, A., MATSUSHITA, S., SHIBATA, H. & NIWA, Y. 1999. A Method for Suppressing Formation of Deposits on Fuel Injector for Direct Injection Gasoline Engine. SAE International 1999-01-3656.

KINTISCH, E. 2007. Energy research. BP bets big on UC Berkeley for novel biofuels center. Science, 315, 747.

KITTELSON, D., PATWARDHAN, U., ZARLING, D., GLADIS, D. & WATTS, W. 2013 Issues associated with measuring nothing or almost nothing: Real-time Measurements of Metallic Ash Emissions from Engines. Presented in Cambridge Particle Meeting.

KITTELSON, D. B. 1998. Engines and nanoparticles: A review. Journal of Aerosol Science, 29, 575-588.

KUME, T., IWAMOTO, Y., IIDA, K., MURAKAMI, M., AKISHINO, K. & ANDO, H. 1996. Combustion control technologies for direct injection SI engine. SAE International 960600.

LABECKI, L., CAIRNS, A., XIA, J., MEGARITIS, A., ZHAO, H. & GANIPPA, L. C. 2012. Combustion and emission of rapeseed oil blends in diesel engine. Applied Energy, 95, 139-146.

LACEY, P., GAIL, S., KIENTZ, J. M., MILOVANOVIC, N. & GRIS, C. 2011. Internal Fuel Injector Deposits. SAE Int. J. Fuels Lubr., 5, 132-145.

LAPUERTA, M., MARTOS, F. J. & HERREROS, J. M. 2007. Effect of engine operating conditions on the size of primary particles composing diesel soot agglomerates. Journal of Aerosol Science, 38, 455-466.

LAPUERTA, M., OLIVA, F., AGUDELO, J. R. & BOEHMAN, A. L. 2012. Effect of fuel on the soot nanostructure and consequences on loading and regeneration of diesel particulate filters. Combustion and Flame, 159, 844-853.

LAPUERTA, M., OLIVA, F. & MART ÍNEZ-MART ÍNEZ, S. 2010. Modeling of the Soot Accumulation in DPF Under Typical Vehicle Operating Conditions. SAE Int. J. Fuels Lubr., 3, 532-542.

LEACH, F. 2012. The Effect of Fuel Volatility and Aromatic Content on Particulate Emissions. Presented in Cambridge Particle Meeting.

LEACH, F., STONE, R. & RICHARDSON, D. 2013. The Influence of Fuel Properties on Particulate Number Emissions from a Direct Injection Spark Ignition Engine. SAE International 2013-01-1558.

LEE, K. O., COLE, R., SEKAR, R., CHOI, M. Y., KANG, J. S., BAE, C. S. & SHIN, H. D. 2002. Morphological investigation of the microstructure, dimensions, and fractal geometry of diesel particulates. Proceedings of the Combustion Institute, 29, 647-653.

LENANE, D. L. 1978. Effect of MMT on Emissions from Production Cars. SAE International 780003.

LI, G. 1999. Modeling fuel preparation and stratified combustion in a gasoline direct injection engine. SAE International 1999-01-0175.

LI, H., LI, C., MA, X., TU, P., XU, H., SHUAI, S.-J. & GHAFOURIAN, A. 2013. Numerical Study of DMF and Gasoline Spray and Mixture Preparation in a GDI Engine. SAE International 2013-01-1592.

LI, Q., FU, J., WU, X., TANG, C. & HUANG, Z. 2012. Laminar flame speeds of DMF-iso-octane-air-N2/CO2 mixtures. . Energy & Fuels, 25, 917-925.

LIANG, B., GE, Y. & TAN, J. 2013. Comparison of PM emissions from a gasoline direct injected (GDI) vehicle and aport fuel injected (PFI) vehicle measured by electrical low pressure impactor (ELPI) with two fuels:Gasoline and M15 methanol gasoline. Journal ofAerosolScience, 57, 22-31.

LINDGREN, R., SKOGSBERG, M., SANDQUIST, H. & DENBRATT, I. 2003. The Influence of Injector Deposits on Mixture Formation in a DISC SI Engine. SAE International 2003-01-1771.

LINDSTRÖM, M. & ÅNGSTRÖM, H.-E. 2008. A Study of Hole Properties in Diesel Fuel Injection Nozzles and its Influence on Smoke Emissions. Proceedings Conference on Thermo- and Fluid Dynamic Processes in Diesel Engines,Conferences & symposia, Valencia, Spain.

MA, X., JIANG, C., XU, H., DING, H. & SHUAI, S. 2014. Laminar burning characteristics of 2-methylfuran and isooctane blend fuels. Fuel, 116, 281-291.

MA, X., JIANG, C., XU, H. & RICHARDSON, S. 2012. In-Cylinder Optical Study on Combustion of DMF and DMF Fuel Blends. SAE International 2012-01-1235.

MA, X., JIANG, C., XU, H., SHUAI, S. & DING, H. 2013. Laminar Burning Characteristics of 2-Methylfuran Compared with 2,5-Dimethylfuran and Isooctane. Energy & Fuels, 27, 6212-6221.

MANSUROV, Z. A. 2005a. Soot formation in combustion processes (review). Combustion Explosion and Shock Waves, 41, 727-744.

MARCH, A., NOURI, J. & YAN, Y. 2010. Spray stability of outwards opening pintle injectors for stratified direct injection spark ignition engine operation. International Journal of Engine Research, 11, 413-437.

MARTIN, P. & BUSTAMANTE, D. 1993. Deposit Forming Tendency of Gasoline Polar Compounds. SAE Internaitonal 932742.

MASON, A., BINNER, J. G. P., GARNER, C. P., GRAUPNER, K., HARRY, J. E., HOARE, D. W., WILLIAMS, A. M. & FOX, N. 2013. Non-Thermal Particulate Filter Regeneration Using Rapid Pulse Electric Discharges. SAE International.

MASUM, B. M., MASJUKI, H. H., KALAM, M. A., RIZWANUL FATTAH, I. M., M PALASH, S. & ABEDIN, M. J. 2013. Effect of ethanol–gasoline blend on NOx emission in SI engine. Renewable and Sustainable Energy Reviews, 24, 209-222.

MATHIEU, F., REDDEMANN, M., MARTIN, D. & KNEER, R. 2010. Experimental Investigation of Fuel Influence on Atomization and Spray Propagation Using an Outwardly Opening GDI-Injector. SAE International

MATHIS, U., MOHR, M. & FORSS, A. M. 2005. Comprehensive particle characterization of modern gasoline and diesel passenger cars at low ambient temperatures. Atmospheric Environment, 39, 107-117.

MATOUSEK, T., DAGEFORDE, H. & BERTSCH, M. Influence of injection pressures up to 300 bar on particle emissions in a GDI engine. 2013. 17th ETH Conference on Combustion Generated Nanoparticles.

MCCABE, R. W., DICICCO, D. M., GUO, G. & HUBBARD, C. P. 2004. Effects of MMT® Fuel Additive on Emission System Components: Comparison of Clear- and MMT®-fueled Escort Vehicles from the Alliance Study. SAE International 2004-01-1084.

MATSUSHITA, S., NIWA, Y., OTANI, H., KINOSHITA, M. & SAITO, A. 1998. Deposit reduction fuel injection valve. European Patent Number EP0828075A1 patent application.

MENDIARA, T., ALZUETA, M. U., MILLERA, A. & BILBAO, R. 2007. Oxidation kinetic study of acetylene soot and two commercial carbon blacks. Available from: http://acs.omnibooksonline.com/data/papers/2007_P074.pdf.

MIYAMOTO, N., OGAWA, H., SHUDO, T. & TAKEYAMA, F. 1994. Combustion and emissions in a new concept DI stratified charge engine with two-stage fuel injection. SAE International 940675.

MOON, S., CHOI, J., ABO-SERIE, E. & BAE, C. 2005. The Effects of Injector Temperature on Spray and Combustion Characteristics in a Single Cylinder DISI Engine. SAE International 2005-01-0101.

MÜLLER, J. O., SU, D. S., JENTOFT, R. E., KRÖHNERT, J., JENTOFT, F. C. & SCHLÖGL, R. 2005. Morphology-controlled reactivity of carbonaceous materials towards oxidation. Catalysis Today, 102–103, 259-265.

MYUNG, C.-L., KIM, J., CHOI, K., HWANG, I. G. & PARK, S. 2012. Comparative study of engine control strategies for particulate emissions from direct injection light-duty vehicle fueled with gasoline and liquid phase liquefied petroleum gas (LPG). Fuel, 94, 348-355.

NOGI, T., SHIRAISHI, T., NAKAYAMA, Y. & OHSUGA, M. 1998. Stability Improvement of Direct Fuel Injection Engine under Lean Combustion Operation. SAE International 982703.

NOGI, T., SHIRAISHI, T., NAKAYAMA, Y. & OHSUGA, M. 1998. Stability Improvement of Direct Fuel Injection Engine under Lean Combustion Operation. SAE International.

NOMA, K., IWAMOTO, Y., MURAKAMI, N., IIDA, K. & NAKAYAMA, O. 1998. Optimized Gasoline Direct Injection Engine for the European Market. SAE International 980150.

OH, Y., LEE, S., KIM, D., CHON, M. & PARK, S. 2012. Experimental and numerical study on spray characteristics of multi-hole type GDI injectors. ILASS Americas 2012 conference.

OHYAMA, Y. 1998. Mixture formation in gasoline direct injection engine. Proceedings of Direkteinspritzung im Ottomotor, 79-106.

OJAPAH, M. M., ZHANG, Y. & ZHAO, H. 2013. Analysis of Gaseous and PM Emissions of 4-Stroke CAI/HCCI and SI Combustion in a DI Gasoline Engine. SAE International 2013-01-1549.

PRICE, P., TWINEY, B., R., S., K., K. & H., W. 2007. Particulate and Hydrocarbon Emissions from a Spray Guided Direct Injection Spark Ignition Engine with Oxygenate Fuel Blends. SAE International 2007-01-0472.

PAPOULIAS, D., GIANNADAKIS, E., MITROGLOU, N., GAVAISES, M. & THEODORAKAKOS, A. 2007. Cavitation in Fuel Injection Systems for Spray-Guided Direct Injection Gasoline Engines. SAE International.

PARK, C., KIM, S., KIM, H. & MORIYOSHI, Y. 2012. Stratified lean combustion characteristics of a spray-guided combustion system in a gasoline direct injection engine. Energy, 41, 401-407.

PARKIN, C. 2008. Update on the UN-ECE particle measurement programme. In: TRANSPORT, U. D. F. (ed.).

PREUSSNER, C., DÖRING, C., FEHLER, S. & KAMPMANN, S. 1998. GDI: Interaction Between Mixture Preparation, Combustion System and Injector Performance. SAE International 980498.

PRICE, P., STONE, R., COLLIER, T., DAVIES, M. & SCHEER, V. 2006. Dynamic Particulate Measurements from a DISI Vehicle: A Comparison of DMS500, ELPI, CPC and PASS. SAE International 2006-01-1077.

PRICE, P., STONE, R., OUDENIJEWEME, D. & CHEN, X. 2007a. Cold Start Particulate Emissions from a Second Generation DI Gasoline Engine. SAE International 2007-01-1931.

PRICE, P., TWINEY, B., R., S., K., K. & H., W. 2007b. Particulate and Hydrocarbon Emissions from a Spray Guided Direct Injection Spark Ignition Engine with Oxygenate Fuel Blends. SAE International 2007-01-0472.

PRICE;, P., STONE;, R., OUDENIJEWEME;, D. & CHEN;, X. Cold Start Particulate Emissions from a Second Generation DI Gasoline Engine. SAE 2007-01-1931.

RAKOPOULOS, D. C., RAKOPOULOS, C. D., PAPAGIANNAKIS, R. G. & KYRITSIS, D. C. 2011. Combustion heat release analysis of ethanol or n-butanol diesel fuel blends in heavy-duty DI diesel engine. Fuel, 90, 1855-1867.

RAMANATHAN, V. & CARMICHAEL, G. 2008. Global and regional climate changes due to black carbon. Nature Geoscience, 1, 221-227.

READING, K., TOMASSEN, H. & EVANS, T. 1992. The Use of Concentration Response Maps to Study the Activity of a High-Performance Diesel Fuel Detergent. SAE International 922187.

RICHARDSON, C., GYOROG, D. & BEARD, L. 1989. A Laboratory Test for Fuel Injector Deposit Studies. SAE International 892116.

RICHTER, J. M., KLINGMANN, R., SPIESS, S. & WONG, K. 2012. Application of Catalyzed Gasoline Particulate Filters to GDI Vehicles. SAE Int. J. Engines, 5, 1361-1370.

RIVERA, E. A. 2014. Fuel injection technology trends. delphi Powertrain Systems.

ROBERT, G. 1980. Fuel injection nozzle with a heat protecting sleeve for internal combustion engines. GB19800038828 19801203

RODRÍGUEZ-FERNÁNDEZ, J., OLIVA, F. & VÁZQUEZ, R. A. 2011. Characterization of the Diesel Soot Oxidation Process through an Optimized Thermogravimetric Method. Energy & Fuels, 25, 2039-2048.

ROMAN-LESHKOV, R., BARRETT, C.J., LIU, Z.Y. DUMESIC, J.A. 2007. Production of dimethylfuran for liquid fuels from biomass-derived carbohydrates. Nature, 447, 982-986.

ROOS, J. W., MEFFERT, M. W., CUNNINGHAM, L. J., HOTCHKISS, A. R. & OPENSHAW, M. J. 2006. A Survey of American and Canadian Consumer Experience - The Performance of Late Model Year Vehicles Operating on Gasoline With and Without the Gasoline Fuel Additive MMT®. SAE International.

RUBINO, L., PHILLIPS, P. R. & TWIGG, M. V. 2005. Measurements of Ultrafine Particle Number Emissions from a Light-Duty Diesel Engine Using SMPS, DMS, ELPI and EEPS. SAE 2005-24-015.

RUBINO, L., PHILLIPS, P. R. & TWIGG, M. V. 2005. Measurements of Ultrafine Particle Number Emissions from a Light-Duty Diesel Engine Using SMPS, DMS, ELPI and EEPS. SAE.

RUSSELL, M., CUMMINGS, J., CUSHING, T. & STUDZINSKI, W. 2013. Cellulosic Ethanol Fuel Quality Evaluation and its Effects on PFI Intake Valve Deposits and GDI Fuel Injector Plugging Performance. SAE International 2013-01-0885.

S. KONO 1995. Study of the stratified charge and stable combustion in DI gasoline engines. SAE International 950688.

SAITO, K.-I. 2000. The Efforts to the Fuel Quality for the Environment Load Reduction - Compatible of the Gasoline Quality to the New Vehicle Technology. Nippon Mitsubishi Oil Vehicle Symposium.

SALADINO, A. J., WILLEY, J. C., LECHNER, J. F., GRAFSTROM, R. C., LAVECK, M. & HARRIS, C. C. 1985. Effects of formaldehyde, acetaldehyde, benzoyl peroxide, and hydrogen peroxide on cultured normal human bronchial epithelial cells. Cancer Res, 45, 2522-6.

SANDFORD, M., PAGE, G. & CRAWFORD, P. 2009. The all new AJV8. SAE International.

SANDQUIST, H., DENBRATT, I., OWRANG, F. & OLSSON, J. 2001. Influence of Fuel Parameters on Deposit Formation and Emissions in a Direct Injection Stratified Charge SI Engine. SAE International 2001-01-2028.

SAYIN, C. 2010. Engine performance and exhaust gas emissions of methanol and ethanol– diesel blends. Fuel, 89, 3410-3415.

SCANIA 2007. New highly efficient diesel-ethanol engine– ready to cut fossil CO2 emissions by 90%, PRESS info.

SCHIFTER, I., DíAZ, L., VERA, M., GUZMÁN, E. & LÓPEZ-SALINAS, E. 2003. Impact of sulphur -in-gasoline on motor vehicle emissions in the metropolitan area of Mexico City. Fuel, 82, 1605-1612.

SCHWAHN, H., LUTZ, U. & KRAMER, U. 2010. Deposit Formation of Flex Fuel Engines Operated on Ethanol and Gasoline Blends. SAE International 2010-01-1464.

SCZOMAK, D. P. 1990. The Poppet Covered Orifice Fuel Injection Nozzle. SAE International 900821.

SHIMIZU, C. & OHTAKA, Y. 2007. Parametric Analysis of Catalytic Converter Plugging Caused by Manganese-Based Gasoline Additives. SAE International 2007-01-1070.

Reference

SKIBA, S. & MELBERT, J. 2012. Dosing Performance of Piezo Injectors and Sensorless Closed-Loop Controlled Solenoid Injectors for Gasoline Direct Injection. SAE Int. J. Engines, 5, 330-335.

SMITH, J., SZEKELY JR, G., SOLOMON, A. & PARRISH, S. 2011. A Comparison of Spray-Guided Stratified-Charge Combustion Performance with Outwardly-Opening Piezo and Multi-Hole Solenoid Injectors. SAE Int. J. Engines, 4, 1481-1497.

SONG, C., ZHAO, Z., LV, G., SONG, J., LIU, L. & ZHAO, R. 2010. Carbonyl compound emissions from a heavy-duty diesel engine fueled with diesel fuel and ethanol–diesel blend. Chemosphere, 79, 1033-1039.

SONG, J. H., ALAM, M., BOEHMAN, A. L. & KIM, U. 2006. Examination of the oxidation behavior of biodiesel soot. Combustion and Flame, 146, 589-604.

STEIN, R. A., ANDERSON, J. E. & WALLINGTON, T. J. 2013. An Overview of the Effects of Ethanol-Gasoline Blends on SI Engine Performance, Fuel Efficiency, and Emissions. SAE Int. J. Engines, 6, 470-487.

STEVENS, E. & STEEPER, R. 2001. Piston Wetting in an Optical DISI Engine: Fuel Films, Pool Fires, and Soot Generation. SAE International 2001-01-1203.

STOREY, J. M., BARONE, T., NORMAN, K. & LEWIS, S. 2010. Ethanol Blend Effects On Direct Injection Spark-Ignition Gasoline Vehicle Particulate Matter Emissions. SAE Int. J. Fuels Lubr., 3, 650-659.

STOREY, J. M. E., BARONE, T. L., THOMAS, J. F. & HUFF, S. P. 2012. Exhaust Particle Characterization for Lean and Stoichiometric DI Vehicles Operating on Ethanol-Gasoline Blends. SAE International 2012-01-0437.

STRATAKIS, G. A. & STAMATELOS, A. M. 2003. Thermogravimetric analysis of soot emitted by a modern diesel engine run on catalyst-doped fuel. Combustion and Flame, 132, 157-169.

TANIGUCHI, B. Y., PEYLA, R. J., PARSONS, G. M., HOEKMAN, S. K. & VOSS, D. A. 1986. Injector Deposits — The Tip of Intake System Deposit Problems. SAE International 861534.

TANIGUCHI, S., YOSHIDA, K. & TSUKASAKI, Y. 2007. Feasibility Study of Ethanol Applications to A Direct Injection Gasoline Engine Journal. SAE International 2007-01-2037.

THEWES, M., MUETHER, M., PISCHINGER, S., BUDDE, M., BRUNN, A., SEHR, A., ADOMEIT, P. & KANKERMAYER, J. 2011. Analysis of the Impact of 2-Methylfuran on Mixture Formation and Combustion in a Direct-Injection Spark-Ignition Engine. Energy & Fuels, 25, 5549-5561.

TIAN, G., DANIEL, R. & XU, H. 2011. DMF-A New Biofuel Candidate.

TIAN, G. H., DANIEL, R., LI, H. Y., XU, H. M., SHUAI, S. J. & RICHARDS, P. 2010. Laminar Burning Velocities of 2,5-Dimethylfuran Compared with Ethanol and Gasoline. Energy & Fuels, 24, 3898-3905.

TIAN, G. H., DANIEL, R., LI, H. Y., XU, H. M., SHUAI, S. J. & RICHARDS, P. 2010b. Laminar Burning Velocities of 2,5-Dimethylfuran Compared with Ethanol and Gasoline. Energy & Fuels, 24, 3898-3905.

TOGBÉ, C., TRAN, L.-S., LIU, D., FELSMANN, D., OẞWALD, P., GLAUDE, P.-A., SIRJEAN, B., FOURNET, R., BATTIN-LECLERC, F. & KOHSE-HÖINGHAUS, K. 2014. Combustion chemistry and flame structure of furan group biofuels using molecule-beam mass spectrometry and gas chromatography − Part III: 2,5-Dimethylfuran. Combustion and Flame, 161, 780-797.

TOMODA, T., SASAKI, S., SAWADA, D., SAITO, A. & SAMI, H. 1997. Development of direct injection gasoline engine—study of stratified mixture formation. SAE International 970539.

TRAN, L.-S., TOGBÉ, C., LIU, D., FELSMANN, D., OẞWALD, P., GLAUDE, P.-A., FOURNET, R., SIRJEAN, B., BATTIN-LECLERC, F. & KOHSE-HÖINGHAUS, K. 2014. Combustion chemistry and flame structure of furan group biofuels using molecule-beam mass spectrometry and gas chromatography − Part II: 2-Methylfuran. Combustion and Flame, 161, 766-779.

TUPA, R. 1987. Port Fuel Injectors-Causes/Consequences/Cures. SAE International.

TUPA, R. C. & KOEHLER, D. E. 1986. Gasoline Port Fuel Injectors - Keep Glean/Clean Up With Additives. SAE International 872113.

UEHARA, T., TAKEI, Y., HOSHI, H. & SHIRATANI, K. 1997. Study on Combustion Chamber Deposit Formation Mechanism -Influence of Fuel Components and Gasoline Detergents. SAE International 971722.

VANDERWEGE, B. A. & HOCHGREB, S. 2000. Effects of Fuel Volatility and Operating Conditions on Fuel Sprays in DISI Engines: (1) Imaging Investigation. SAE International 2000-01-0535.

VONBACHO, P. S., FOX, J. G. & SANT, D. W. 2005. Development of a Robust Injector Design for Superior Deposit Resistance. SAE International 2005-01-3841.

WALLNER, T. 2011. Correlation Between Speciated Hydrocarbon Emissions and Flame Ionization Detector Response for Gasoline/Alcohol Blends. Journal of Engineering for Gas Turbines and Power-Transactions of the Asme, 133.

WALLNER, T. & MIERS, S. A. 2008. Combustion Behavior of Gasoline and Gasoline/Ethanol Blends in a Modern Direct-Injection 4-Cylinder Engine. SAE International 2008-01-0077.

WANG, C. M., XU, H. M., DANIEL, R., GHAFOURIAN, A., HERREROS, J. M., SHUAI, S. J. & MA, X. 2013a. Combustion characteristics and emissions of 2-methylfuran compared to 2,5-dimethylfuran, gasoline and ethanol in a DISI engine. Fuel, 103, 200-211.

WANG, L., SONG, C., SONG, J., LV, G., PANG, H. & ZHANG, W. 2013b. Aliphatic C–H and oxygenated surface functional groups of diesel in-cylinder soot: Characterizations and impact on soot oxidation behavior. Proceedings of the Combustion Institute, 34, 3099-3106.

WEI, L., LI, Z., TONG, L., WANG, Z., JIN, H., YAO, M., ZHENG, Z., WANG, C. & XU, H. 2012. Primary Combustion Intermediates in Lean and Rich Low-Pressure Premixed Laminar 2-Methylfuran/Oxygen/Argon Flames. Energy & Fuels, 26, 6651-6660.

WEAVER, C. E. 2011. Advanced Gasoline Turbocharged Direct Injection (GTDI) Engine Development. DOE Vehicle Technologies Program Review.

WHITEHEAD, M. A., BUCKINGHAM, J. P. & BRUNNER, J. K. 1998. The Port Fuel Injector Deposit Test - A Statistical Review. SAE International 982713.

WU, X., HUANG, Z., JIN, C., WANG, X., ZHENG, B. & ZHANG, Y. 2009a. Identification of combustion intermediates in a low-pressure premixed laminar 2,5-dimethylfuran/oxygen/argon flame with tunable synchrotron photoionization. Combustion and Flame, 156, 1365-76.

WU, X. S., DANIEL, R., TIAN, G. H., XU, H. M., HUANG, Z. H. & RICHARDSON, D. 2011. Dual-injection: The flexible, bi-fuel concept for spark-ignition engines fuelled with various gasoline and biofuel blends. Applied Energy, 88, 2305-2314.

WU, X. S., HUANG, Z. H., JIN, C., WANG, X. G., ZHENG, B., ZHANG, Y. J. & WEI, L. X. 2009b. Measurements of Laminar Burning Velocities and Markstein Lengths of 2,5-Dimethylfuran-Air-Diluent Premixed Flames. Energy & Fuels, 23, 4355-4362.

WU, X. S., LI, Q. Q., FU, J., TANG, C. L., HUANG, Z. H., DANIEL, R., TIAN, G. H. & XU, H. M. 2012. Laminar burning characteristics of 2,5-dimethylfuran and iso-octane blend at elevated temperatures and pressures. Fuel, 95, 234-240.

WWFC 2012. Worldwide fuel charter, proposed fifth edition.

XU, F. 2012. Experimental research on particulate matter emissions from gasoline direct injection engines. PhD thesis, University of Oxford.

YANG, S., LEE, K. & CHONG, H. 2010. Characterization of Oxidation Behaviors and Chemical-Kinetics Parameters of Diesel Particulates Relevant to DPF Regeneration. SAE International 2010-01-2166.

YAO, Y. C., TSAI, J. H., CHANG, A. L. & JENG, F. T. 2008. Effects of sulphur and aromatic contents in gasoline on motorcycle emissions. Atmospheric Environment, 42, 6560-6564.

YEHLIU, K., VANDER WAL, R. L., ARMAS, O. & BOEHMAN, A. L. 2012. Impact of fuel formulation on the nanostructure and reactivity of diesel soot. Combustion and Flame, 159, 3597-3606.

YELIANA, COONEY, C., WORM, J. & NABER, J. D. 2008. The calculation of mass fraction burn of ethanol–gasoline blended fuels using single and two-zone models. SAE International 2008- 01-0320.

YURIY ROMÁN-LESHKOV 2009. Biomass-derived furanic compounds for the production of fuels and chemical intermediates.

ZHANG, S., MCMAHON, W., TOUTOUNDJIAN, H., CRUZ, M. & FRODIN, B. 2010. Particulate Mass and Number Emissions from Light-duty Low Emission Gasoline Vehicles. SAE International 2010-01-0795.

ZHAO, F., LAI, M. C. & HARRINGTON, D. L. 1999. Automotive spark-ignited direct-injection gasoline engines. Progress in Energy and Combustion Science, 25, 437-562.

ZHAO, H., HOLLADAY, J.E., BROWN, H. AND ZHANG, Z.C. 2007. Metal Chlorides in Ionic Liquid Solvents Convert Sugars to 5-Hydroxymethylfurfural. Science, 316, 1597-1600.

ZHONG, S. H., DANIEL, R., XU, H., ZHANG, J., TURNER, D., WYSZYNSKI, M. L. & RICHARDS, P. 2010. Combustion and Emissions of 2,5-Dimethylfuran in a Direct-Injection Spark-Ignition Engine. Energy & Fuels, 24, 2891-2899.

ZHU, J. Y., LEE, K. O., YOZGATLIGIL, A. & CHOI, M. Y. 2005. Effects of engine operating conditions on morphology, microstructure, and fractal geometry of light-duty diesel engine particulates. Proceedings of the Combustion Institute, 30, 2781-2789.

ZHU, Z., LI, D. K., LIU, J., WEI, Y. J. & LIU, S. H. 2012. Investigation on the regulated and unregulated emissions of a DME engine under different injection timing. Applied Thermal Engineering, 35, 9-14.